

Engineering of *Saccharomyces pastorianus* Old Yellow Enzyme 1 for the Synthesis of Pharmacologically Active (S)-Profen Derivatives

Guigao Liu, Shang Li, Qinghua Shi, Hengyu Li, Jiyang Guo, Jingping Ouyang, Xian Jia, Lihan Zhang, Song You, **Bin Qin**

Submitted date: 29/08/2020 · Posted date: 31/08/2020

Licence: CC BY-NC-ND 4.0

Citation information: Liu, Guigao; Li, Shang; Shi, Qinghua; Li, Hengyu; Guo, Jiyang; Ouyang, Jingping; et al. (2020): Engineering of *Saccharomyces pastorianus* Old Yellow Enzyme 1 for the Synthesis of Pharmacologically Active (S)-Profen Derivatives. ChemRxiv. Preprint.

<https://doi.org/10.26434/chemrxiv.12894056.v1>

2-Arylpropionic acid derivatives, such as ibuprofen, constitute an important group of non-steroidal anti-inflammatory drugs (NSAIDs). Biocatalytic asymmetric reduction of 2-arylacrylic acid derivatives by ene reductases (EREDs) is a valuable approach for synthesis of these derivatives. However, previous bioreduction of 2-arylacrylic acid derivatives by either ERED wild-types or variants resulted solely in nonpharmacological (R)-enantiomers as the products. Here, we present the engineering of *Saccharomyces pastorianus* old yellow enzyme 1 (OYE1) into (S)-stereoselective enzymes, which afford pharmacologically active (S)-profen derivatives. By structural comparison of substrate recognition in related EREDs and analysis of non-covalent contacts in the pro-S model of OYE1, the key residues of OYE1 that switch its stereoselectivity to an (S)-stereopreference were identified. Systematic site-directed mutagenesis screening at these positions successfully provided the (S)-stereoselective OYE1 variants, which catalyzed stereoselective bioreduction of various profen precursors to afford pharmacologically active (S)-derivatives including (S)-ibuprofen and (S)-naproxen methyl esters with up to >99% ee values. Moreover, the key residues and mutation strategy obtained from OYE1 could be further transferred to OYE 2.6 (from *Pichia stipitis*) and KnOYE1 (from *Kazachstania naganishii*) to create the (S)-stereoselective EREDs. Our results may provide a generalizable strategy for stereocontrol of OYEs and set the basis for biocatalytic production of (S)-profens.

File list (2)

Manuscript.pdf (1.84 MiB)

[view on ChemRxiv](#) · [download file](#)

Supplementary Information.pdf (9.96 MiB)

[view on ChemRxiv](#) · [download file](#)

Engineering of *Saccharomyces pastorianus* Old Yellow Enzyme 1 for the Synthesis of Pharmacologically Active (*S*)-Profen Derivatives

Guigao Liu,^{1,‡} Shang Li,^{1,‡} Qinghua Shi,² Hengyu Li,² Jiyang Guo,² Jingping Ouyang,³ Xian Jia,³
Lihan Zhang,^{*,4} Song You,^{*,2} and Bin Qin^{*,1}

¹Wuya College of Innovation, Shenyang Pharmaceutical University, 103 Wenhua Road, Shenhe,
Shenyang 110016, People's Republic of China

²School of Life Sciences and Biopharmaceutical Sciences, Shenyang Pharmaceutical University,
103 Wenhua Road, Shenhe, Shenyang 110016, People's Republic of China

³School of Pharmaceutical Engineering, Shenyang Pharmaceutical University, 103 Wenhua
Road, Shenhe, Shenyang 110016, People's Republic of China

⁴School of Science, Westlake University, 18 Shilongshan Road, Xihu, Hangzhou 310024,
People's Republic of China

‡ G.L. and S.L. contributed equally.

*Corresponding author: to-qinbin@163.com (B.Q.); yousong206@aliyun.com (S.Y.);
zhanglihan@westlake.edu.cn (L.Z.).

Abstract

2-Arylpropionic acid derivatives, such as ibuprofen, constitute an important group of non-steroidal anti-inflammatory drugs (NSAIDs). Biocatalytic asymmetric reduction of 2-arylacrylic acid derivatives by ene reductases (EREDs) is a valuable approach for synthesis of these derivatives. However, previous bioreduction of 2-arylacrylic acid derivatives by either ERED wild-types or variants resulted solely in nonpharmacological (*R*)-enantiomers as the products. Here, we present the engineering of *Saccharomyces pastorianus* old yellow enzyme 1 (OYE1) into (*S*)-stereoselective enzymes, which afford pharmacologically active (*S*)-profen derivatives. By structural comparison of substrate recognition in related EREDs and analysis of non-covalent contacts in the pro-*S* model of OYE1, the key residues of OYE1 that switch its stereoselectivity to an (*S*)-stereopreference were identified. Systematic site-directed mutagenesis screening at these positions successfully provided the (*S*)-stereoselective OYE1 variants, which catalyzed stereoselective bioreduction of various profen precursors to afford pharmacologically active (*S*)-derivatives including (*S*)-ibuprofen and (*S*)-naproxen methyl esters with up to >99% *ee* values. Moreover, the key residues and mutation strategy obtained from OYE1 could be further transferred to OYE 2.6 (from *Pichia stipitis*) and KnOYE1 (from *Kazachstania naganishii*) to create the (*S*)-stereoselective EREDs. Our results may provide a generalizable strategy for stereocontrol of OYEs and set the basis for biocatalytic production of (*S*)-profens.

Keywords: ene reductases, profen, OYE1, biocatalysis, protein engineering

Introduction

Ene reductases (EREDs), which catalyze the reduction of activated C=C bonds and thus generate two chiral centers, are powerful and valuable biocatalysts in asymmetric synthesis.¹⁻⁵ Among the families of EREDs, the prototypical flavin mononucleotide (FMN)-containing old yellow enzymes (OYEs) catalyze bioreduction of a broad variety of substrates, including α , β -unsaturated aldehydes, ketones, esters, nitriles, and nitro compounds.^{1,4} The increasing studies on discovery and engineering of EREDs, and combining EREDs with chemocatalysis raise the potential for application of EREDs in pharmaceutical synthesis and organic synthesis.^{1-2,5-10}

The “profen” drugs, such as ibuprofen, flurbiprofen, ketoprofen, and naproxen, which have the 2-arylpropionic acid skeletons, belong to an important and frequently used group of non-steroidal anti-inflammatory drugs (NSAIDs). Although ibuprofen and ketoprofen are often used as racemic mixtures, the (*S*)-enantiomers of “profens” are the main bioactive enantiomers for cyclooxygenase (COX) inhibition, whereas the (*R*)-enantiomers are generally not considered as COX inhibitors. To prepare the optically pure (*S*)-profens, several biocatalytic methods have been tried in the past several decades.¹¹⁻²¹ The lipase-catalyzed kinetic resolution of racemic profen derivatives using wild-type (WT) or engineered enzymes is well studied in both industrial and lab scale, though the yield is theoretically limited to 50% at maximum.¹¹⁻¹⁴ An alternative approach is the use of alcohol dehydrogenases for dynamic kinetic resolution of tautomeric aldehyde derivatives, though this is only applicable to the production of chiral “profenols”.¹⁵ The dehydrogenase-mediate asymmetric disproportionation of aldehydes was further developed to produce (*S*)-profens, but the reaction efficiency is compromised by modest conversion rate and products being nearly 1:1 mixture of the profens and the profenols.¹⁶

The asymmetric C=C bond reduction of profen precursors by EREDs is an alternative and attractive biocatalytic route to prepare optically pure profens (**Figure 1**).^{1,17-21} Recent studies showed that some OYEs, such as YqjM (from *Bacillus subtilis*) and KYE2 (from *Kluyveromyces marxianus*), displayed the ability to stereoselectively reduce 2-arylacrylic acid methyl esters to afford (*R*)-2-arylpropionic acid methyl esters (**Figure 1a** and **Figure S1**).¹⁷⁻¹⁹ The Gröger group and Scrutton group also reported that several OYEs (GOx-ER from *Gluconobacter oxydans* and XenA from *Pseudomonas putida*) can catalyze the direct reduction of 2-arylacrylic acids, whose carboxyl moiety was previously thought to be too weak as an electron-withdrawing group for OYEs (**Figure 1a**).²⁰⁻²¹ Nevertheless, the bioreduction of profen precursors by the aforementioned wild-type OYEs gave the nonpharmacological (*R*)-enantiomers as the products (**Figure 1a** and **Figure S1**).¹⁷⁻²¹ Although some OYEs have been engineered into the (*S*)-selective enzymes in the reduction of carvones and other substrates (**Figure S2**),^{18,22-28} the challenge has remained for direct reductive production of (*S*)-profens.¹⁸ Herein, we report the engineering of ene reductase OYE1 (from *Saccharomyces pastorianus*) into (*S*)-selective enzymes, which can catalyze the stereoselective C=C bond reduction of various profen precursors to afford pharmacologically active (*S*)-profen derivatives, such as (*S*)-ibuprofen and (*S*)-naproxen methyl esters with up to >99% enantiomeric excess (*ee*) values (**Figure 1b**).

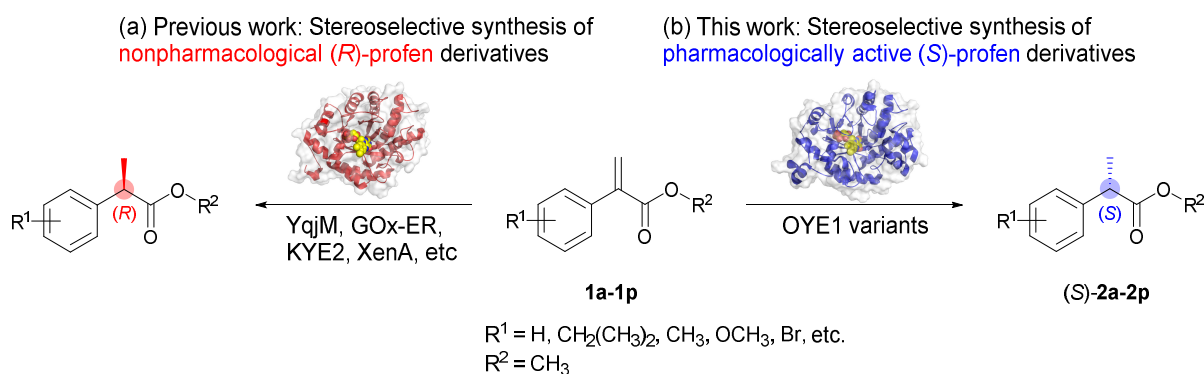


Figure 1. Asymmetric C=C bond bioreduction of 2-arylacrylic acid derivatives (profen precursors) by ene reductases (EREDs).

Results & discussion

In contrast to other reductive enzymes (e.g. ketoreductases), the studies on switching the stereopreference of EREDs are limited.^{1,26} We thus started from structural analyses of EREDs to better understand their stereochemical outcome and to design the binding mode for the unnatural pro-*S* orientation of 2-arylacrylic acid derivatives. A series of pioneering works by Stewart and Scrutton established the binding mode of OYE enzymes and proposed a “normal” binding mode and a “flipped” binding mode to explain the stereoselectivity (**Figure 2** and **Figure S2**).^{21,27-28} As shown in **Figure 2a**, the co-crystal structure of OYE1 W116L variant and the (4*R*)-carvone substrate (PDB:4GWE) shows a “normal” binding mode, where the larger moiety of (4*R*)-carvone that contains isopropenyl group is located in the left side of the binding pocket (pocket L) of OYE1 W116L variant to afford (1*R*,4*R*)-dihydrocarvone.²⁷ Similarly, the co-crystal structure of XenA with 2-phenylacrylic acid (PDB:5N6Q) shows that the larger phenyl group of 2-phenylacrylic acid is also positioned in the pocket L in a “normal” binding mode, which yields (*R*)-2-phenylpropionic acid as the product (**Figure 2c**).²¹ In contrast, in the OYE1 W116A variant, the (4*R*)-carvone substrate binds in a “flipped” mode, with the larger isopropenyl group located in the right side of the pocket (pocket R), which is created by the W116A substitution (**Figure 2b**).²⁷ This flipped orientation of (4*R*)-carvone would lead to the production of (1*S*,4*R*)-dihydrocarvone with the opposite stereochemistry at C1 position.²⁷ These analyses suggest that creating a “flipped” substrate binding mode²⁷⁻²⁸ by modifying the pockets L and R might be critical for the (*S*)-stereoselective reduction in EREDs.

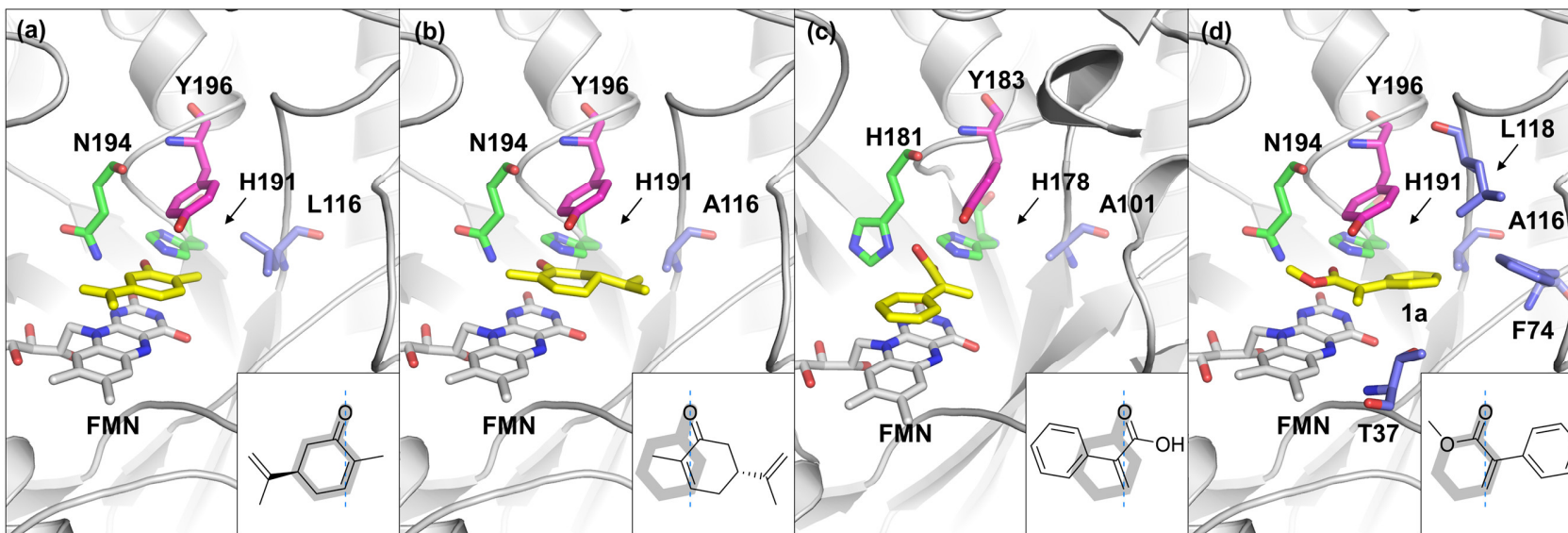


Figure 2. Structural comparison of reported (*R/S*)-stereoselective EREDs and the pro-*S* model of OYE1 with methyl 2-phenylacrylate (**1a**). FMN, the substrate, His/Asn (or His/His) catalytic diad, active site Tyr, and key residues forming the binding pocket R, are shown in white, yellow, green, magenta, and blue, respectively. The bottom right corner of each panel shows a simplified model of substrate recognition, with an asymmetry axis (blue dashed line) crossing the carbonyl oxygen (forming hydrogen bonds with enzymes) and β -carbon (accepting hydride from FMN). The gray highlight shows the comparison with “normal” binding of 2-cyclohexenone backbone²⁷⁻²⁸ (**Figure S2**). **(a)** OYE1 W116L with (4*R*)-carvone in a “normal” pro-*R* binding mode (PDB: 4GWE).²⁷ **(b)** OYE1 W116A with (4*R*)-carvone in a “flipped” pro-*S* binding mode (PDB: 4K7V).²⁷ **(c)** XenA with 2-phenylacrylic acid in a “normal” pro-*R* binding mode (PDB: 5N6Q).²¹ **(d)** OYE W116A with methyl 2-phenylacrylate (**1a**) in a “flipped” pro-*S* binding mode. This model was manually modified based on 4K7V with bound (4*R*)-carvone ligand,²⁷ then optimized by molecular dynamic simulation and the snapshot from MD trajectory was used for analysis.

To model the pro-*S* orientation of profen precursors, we manually modified the structure of (4*R*)-carvone in OYE1 W116A variant (PDB: 4K7V)²⁷ to methyl 2-phenylacrylate (**1a**, **Figure 2d** and **Table 1**) and optimized this model by molecular dynamic (MD) simulation. As show in **Figure 2d**, in a productive orientation from MD trajectory, the phenyl group of **1a** was positioned in the pocket R in a “flipped” manner, in contrast to the “normal” binding as observed in XenA (**Figure 2c**). Additionally, the carbonyl oxygen of **1a** is 2.3 Å and 2.4 Å from the side chains of H191 and N194, which is sufficient for formation of hydrogen bonds.²⁸⁻²⁹ Moreover, the C β and C α of **1a** is 3.5 Å and 3.0 Å from the N5 atom of FMN and the side chain of Y196, while the angle formed by FMN N10-N5-C β of **1a** is 107.0°, which is in a proper range for hydride attack.²⁸⁻²⁹ These evidences suggest that the OYE1 W116A variant may accept **1a** with a pro-*S* orientation in its binding pocket, and thus displays (*S*)-stereoselectivity in the asymmetric reduction of **1a**.

Next, to scrutinize the key amino acid interactions, we analyzed non-covalent contacts between the constructed pro-*S* model of substrate **1a** and residues of OYE1 W116A by the Protein Contacts Atlas online tool³⁰ (**Figure 3**). The result illustrated close contact between **1a** and the residues T37, M39, G72, F74, Y82, A85, A116, L118, Y375 (creating pocket R), and F250, P295, F296 (creating pocket L). In addition, residues T37, A116, F74, Y82, and L118 of pocket R displayed larger atomic contacts with **1a** (**Figure 3b**). On the basis of these observations, we hypothesized that protein engineering at these positions could reshape the binding pocket R (**Figure 3d**), which might switch the selectivity of OYE1 to the (*S*)-stereopreference and make it accept more bulky substrates.

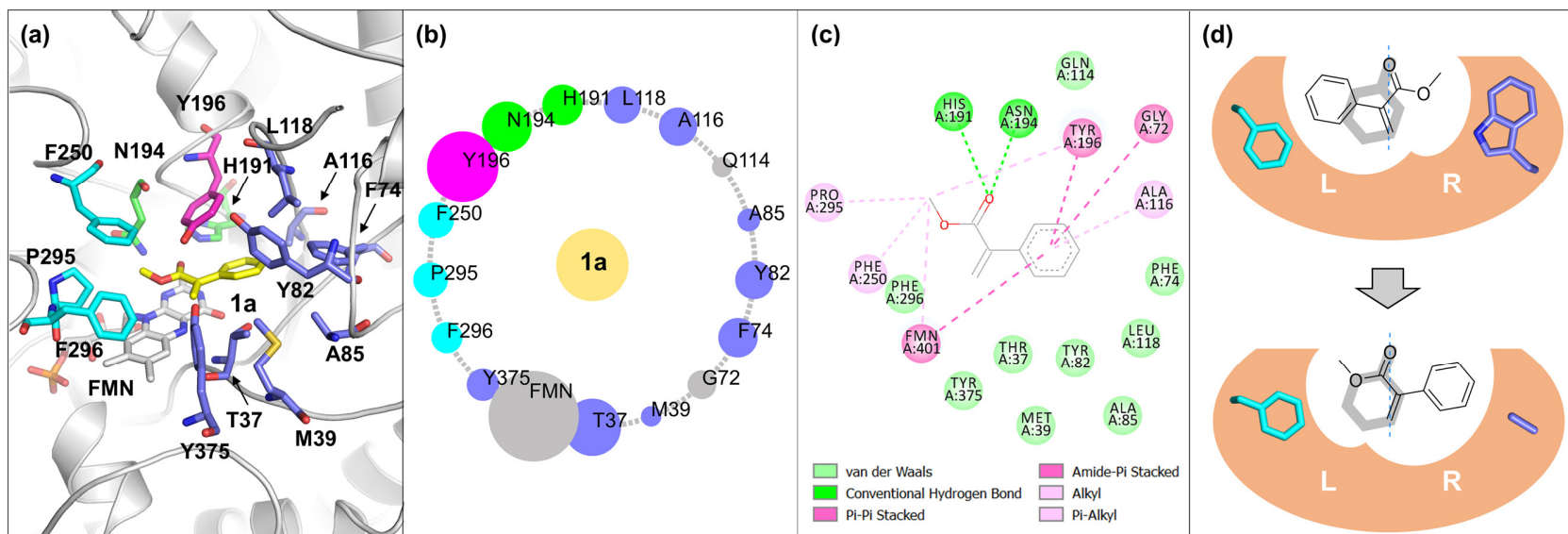
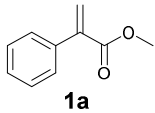
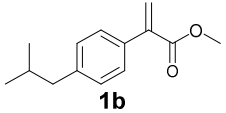
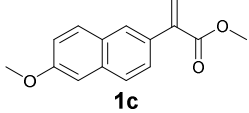
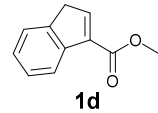


Figure 3. Analyses of the key residues and non-covalent contacts in the refined pro-*S* model of OYE1 W116A with methyl 2-phenylacrylate (**1a**). This model was constructed based on the modification of OYE1 W116A with bound (*4R*)-carvone (PDB: 4K7V).²⁷ **(a)** The pro-*S* model of OYE W116A with **1a**. The residues that create the left and the right binding pockets are shown in cyan and blue, respectively. **(b)** Non-covalent contacts of OYE1 W116A with **1a** that analyzed and visualized by the Protein Contacts Atlas online tool. Directly contacting residues are shown in the circle, while **1a** is shown as central node in the asteroid plot. The residues are colored according to different functions (green and magenta for catalytic residues, cyan for pocket L forming residues, and blue for pocket R forming residues), and the size of each circle is scaled to denote the strength of atomic contacts.³⁰ **(c)** Interaction between OYE1 W116A and **1a** analyzed by the Discovery Studio Visualizer. The residues are colored according to different types of interactions. **(d)** Simple models of pro-*R* OYE1 (top) and pro-*S* OYE1 (bottom).

Table 1. Asymmetric Reduction of 2-Arylacrylic Acid Derivatives 1a–1d by YqjM, OYE1, and OYE1 Variants.

ERED	 1a	 1b	 1c	 1d
YqjM WT	>99 ^a , >99 ^b (<i>R</i>) ^c	77.2, 98.3 (<i>R</i>)	97.8, >99 (<i>R</i>)	96.4, >99 (<i>R</i>)
OYE1 WT	96.9, >99 (<i>R</i>)	88.0, 97.5 (<i>R</i>)	97.1, >99 (<i>R</i>)	50.0, >99 (<i>R</i>)
OYE1 W116G	98.2, 78.4 (<i>S</i>)	NA	NA	52.3, 49.5 (<i>S</i>)
OYE1 W116A	77.9, 81.4 (<i>S</i>)	NA	NA	98.6, 49.6 (<i>S</i>)
OYE1 W116V	NA ^d	NA	NA	NA
OYE1 W116S	73.4, 56.7 (<i>R</i>)	NA	NA	38.9, 82.4 (<i>R</i>)
OYE1 W116A/T37G	30.9, 91.6 (<i>S</i>)	NA	NA	98.5, >99 (<i>S</i>)
OYE1 W116A/T37A	>99, 98.1 (<i>S</i>)	NA	NA	99.4, >99 (<i>S</i>)
OYE1 W116A/T37V	66.9, 95.7 (<i>S</i>)	NA	NA	NA
OYE1 W116A/T37S	28.0, 92.3 (<i>S</i>)	NA	NA	96.9, 91.7 (<i>S</i>)
OYE1 W116A/T37A/F74G	32.1, 80.4 (<i>S</i>)	3.6, 96.6 (<i>S</i>)	5.6, 96.8 (<i>S</i>) ^e	29.2, 89.8 (<i>S</i>)
OYE1 W116A/T37A/F74A	>99, 95.4 (<i>S</i>)	4.6, 96.6 (<i>S</i>)	4.1, 89.7 (<i>S</i>) ^e	99.2, 91.9 (<i>S</i>)
OYE1 W116A/T37A/F74V	26.3, 94.1 (<i>S</i>)	12.7, 96.7 (<i>S</i>)	NA	57.0, 97.7 (<i>S</i>)
OYE1 W116A/T37A/F74S	35.3, 96.3 (<i>S</i>)	13.2, 97.7 (<i>S</i>)	NA	86.1, 89.8 (<i>S</i>)
OYE1 W116G/T37A/F74A	NA	68.5, 99.4 (<i>S</i>)	4.2, 89.1 (<i>S</i>) ^e	33.9, 53.6 (<i>S</i>)
OYE1 W116A/T37A/F74A/L118A	NA	92.9, 97.4 (<i>S</i>)	60.0, 93.1 (<i>S</i>) ^e	NA
OYE1 W116G/T37A/F74A/L118A	NA	19.0, 97.3 (<i>S</i>)	95.9, 99.7 (<i>S</i>)^e	NA

^aThe conversions in percent were determined by chiral HPLC analysis. ^bThe enantiomeric excess (*ee*) values of resultant products in percent were measured by chiral HPLC analysis. ^cThe absolute configurations of the resultant products were identified by comparing the retention times of chiral HPLC with authentic samples, literature data, or the different stereopreferences of YqjM and OYE1 variants (Table S2 in the Supplementary Information). ^dNA, no measurable activity. ^eReaction was performed using the purified enzyme (See Supplementary Information for details). Reaction condition: The reactions were carried out at analytical scale using the cell lysate of *E. coli* expressing EREDs (0.2 g wet cells) and GDH (0.1 g wet cells) with substrate (3 mM, in 50 μ L EtOH or DMSO), glucose (44 mM), NADP⁺ (0.4 mM), and PBS buffer (100 mM, pH 7.0, 950 μ L) at 30 °C, stirring at 200 rpm for 24 h. For reactions using purified enzymes, the reactions were carried out using purified EREDs (10 μ M) with **1c** (3 mM, in 50 μ L DMSO) and NADPH (6 mM) at 30 °C and 200 rpm for 24 h.

To test the above hypothesis of “flipped” binding mode controlled by the left and the right pocket size, we first focused on the W116 position of OYE1. While our pro-*S* model of OYE1 was prepared based on the W116A variant, we systematically mutated the residue 116 with amino acids Gly, Ala, Val, and Ser to investigate the size effect of the side chain’s size (namely shrinkage scanning hereafter). As shown in **Table 1**, in accordance with the stereoselectivity of characterized wild-type EREDs, YqjM WT and OYE1 WT displayed high (*R*)-stereoselectivity toward **1a**, yielding methyl (*R*)-2-phenylpropanoate (**2a**) with >99% *ee* values. In contrast, the reduction of **1a** by OYE1 W116G and W116A variants gave the product **2a** with an *S* configuration. Although the (*S*)-stereoselectivity of OYE1 variants toward **1a** was not high enough (78.4% *ee* for W116G variant and 81.4% *ee* for W116A variant), this result revealed that the bulky phenyl group of **1a** was located with a “flipped”, pro-*S* conformation in the enlarged pocket R created by the W116G/A substitutions. In case of the W116V and W116S variants, the slightly larger side chain of Val and polar Ser might disfavor the positioning of the substrate’s phenyl group in pocket R, leading to the loss of activity and the (*R*)-stereoselectivity, respectively.

Having established a mutant with modest (*S*)-stereoselectivity against the profen substrate analog, we aimed to improve the stereoselectivity by structure-guided rational design. We noticed that the residue T37 of the pocket R (**Figure 3b**) had the largest non-covalent contacts (except catalytic Y196) with **1a**. The polar side chain of T37 could disfavor the orientation of the phenyl group of **1a** in this region, which might have decreased the (*S*)-stereoselectivity. Although the conserved T37 (**Figure S3**) was previously known to be important for catalytic activity,³¹ our recent study on engineering the T37 of OYE1 toward (4*R*)-carvone³² and other studies of engineering the corresponding C26 residue (of YqjM) in classical and thermophilic-like OYEs³³⁻³⁴ indicated the mutability at this position. Therefore, the shrinkage scanning with Gly, Ala, Val,

or Ser substitutions was also applied to the residue T37 of the OYE1 W116A variant. As shown in **Table 1**, enhanced (*S*)-stereoselectivity was found in asymmetric reduction of **1a** by all the constructed variants. Notably, the OYE1 W116A/T37A variant displayed the highest activity and selectivity toward **1a**, yielding methyl (*S*)-2-phenylpropanoate ((*S*)-**2a**) as the product with a 98.1% *ee* value.

Motivated by these results, we next tried the biocatalytic reduction of methyl 2-(4-isobutylphenyl)acrylate (**1b**) and methyl 2-(6-methoxynaphthalen-2-yl)acrylate (**1c**), which are the precursors of ibuprofen and naproxen, respectively. Unfortunately, the OYE1 W116A/T37A variant and the other T37 variants did not show any activity toward **1b** and **1c** (**Table 1**). We then constructed the pro-*S* models of OYE1 W116A/T37A with **1b** and **1c** (**Figure S4**) to identify a potential clash in the pocket R with substrates. The model indicated that the bulky side chain of F74 can block the bulkier aryl moiety of **1b/1c**. Moreover, since the F74 position in homologues of OYE1 showed several variants at this position (**Figure S3**), we targeted F74 by the shrinkage scanning with the aim of creating a larger pocket R for the binding of these bulky substrates. The resulting four mutants, although with low activity, displayed high (*S*)-stereoselectivity in the asymmetric reduction of **1b**, and the F74G and F74A mutants even accepted **1c** with 90% stereoselectivity. The OYE1 W116A/T37A/F74A variant was next selected for further mutation rather than the F74G variant since the F74A substitution might stabilize the substrate binding by alkyl interaction. The L118 residue forming the pocket R was also mutated to smaller Ala with the intent to further enlarge the pocket R. As shown in **Table 1**, the conversion rate of the OYE1 W116A/T37A/F74A/L118A variant toward the ibuprofen analog **1b** was dramatically improved to 92.9% from 4.9%, while the (*S*)-stereoselectivity was maintained at high (97.4% *ee*). The conversion rate of the OYE1 W116A/T37A/F74A/L118A variant toward the naproxen analog **1c**

was further improved to 95.9% by an Ala to Gly mutation (W116G/T37A/F74A/L118A variant) with an excellent 99.7% *ee* value for the (*S*)-enantiomer. To the best of our knowledge, these results demonstrate the first OYE enzymes capable of producing (*S*)-profen derivatives.

In addition, we also investigated the asymmetric reduction of substrate **1d**, whose reduction product was previously used as the precursor for the synthesis of human peptidyl-prolyl-*cis/trans*-isomerase (Pin1) inhibitors.³⁵ The binding mode of **1d** in the pocket R of the OYE1 W116A variant was similar as that of **1a**, albeit its bicyclic structure, making it a promising substrate for asymmetric reduction (**Figure S5**). As shown in **Table 1**, the OYE1 WT displayed a high (*R*)-stereoselectivity toward **1d** with a >99% *ee* value, whereas the OYE1 W116A/T37A variant exhibited a high (*S*)-stereoselectivity ((*S*)-**2d** with a >99% *ee* value). Consistent with our modeling prediction, the stereochemical preference was identical between **1a** and **1d** across all OYE1 variants we tested. These results also indicated that the stereocomplementary reduction of **1d** was achieved through the OYE1 WT and the obtained OYE1 variants.

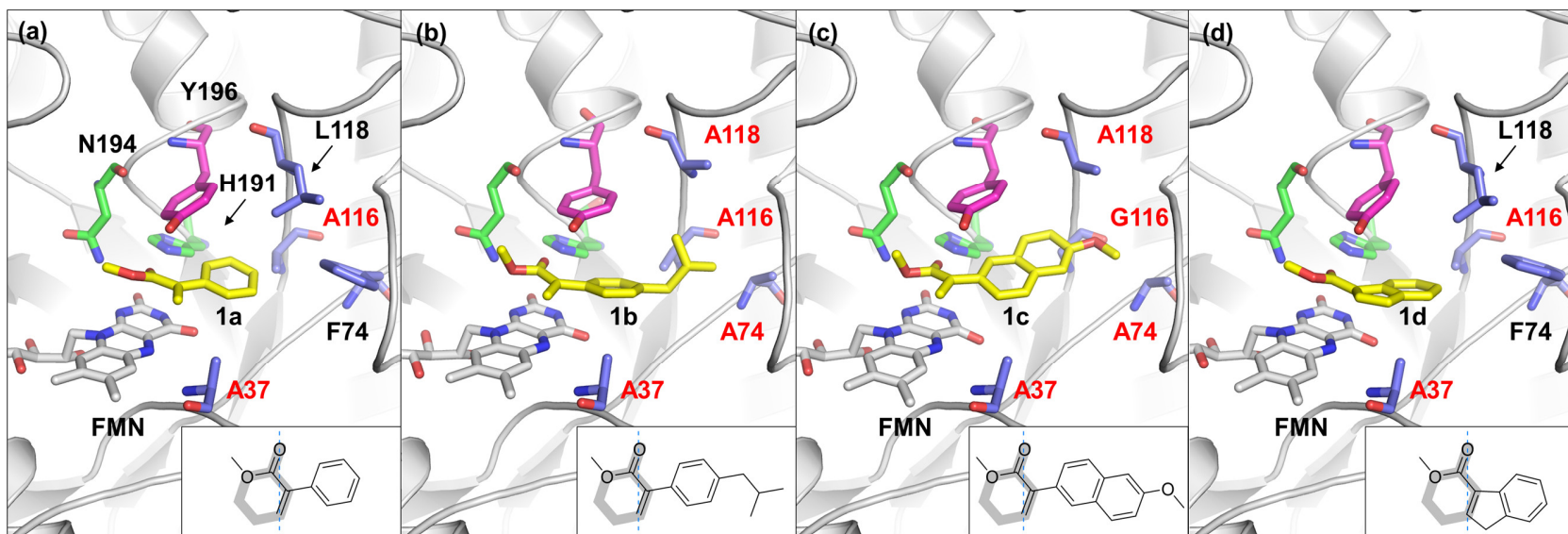


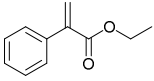
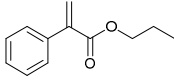
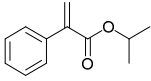
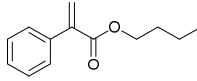
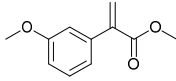
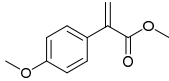
Figure 4. Results from the MD simulation of OYE1 variants with corresponding substrates. **(a)** Snapshot of the MD trajectory for OYE1 W116A/T37A variant with methyl 2-phenylacrylate (**1a**). Key residues in the binding pocket R are shown as blue sticks and labels for mutations are shown in red. **(b)** Snapshot of the MD trajectory for OYE1 W116A/T37A/F74A/L118A variant with methyl 2-(4-isobutylphenyl)acrylate (**1b**, ibuprofen precursor). **(c)** Snapshot of the MD trajectory for OYE1 W116G/T37A/F74A/L118A variant with methyl 2-(6-methoxynaphthalen-2-yl)acrylate (**1c**, naproxen precursor). **(d)** Snapshot of the MD trajectory for OYE1 W116A/T37A variant with methyl 1H-indene-3-carboxylate (**1d**, precursor of Pin1 inhibitors³⁵).

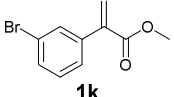
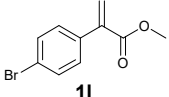
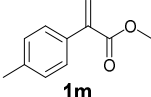
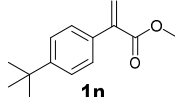
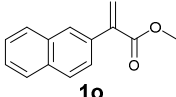
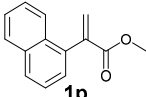
To scrutinize the molecular basis of the (*S*)-stereoselectivity of the OYE1 variants, four pro-*S* models of the OYE1 variants, W116A/T37A with **1a**, W116A/T37A/F74A/L118A with **1b**, W116G/T37A/F74A/L118A with **1c**, and W116A/T37A with **1d** were constructed and then optimized by molecular dynamics simulations. Analyses of the distance between the carbonyl oxygen of the substrate and the side chains of H191/N194, the distance between the $C\beta/C\alpha$ of the substrate and FMN-N5 or Y196, and the angle of FMN and substrate (N10-N5- $C\beta$) indicated that most models were stable and some orientations were productive (**Figure 4** and **Figure S6**). For example, the stability of OYE1 W116A variant with **1a** was improved by the W116A/T37A variant, which might explain the improved (*S*)-stereoselectivity. Although the stability of the W116A/T37A/F74A/L118A with **1b** was lower than that of the W116G/T37A/F74A/L118A with **1c**, enhanced stability was found in the W116G/T37A/F74A/L118A variant toward **1b**, which also displayed a high (*S*)-selectivity toward **1b**. Moreover, the calculated volume of substrate binding pockets (by CASTp 3.0)³⁶ revealed that the shrinkage mutations W116G/A, T37A, F74A, and L118A have contributed to the enlarged binding pocket volume (**Figure S7**). In addition, the analysis of non-covalent contacts indicated that the newly generated π -alkyl or alkyl-alkyl interactions between the introduced residue substitutions (W116A, T37A, F74A, or L118A) and substrates could stabilize the binding of substrates, which might contribute to the better “flipped” binding mode required for the (*S*)-stereoselectivity (**Figure 4** and **Figure S8**). We also compared the structure of the (*R*)-stereopreferred XenA²¹ and the model of OYE1 W116A/T37A to understand the unique (*S*)-selectivity of the obtained OYE1 variants. Although XenA does have an A101 residue that corresponds to the W116 in OYE1 and smaller residues at the sites corresponding to T37, F74, and L118 in the pocket R of OYE1 (**Figure S9**), the loops β_{11}/α_7 and β_{10}/α_6 of XenA are slightly away from its substrate binding pocket, resulting in an open pocket L

(**Figure S10**). In contrast, the equivalent loops $\beta 11/\alpha 10$ and $\beta 10/\alpha 9$ of OYE1 are closer around the substrate binding pocket, and the volume of pocket L is restricted by the residues F250, P295, and F296 in these loops (**Figure S10**). Thus, the restricted pocket L of OYE1 might promote the bulky phenyl group of the substrates to locate in the enlarged pocket R created by the W116A and T37A substitutions, leading to the (*S*)-stereoselectivity.

Next, we explored the substrate scope of the obtained (*S*)-stereoselective OYE1 variants. To evaluate the contribution of pocket L and pocket R in substrate recognition, we prepared a range of substitutions in the ester moiety and the aryl moiety of the substrates (**1e-1p**) and tested them against YqjM and OYE1 (**Table 2**). In agreement with our hypothesis and previously reported stereoselectivity, YqjM and OYE1 WT exhibited an (*R*)-stereoselectivity toward all accepted substrates, whereas the OYE1 variants exhibited an (*S*)-stereoselectivity to a variety of substrates that have modified aryl group (**1i-1o**) with high to excellent selectivity. Notably, the triple mutations W116G/T37A/F74A were essential to accommodate *p*-substituted substrates (**1j, 1l-1n**) in a “flipped” manner in pocket R. The substrates with longer ester side chain (**1f-1h**) were not accepted by YqjM and OYE1 WT presumably due to the limited size of their binding pocket, and we observed an (*R*)-stereoselectivity even with the engineered OYE1 W116A/T37A mutant for **1f** and **1h**. This was reasonable because the longer propyl and butyl ester may clash with the small pocket L, thus flipping back the substrate to the “normal” binding mode, with longer ester moiety positioned in the enlarged pocket R. None of the enzymes displayed activity toward **1g** and **1p**, indicating the substrate size limit for these OYE1 variants.

Table 2. Asymmetric Reduction of 2-Arylacrylic Acid Derivatives 1e–1p by YqjM, OYE1, and Selected OYE1 Variants.

ERED	 1e	 1f	 1g	 1h	 1i	 1j
YqjM WT	5.4 ^a , 98.2 ^b (<i>R</i>)	NA	NA	NA	>99, >99 (<i>R</i>)	>99, >99 (<i>R</i>)
OYE1 WT	NA	NA	NA	NA	>99, >99 (<i>R</i>)	>99, >99 (<i>R</i>)
OYE1 selected variant (Variant)	94.2, 89.2 (<i>S</i>) (W116A/T37A)	42.7, 78.9 (<i>R</i>) (W116A/T37A)	NA	91.6, 93.3 (<i>R</i>) (W116A/T37A)	>99, 97.7 (<i>S</i>) (W116A/T37A)	>99, 99.8 (<i>S</i>) (W116G/T37A/F 74A)

EREDs	 1k	 1l	 1m	 1n	 1o	 1p
YqjM WT	>99, >99 (<i>R</i>)	>99, >99 (<i>R</i>)	>99, >99 (<i>R</i>)	94.7, >99 (<i>R</i>)	96.7, >99 (<i>R</i>)	NA
OYE1 WT	>99, >99 (<i>R</i>)	>99, >99 (<i>R</i>)	>99, >99 (<i>R</i>)	57.2, >99 (<i>R</i>)	88.4, >99 (<i>R</i>)	NA
OYE1 selected variant (Variant)	>99, >99 (<i>S</i>) (W116A/T37A)	>99, >99 (<i>S</i>) (W116G/T37A/F 74A)	>99, >99 (<i>S</i>) (W116G/T37A/F 74A)	91.5, >99 (<i>S</i>) (W116G/T37A/F 74A)	81.8, 90.8 (<i>S</i>) (W116G/T37A/F 74A)	NA

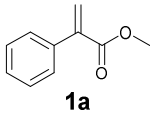
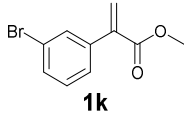
^aThe conversions in percent, determined by chiral HPLC analysis. ^bThe enantiomeric excess (*ee*) values of resultant products in percent, measured by chiral HPLC analysis. Reaction condition: The reactions were carried out at analytical scale using the cell lysate of *E. coli* expressing EREDs (0.2 g wet cells) and GDH (0.1 g wet cells) with substrate (3 mM, in 50 μ L EtOH or DMSO), glucose (44 mM), NADP⁺ (0.4 mM), and PBS buffer (100 mM, pH 7.0, 950 μ L) at 30 °C, stirring at 200 rpm for 24 h.

Table 3. Kinetic Parameters of OYE1 WT and Variants toward 2-Arylacrylic Acid Derivatives.

Substrate	ERED	K_m [mM]	k_{cat} [s ⁻¹]	k_{cat}/K_m [mM ⁻¹ s ⁻¹]
1a	WT	5.05 ± 0.56	0.10 ± 0.06	0.019
	W116A/T37A	11.09 ± 4.8	0.26 ± 0.08	0.024
1b	W116A/T37A/F74A/L118A	0.37 ± 0.06	0.016 ± 0.001	0.045
1c	W116G/T37A/F74A/L118A	2.49 ± 2.3	0.031 ± 0.026	0.013
1i	WT	2.42 ± 0.84	0.040 ± 0.007	0.016
	W116A/T37A	1.05 ± 0.53	0.042 ± 0.008	0.040
1j	WT	4.05 ± 0.48	0.035 ± 0.002	0.0088
	W116G/T37A/F74A	5.87 ± 0.89	0.047 ± 0.005	0.0081
1k	WT	2.81 ± 0.52	0.063 ± 0.008	0.022
	W116A/T37A	1.29 ± 0.56	0.16 ± 0.04	0.12
1l	WT	1.20 ± 0.19	0.094 ± 0.008	0.078
	W116G/T37A/F74A	0.62 ± 0.25	0.028 ± 0.005	0.045

The kinetic assays were carried out in 200 μ L PBS buffer (100 mM, pH 7.0) containing FMN (12.5 μ M), NADPH (1.5 mM), glucose oxidase (*ca.* 10 U), glucose (50 mM), at 30 °C using 5.6 μ M to 7.4 μ M of the OYEs at substrate concentrations ranging from 0.15 mM to 6.6 mM.

Table 4. Asymmetric Reduction of 2-Arylacrylic Acid Derivatives 1a and 1k by OYE1, OYE2.6, KnOYE1 and Their Variants.

ERED	 1a	 1k
OYE1 WT	96.9 ^a , >99 ^b (<i>R</i>)	>99, >99 (<i>R</i>)
OYE1 W116A	77.9, 81.4 (<i>S</i>)	85.3, 72.6 (<i>S</i>)
OYE1 W116A/T37A	>99, 98.1 (<i>S</i>)	>99, >99 (<i>S</i>)
OYE2.6 WT	NA	13.0, 94.7 (<i>R</i>)
OYE2.6 I113A	53.4, 49.1 (<i>S</i>)	94.3, 75.1 (<i>S</i>)
OYE2.6 I113A/T35A	NA	12.7, 75.8 (<i>S</i>)
OYE2.6 N293F/I113A	35.0, 45.4 (<i>S</i>)	83.9, 80.9 (<i>S</i>)
OYE2.6 N293F/I113A/T35A	NA	99.4, 99.4 (<i>S</i>)
KnOYE1 WT	NA	4.1, 94.4 (<i>R</i>)
KnOYE1 R119A	>99, 92.4 (<i>R</i>)	>99, 85.4 (<i>R</i>)
KnOYE1 R119A/T40A	NA	74.8, 0.9 (<i>R</i>)
KnOYE1 S299F/R119A	92.0, 74.0 (<i>R</i>)	90.2, 24.8 (<i>R</i>)
KnOYE1 S299F/R119A/T40A	24.0, 84.4 (<i>S</i>)	30.1, 67.7 (<i>S</i>)
KnOYE1 S299F/R119A/T40A/W42A	>99, 70.0 (<i>S</i>)	94.6, 79.7 (<i>S</i>)

^aThe conversions in percent, determined by chiral HPLC analysis. ^bThe enantiomeric excess (*ee*) values of resultant products in percent, measured by chiral HPLC analysis. Reaction condition: The reaction was carried out at analytical scale using the cell lysate of *E. coli* expressing EREDs (0.2 g wet cells) and GDH (0.1 g wet cells) with substrate (3 mM, in 50 μ L EtOH or DMSO), glucose (44 mM), NADP⁺ (0.4 mM), and PBS buffer (100 mM, pH 7.0, 950 μ L) at 30 °C, stirring at 200 rpm for 24 h.

The kinetic studies of the OYE1 WT and variants with selected substrates were also carried out to investigate the catalytic efficiency. As shown in **Table 3**, the OYE1 W116A/T37A variant displayed higher catalytic efficiency (k_{cat}/K_m) than the WT enzyme against **1a**, **1i**, and **1k**. Notably, the highest catalytic efficiency was found in the bioreduction of **1k** by the W116A/T37A variant. Overall, the OYE1 variants producing the (*S*)-profen derivatives exhibited comparable catalytic efficiency to the (*R*)-stereoselective OYE1 WT, demonstrating the robustness of the engineered variants. The aryl moiety of the substrates could also influence the activity, as both WT and the variants displayed higher catalytic efficiency against the *p*-/*m*-Br substituted substrates (**1k** and **1l**) than that against the *p*-/*m*-OMe substituted substrates (**1i** and **1j**). The OYE1 variants have modest changes in both K_m and k_{cat} values when compared with the WT or against different substrates, suggesting their complicated effects in substrate binding and reaction turnover.

To determine the yield of the OYE-catalyzed (*S*)-profen production, we used substrates **1b**, **1d**, **1i**, **1j**, and **1l**, for biocatalytic C=C bond reduction by the appropriate OYE1 variants. With 0.08 mmol of the substrates, we furnished (*S*)-**2b**, (*S*)-**2d**, (*S*)-**2i**, (*S*)-**2j**, and (*S*)-**2l** in 16-31% isolated yields. The low yields are presumably due to the loss of products during the extraction and purification process. In the enlarged reactions on 0.19 mmol for **1a** and 1.0 mmol for **1k**, the OYE1 W116A/T37A variant delivered (*S*)-**2a** and (*S*)-**2k** in improved 66% (98% *ee*) and 68% (99% *ee*) yields, respectively, which raises the potential applications of these (*S*)-stereoprefered OYEs.

Finally, with the OYE1 variants that could prepare the pharmacologically active (*S*)-profen derivatives in hand, we turned to find and engineer more EREDs with an (*S*)-stereopreference toward profen precursors. BLAST search and multiple-sequence alignment of OYE1 homologues revealed that the W116 and T37 were highly conserved among these enzymes (**Figure S3**), which might explain why most EREDs show an (*R*)-stereopreference. Notably, OYE2.6 (from *Pichia*

stipitis) is known to display an (*S*)-stereopreference toward a series of substrates and has the Ile113 (corresponding to W116 of OYE1, **Figure S11** and **Figure S12**).³⁷⁻³⁸ Additionally, we identified KnOYE1 from *Kazachstania naganishii* by genome mining (NCBI accession: XP_022464309), which has a 63% sequence identity with OYE1 and contains an Arg residue at the 119 position (corresponding to the W116 position of OYE1, **Figure S11** and **Figure S12**). We tested the two enzymes using compounds **1a** and **1k** to investigate whether the mutation corresponding to the W116 of OYE1 can yield the (*S*)-stereopreference. Although OYE2.6 WT and KnOYE1 WT did not show activity toward **1a**, introduction of the I113A mutation in analogy to the OYE1 W116A, with the aim of expanding the pocket R in OYE2.6 resulted in the (*S*)-stereoselective reduction of **1a** (**Table 4**). However, the equivalent mutations R119A and R119A/T40A in KnOYE1 did not show the (*S*)-stereopreference toward **1a**, suggesting that expansion of the pocket R is not enough for accommodating the substrate. To facilitate substrate binding in the pocket R of KnOYE1, we designed the S299F mutation to limit the size of pocket L, and the W42A mutation to enlarge the pocket R (**Figure S12**). The assay results revealed that a combination of mutations in pocket L (S299F) and pocket R (T40A/W42A) effectively converted the stereoselectivity from (*R*)- to (*S*)-form toward **1a**. For substrate **1k**, the enhanced (*S*)-stereoselectivity was found in related OYE2.6 variants with further mutation of N293F (corresponding to the F296 of OYE1 and S299 of KnOYE1). Similarly, the S299F and W42A substitution also contributed to the (*S*)-stereopreference of KnOYE1 variants toward **1k**. These results suggest that the rational binding site design of the pockets L and R can be a general strategy to modify the stereoselectivity of OYE family enzymes.

Conclusions

Biocatalytic reduction of the C=C bonds of 2-arylacrylic acid derivatives by EREDs is an attractive route to synthesize optically pure profens. However, most EREDs catalyzed asymmetric reactions display the same stereoselectivity, yielding the nonpharmacological (*R*)-profen derivatives as the products, which limits further application of EREDs. In this research, we engineered OYE1 into (*S*)-stereoselective enzymes that could synthesize the pharmacologically active (*S*)-profen derivatives by asymmetric reduction of the prochiral precursors. Through careful comparison of the substrate recognition in structures of EREDs and analysis of the non-covalent contacts in the pro-*S* model of OYE1 with substrate, the key residues in the binding pocket R that control stereoselectivity were identified in OYE1. Expanding the substrate binding pocket R of OYE1 by mutagenesis with smaller substitutions at these residues switched its (*R*)-stereoselectivity to (*S*)-stereoselectivity, resulting in the production of (*S*)-ibuprofen, (*S*)-naproxen, and other (*S*)-2-arylpropionic acid derivatives with up to >99% *ee* values. Furthermore, mutagenesis of OYE2.6 and KnOYE1 at the positions corresponding to OYE1 successfully switched their stereopreferences to the (*S*)-form toward 2-arylacrylic acid derivatives. Although our study remains in laboratory-scale biocatalysis, the OYEs mediated reductions on preparative scale have been reported recently, for example including the reduction of methyl-3-oxocyclohex-1-enecarboxylate in an astonishing 100-gram scale.^{3,5,39} The generalizable binding site design strategy in this research and the obtained (*S*)-stereoprefered EREDs will set the basis for the application of related biocatalysts.

Conflicts of interest

There are no conflicts to declare

Acknowledgment

This work was financially supported by the National Natural Science Foundation of China (31971207, 81602993), LiaoNing Revitalization Talents Program (XLYC1907153), and Young Elite Scientists Sponsorship Program by CAST (2016QNRC001).

References

- (1) H. S. Toogood and N. S. Scrutton, *ACS Catal.*, 2018, **8**, 3532-3549.
- (2) P. N. Devine, R. M. Howard, R. Kumar, M. P. Thompson, M. D. Truppo and N. J. Turner, *Nat. Rev. Chem.*, 2018, **2**, 409-421.
- (3) C. K. Winkler, K. Faber and M. Hall, *Curr. Opin. Chem. Biol.*, 2018, **43**, 97-105.
- (4) M. Hall and A. S. Bommarius, *Chem. Rev.*, 2011, **111**, 4088-4110.
- (5) F. Hollmann, D. J. Opperman and C. E. Paul, *Angew. Chem., Int. Ed.*, 2020, DOI: 10.1002/anie.202001876.
- (6) Z. C. Litman, Y. Wang, H. Zhao and J. F. Hartwig, *Nature*, 2018, **560**, 355-359.
- (7) X. Huang, B. Wang, Y. Wang, G. Jiang, J. Feng and H. Zhao, *Nature*, 2020, **584**, 69-74.
- (8) K. F. Biegasiewicz, S. J. Cooper, X. Gao, D. G. Oblinsky, J. H. Kim, S. E. Garfinkle, L. A. Joyce, B. A. Sandoval, G. D. Scholes and T. K. Hyster, *Science*, 2019, **364**, 1166-1169.
- (9) B. A. Sandoval, S. I. Kurtoic, M. M. Chung, K. F. Biegasiewicz and T. K. Hyster, *Angew. Chem., Int. Ed.*, 2019, **58**, 8714-8718.

- (10) T. W. Thorpe, S. P. France, S. Hussain, J. R. Marshall, W. Zawodny, J. Mangas-Sanchez, S. L. Montgomery, R. M. Howard, D. S. B. Daniels, R. Kumar, F. Parmeggiani and N. J. Turner, *J. Am. Chem. Soc.*, 2019, **141**, 19208-19213.
- (11) R. Kourist, P. Domínguez de María and K. Miyamoto, *Green Chem.*, 2011, **13**, 2607-2618.
- (12) A. G. Sandström, Y. Wikmark, K. Engström, J. Nyhlén and J.-E. Bäckvall, *Proc. Natl. Acad. Sci. U. S. A.*, 2012, **109**, 78-83.
- (13) Q. Wu, P. Soni and M. T. Reetz, *J. Am. Chem. Soc.*, 2013, **135**, 1872-1881.
- (14) B. Qin, P. Liang, X. Jia, X. Zhang, M. Mu, X.-Y. Wang, G.-Z. Ma, D.-N. Jin and S. You, *Catal. Commun.*, 2013, **38**, 1-5.
- (15) J. A. Friest, Y. Maezato, S. Broussy, P. Blum and D. B. Berkowitz, *J. Am. Chem. Soc.*, 2010, **132**, 5930-5931.
- (16) E. Tassano, K. Faber and M. Hall, *Adv. Synth. Catal.*, 2018, **360**, 2742-2751.
- (17) J. Pietruszka and M. Schölzel, *Adv. Synth. Catal.*, 2012, **354**, 751-756.
- (18) E. Rühllein, T. Classen, L. Dobnikar, M. Schölzel and J. Pietruszka, *Adv. Synth. Catal.*, 2015, **357**, 1775-1786.
- (19) Z. Li, Z. Wang, G. Meng, H. Lu, Z. Huang and F. Chen, *Asian J. Org. Chem.*, 2018, **7**, 763-769.
- (20) T. Reiß, W. Hummel, S. P. Hanlon, H. Iding and H. Gröger, *ChemCatChem*, 2015, **7**, 1302-1311.
- (21) J. Waller, H. S. Toogood, V. Karuppiyah, N. J. W. Rattray, D. J. Mansell, D. Leys, J. M. Gardiner, A. Fryszkowska, S. T. Ahmed, R. Bandichhor, G. P. Reddy and N. S. Scrutton, *Org. Biomol. Chem.*, 2017, **15**, 4440-4448.

- (22) E. Brenna, M. Crotti, F. G. Gatti, D. Monti, F. Parmeggiani, R. W. Powell Iii, S. Santangelo and J. D. Stewart, *Adv. Synth. Catal.*, 2015, **357**, 1849-1860.
- (23) A. B. Daugherty, S. Govindarajan and S. Lutz, *J. Am. Chem. Soc.*, 2013, **135**, 14425-14432.
- (24) A. B. Daugherty, J. R. Horton, X. Cheng and S. Lutz, *ACS Catal.*, 2015, **5**, 892-899.
- (25) L. T. Quertinmont and S. Lutz, *Tetrahedron*, 2016, **72**, 7282-7287.
- (26) E. D. Amato and J. D. Stewart, *Biotechnol. Adv.*, 2015, **33**, 624-631.
- (27) Y. A. Pompeu, B. Sullivan and J. D. Stewart, *ACS Catal.*, 2013, **3**, 2376-2390.
- (28) S. K. Padhi, D. J. Bougioukou and J. D. Stewart, *J. Am. Chem. Soc.*, 2009, **131**, 3271-3280.
- (29) M. W. Fraaije and A. Mattevi, *Trends Biochem. Sci.*, 2000, **25**, 126-132.
- (30) M. Kayikci, A. J. Venkatakrishnan, J. Scott-Brown, C. N. J. Ravarani, T. Flock and M. M. Babu, *Nat. Struct. Mol. Biol.*, 2018, **25**, 185-194.
- (31) D. Xu, R. M. Kohli and V. Massey, *Proc. Natl. Acad. Sci. U. S. A.*, 1999, **96**, 3556.
- (32) J. Guo, R. Zhang, J. Ouyang, F. Zhang, F. Qin, G. Liu, W. Zhang, H. Li, X. Ji, X. Jia, B. Qin and S. You, *ChemCatChem*, 2018, **10**, 5496-5504.
- (33) N. Nett, S. Duewel, A. A. Richter and S. Hoebenreich, *ChemBioChem*, 2017, **18**, 685-691.
- (34) D. J. Bougioukou, S. Kille, A. Taglieber and M. T. Reetz, *Adv. Synth. Catal.*, 2009, **351**, 3287-3305.
- (35) S. Daum, F. Erdmann, G. Fischer, B. Féaux de Lacroix, A. Hessamian-Alinejad, S. Houben, W. Frank and M. Braun, *Angew. Chem. Int. Ed.*, 2006, **45**, 7454-7458.
- (36) W. Tian, C. Chen, X. Lei, J. Zhao and J. Liang, *Nucleic Acids Res.*, 2018, **46**, W363-W367.
- (37) A. Z. Walton, W. C. Conerly, Y. Pompeu, B. Sullivan and J. D. Stewart, *ACS Catal.*, 2011, **1**, 989-993.

(38) A. Z. Walton, B. Sullivan, A. C. Patterson-Orazem and J. D. Stewart, *ACS Catal.*, 2014, **4**, 2307-2318.

(39) T. Hadi, A. Díaz-Rodríguez, D. Khan, J. P. Morrison, J. M. Kaplan, K. T. Gallagher, M. Schober, M. R. Webb, K. K. Brown, D. Fuerst, R. Snajdrova and G.-D. Roiban, *Org. Process Res. Dev.*, 2018, **22**, 871-879.

Manuscript.pdf (1.84 MiB)

[view on ChemRxiv](#) • [download file](#)

Engineering of *Saccharomyces pastorianus* Old Yellow Enzyme 1 for the Synthesis of Pharmacologically Active (*S*)-Profen Derivatives

Guigao Liu,^{1,‡} Shang Li,^{1,‡} Qinghua Shi,² Hengyu Li,² Jiyang Guo,² Jingping Ouyang,³ Xian Jia,³ Lihan Zhang,^{*,4} Song You,^{*,2} and Bin Qin^{*,1}

¹Wuya College of Innovation, Shenyang Pharmaceutical University, 103 Wenhua Road, Shenhe, Shenyang 110016, People's Republic of China

²School of Life Sciences and Biopharmaceutical Sciences, Shenyang Pharmaceutical University, 103 Wenhua Road, Shenhe, Shenyang 110016, People's Republic of China

³School of Pharmaceutical Engineering, Shenyang Pharmaceutical University, 103 Wenhua Road, Shenhe, Shenyang 110016, People's Republic of China

⁴School of Science, Westlake University, 18 Shilongshan Road, Xihu, Hangzhou 310024, People's Republic of China

‡ G.L. and S.L. contributed equally.

*Corresponding author: to-qinbin@163.com (B.Q.); yousong206@aliyun.com (S.Y.); zhanglihan@westlake.edu.cn (L.Z.).

Table of Contents

Supplementary Materials and Methods	S2-S8
Tables S1-S2	S9-S12
Figures S1-S81	S13-S93

Supplementary Materials and Methods

Chemicals and equipment

The substrates for EREDs and related racemic products were synthesized by following the reported procedures.¹ The other chemicals were purchased from Aladdin-reagent (Shanghai, China), J&K (Beijing, China), CASmart (Beijing, China), and Integle (Shanghai, China). The molecular biological reagents were purchased from TaKaRa (Dalian, China), Sangon (Shanghai, China), and Tiangen (Beijing, China). Primers were ordered from Genewiz (Suzhou, China).

The HPLC-grade hexane and 2-propanol were purchased from Dikma (Beijing, China). Chiral HPLC analysis was performed on a JASCO LC-1500 system using chiral columns (Daicel Chiral Technologies Co., LTD, Shanghai, China) with a JASCO UV-2075 detector and a JASCO CD-2095 detector. T100 Thermal Cycler (Bio-Rad) was used for polymerase chain reaction (PCR). Protein concentrations and kinetic parameters of EREDs were determined using a BioTek Epoch microplate spectrophotometer. NMR spectra were recorded using a Bruker AVANCE-400 in CDCl₃ with TMS as an internal standard.

Cloning, expression, purification and site-directed mutagenesis of EREDs

The codon-optimized genes of OYE1, YqjM, and OYE2.6 were ordered from Genewiz (Suzhou, China). The hypothetical protein KNAG_0D03170 (NCBI Accession: XP_022464309) [*Kazachstania naganishii* CBS 8797] was truncated (N14-N413) as KnOYE1X. The KnOYE1X S75G/S198G variant (for binding of FMN) was renamed as KnOYE1 in this research. The codon-optimized gene of KnOYE1 was also ordered from Genewiz (Suzhou, China). The ERED genes were inserted into pET28b_NhisMBP-V vector and then transformed into *E. coli* Rosetta2 (DE3) for expression as described previously.² The mutations at the corresponding sites of EREDs were created by the overlap extension PCR method.³ The gene fragments with mutations were inserted into pET28b_NhisMBP-V and then transformed into *E. coli* Rosetta2 (DE3) cells for the expression the ERED variants. The primers used for cloning and mutagenesis are shown in Table S1. The expression and purification of EREDs were performed following the standard procedures as described previously.²

Asymmetric reduction of substrates 1a-1p

The asymmetric reduction of substrates **1a-1p** was carried out using a NAD(P)H recycling system as described previously.² Substrates **1a-1b**, and **1d-1p** (3 mM final) in 50 μ L ethanol or DMSO were

respectively added to a mixture of cell lysate of *E. coli* Rosetta2 (DE3) harboring an ERED (0.2 g wet cells), GDH (0.1 g wet cells), glucose (8.0 mg, 44 mM), and NADP⁺ (0.3 mg, 0.4 mM) in 950 μ L PBS buffer (100 mM, pH 7.0). The mixture was incubated at 30 °C and 200 rpm for 24 h, and then extracted twice with ethyl acetate. The combined organic layers were concentrated *in vacuo*. The enantiomeric excess (*ee*) values of the products were determined by chiral HPLC analyses (See **Table S2** for detail). Each of the analytical reactions was performed at least three times to ensure the accuracy and repeatability of the data.

For reactions with purified enzymes, substrate **1c** (3 mM final) in 50 μ L DMSO was added to a mixture of a purified ERED (10 μ M), and NADPH (6.0 mg, 8 mM) in 950 μ L PBS buffer (100 mM, pH 7.0). The mixture was incubated and analyzed as that of the crude EREDs. Each of the analytical reactions was performed at least three times to ensure the accuracy and repeatability of the data.

For preparative-synthesis of (*S*)-**2b**, (*S*)-**2d**, (*S*)-**2i**, (*S*)-**2j**, and (*S*)-**2l**, the substrate (2 mM final, 17.6 mg for **1b**, 13.9 mg for **1d**, 15.4 mg for **1i**, 15.4 mg for **1j**, and 19.2mg for **1l**) in 2.0 mL DMSO was added to a mixture of cell lysate of *E. coli* Rosetta2 (DE3) harboring an ERED (8.0 g wet cells) and GDH (4.0 g wet cells), glucose (320.0 mg, 44 mM), and NADP⁺ (12.4 mg, 0.4 mM) in 38.0 mL PBS buffer (100 mM, pH 7.0). The mixture was incubated at 30 °C and 200 rpm for 24 h, and then extracted with ethyl acetate. The combined organic layers were concentrated *in vacuo*. The obtained products were purified by flash chromatography (silica gel, PE-EA), affording (*S*)-**2b** (4.8 mg, 0.021 mmol, 27% isolated yield), (*S*)-**2d** (3.2 mg, 0.018 mmol, 23%), (*S*)-**2i** (4.8 mg, 0.025 mmol, 31%), (*S*)-**2j** (2.6 mg, 0.013 mmol, 16%), and (*S*)-**2l** (5.9 mg, 0.024 mmol, 30%), respectively.

For preparative-synthesis of (*S*)-**2a**, the substrate **1a** (4.7 mM final, 30.4 mg, 0.19 mmol) in 2.0 mL ethanol was added to a mixture of cell lysate of *E. coli* Rosetta2 (DE3) harboring OYE1 W116A/T37A (8.0 g wet cells) and GDH (4.0 g wet cells), glucose (320.0 mg, 44 mM), and NADP⁺ (12.4 mg, 0.4 mM) in 38.0 mL PBS buffer (100 mM, pH 7.0). The mixture was incubated at 30 °C and 200 rpm for 24 h, and then extracted with ethyl acetate. The combined organic layers were concentrated *in vacuo*. The obtained products were purified by flash chromatography (silica gel, PE-EA), affording (*S*)-**2a** (20.2 mg, 0.12 mmol, 66% isolated yield, 98% *ee*).

For preparative-synthesis of (*S*)-**2k**, the substrate **1k** (4.6 mM final, 240.0 mg, 1.0 mmol) in 12.0 mL DMSO was added to a mixture of cell lysate of *E. coli* Rosetta2 (DE3) harboring OYE1 W116A/T37A (48.0 g wet cells) and GDH (24.0 g wet cells), glucose (1.9 g, 44 mM), and NADP⁺ (71.3 mg, 0.4 mM)

in 228.0 mL PBS buffer (100 mM, pH 7.0). The mixture was incubated at 30 °C and 200 rpm for 24 h, and then extracted with ethyl acetate. The combined organic layers were concentrated *in vacuo*. The obtained products were purified by flash chromatography (silica gel, PE-EA), affording (*S*)-**2k** (165 mg, 0.68 mmol, 68% isolated yield, 99% *ee*).

The ¹H and ¹³C NMR spectra of synthesized substrates for EREDs and related racemic products are shown in **Figures S26-S67**. Chemical shifts of each compound shown below were determined by referencing to the solvent peak.

1a: ¹H NMR (400 MHz, CDCl₃) δ 7.46 – 7.30 (m, 5H), 6.37 (d, *J* = 1.2 Hz, 1H), 5.89 (d, *J* = 1.2 Hz, 1H), 3.82 (s, 3H). ¹³C NMR (101 MHz, CDCl₃) δ 167.40, 141.46, 136.85, 128.42, 128.31, 128.25, 126.99, 52.31.

1b: ¹H NMR (400 MHz, CDCl₃) δ 7.36 – 7.29 (m, 2H), 7.13 (d, *J* = 8.1 Hz, 2H), 6.31 (d, *J* = 1.3 Hz, 1H), 5.88 (d, *J* = 1.3 Hz, 1H), 3.82 (s, 3H), 2.48 (d, *J* = 7.2 Hz, 2H), 1.87 (dp, *J* = 13.5, 6.8 Hz, 1H), 0.91 (d, *J* = 6.6 Hz, 6H). ¹³C NMR (101 MHz, CDCl₃) δ 167.65, 142.02, 141.33, 134.15, 129.02, 128.10, 126.16, 52.28, 45.29, 30.29, 22.54.

1c: ¹H NMR (400 MHz, CDCl₃) δ 7.85 – 7.80 (m, 1H), 7.77 – 7.66 (m, 2H), 7.49 (dd, *J* = 8.5, 1.8 Hz, 1H), 7.19 – 7.08 (m, 2H), 6.39 (d, *J* = 1.2 Hz, 1H), 5.98 (d, *J* = 1.3 Hz, 1H), 3.92 (s, 3H), 3.85 (s, 3H). ¹³C NMR (101 MHz, CDCl₃) δ 167.68, 158.22, 141.41, 134.41, 132.04, 129.94, 128.68, 127.42, 126.72, 126.61, 126.52, 119.22, 105.72, 55.46, 52.36.

1d: ¹H NMR (400 MHz, CDCl₃) δ 8.05 (dd, *J* = 7.6, 1.0 Hz, 1H), 7.51 – 7.44 (m, 2H), 7.36 (td, *J* = 7.5, 1.1 Hz, 1H), 7.29 – 7.23 (m, 1H), 3.91 (s, 3H), 3.53 (d, *J* = 2.0 Hz, 2H). ¹³C NMR (101 MHz, CDCl₃) δ 164.67, 144.61, 143.48, 140.83, 136.27, 126.79, 125.70, 123.90, 122.56, 51.69, 38.57.

1e: ¹H NMR (400 MHz, CDCl₃) δ 7.45 – 7.39 (m, 2H), 7.39 – 7.30 (m, 3H), 6.35 (d, *J* = 1.3 Hz, 1H), 5.89 (d, *J* = 1.3 Hz, 1H), 4.29 (q, *J* = 7.1 Hz, 2H), 1.33 (t, *J* = 7.1 Hz, 3H). ¹³C NMR (101 MHz, CDCl₃) δ 166.95, 141.74, 136.93, 128.42, 128.25, 128.21, 126.57, 61.23, 14.35.

1f: ¹H NMR (400 MHz, CDCl₃) δ 7.47 – 7.29 (m, 5H), 6.35 (d, *J* = 1.3 Hz, 1H), 5.89 (d, *J* = 1.3 Hz, 1H), 4.19 (t, *J* = 6.7 Hz, 2H), 1.72 (h, *J* = 7.2 Hz, 2H), 0.97 (t, *J* = 7.4 Hz, 3H). ¹³C NMR (101 MHz, CDCl₃) δ 167.03, 141.78, 136.96, 128.44, 128.24, 128.21, 126.59, 66.85, 22.15, 10.64.

1i: ¹H NMR (400 MHz, CDCl₃) δ 7.31 – 7.21 (m, 1H), 7.02 – 6.94 (m, 2H), 6.89 (ddd, *J* = 8.3, 2.6, 1.0 Hz, 1H), 6.36 (d, *J* = 1.2 Hz, 1H), 5.89 (d, *J* = 1.3 Hz, 1H), 3.82 (d, *J* = 0.9 Hz, 6H). ¹³C NMR (101 MHz,

CDCl₃) δ 167.33, 159.44, 141.33, 138.19, 129.26, 127.12, 120.91, 114.23, 113.86, 55.41, 52.34.

1j: ¹H NMR (400 MHz, CDCl₃) δ 7.39 – 7.33 (m, 2H), 6.92 – 6.85 (m, 2H), 6.27 (d, *J* = 1.2 Hz, 1H), 5.83 (d, *J* = 1.2 Hz, 1H), 3.82 (s, 6H). ¹³C NMR (101 MHz, CDCl₃) δ 167.70, 159.78, 140.80, 129.63, 129.29, 125.50, 113.70, 55.43, 52.29.

1k: ¹H NMR (400 MHz, CDCl₃) δ 7.57 (t, *J* = 1.9 Hz, 1H), 7.47 (ddd, *J* = 7.9, 2.0, 1.1 Hz, 1H), 7.34 (dt, *J* = 7.9, 1.3 Hz, 1H), 7.28 – 7.20 (m, 1H), 6.41 (d, *J* = 1.0 Hz, 1H), 5.91 (d, *J* = 1.0 Hz, 1H), 3.83 (s, 3H). ¹³C NMR (101 MHz, CDCl₃) δ 166.74, 140.14, 138.83, 131.45, 131.32, 129.74, 128.12, 127.16, 122.27, 52.46.

1l: ¹H NMR (400 MHz, CDCl₃) δ 7.51 – 7.44 (m, 2H), 7.32 – 7.26 (m, 2H), 6.39 (d, *J* = 1.1 Hz, 1H), 5.90 (d, *J* = 1.1 Hz, 1H), 3.82 (s, 3H). ¹³C NMR (101 MHz, CDCl₃) δ 166.87, 140.36, 135.72, 131.40, 130.11, 127.53, 122.58, 52.42.

1m: ¹H NMR (400 MHz, CDCl₃) δ 7.34 – 7.28 (m, 2H), 7.17 (d, *J* = 7.9 Hz, 2H), 6.31 (d, *J* = 1.2 Hz, 1H), 5.86 (d, *J* = 1.3 Hz, 1H), 3.82 (s, 3H), 2.36 (s, 3H). ¹³C NMR (101 MHz, CDCl₃) δ 167.59, 141.32, 138.21, 133.97, 128.96, 128.28, 126.24, 52.28, 21.31.

1o: ¹H NMR (400 MHz, CDCl₃) δ 7.93 – 7.88 (m, 1H), 7.87 – 7.78 (m, 3H), 7.50 (ddd, *J* = 15.6, 7.4, 2.6 Hz, 3H), 6.44 (d, *J* = 1.2 Hz, 1H), 6.01 (d, *J* = 1.2 Hz, 1H), 3.85 (s, 3H). ¹³C NMR (101 MHz, CDCl₃) δ 167.49, 141.45, 134.27, 133.22, 133.15, 128.41, 127.75, 127.71, 127.62, 127.27, 126.47, 126.36, 126.24, 52.38.

2a: ¹H NMR (400 MHz, CDCl₃) δ 7.37 – 7.20 (m, 5H), 3.73 (q, *J* = 7.2 Hz, 1H), 3.66 (s, 3H), 1.50 (d, *J* = 7.2 Hz, 3H). ¹³C NMR (101 MHz, CDCl₃) δ 175.15, 140.71, 128.78, 127.61, 127.28, 52.16, 45.57, 18.74.

2b: ¹H NMR (400 MHz, CDCl₃) δ 7.22 – 7.16 (m, 2H), 7.11 – 7.05 (m, 2H), 3.70 (q, *J* = 7.2 Hz, 1H), 3.66 (s, 3H), 2.44 (d, *J* = 7.2 Hz, 2H), 1.83 (dh, *J* = 13.5, 6.7 Hz, 1H), 1.49 (d, *J* = 7.2 Hz, 3H), 0.90 (d, *J* = 6.6 Hz, 6H). ¹³C NMR (101 MHz, CDCl₃) δ 175.36, 140.70, 137.91, 129.50, 127.27, 52.11, 45.19, 30.31, 22.54, 18.76.

2c: ¹H NMR (400 MHz, CDCl₃) δ 7.73 – 7.64 (m, 3H), 7.40 (dd, *J* = 8.5, 1.8 Hz, 1H), 7.16 – 7.08 (m, 2H), 3.91 (s, 3H), 3.86 (q, *J* = 7.1 Hz, 1H), 3.66 (s, 3H), 1.57 (d, *J* = 7.2 Hz, 3H). ¹³C NMR (101 MHz, CDCl₃) δ 175.28, 157.80, 135.83, 133.85, 129.42, 129.08, 127.32, 126.33, 126.08, 119.14, 105.76, 55.45, 52.17, 45.50, 18.73.

2d: ¹H NMR (400 MHz, CDCl₃) δ 7.40 – 7.35 (m, 1H), 7.24 – 7.12 (m, 3H), 4.06 (dd, *J* = 8.2, 6.6 Hz,

1H), 3.73 (s, 3H), 3.10 (ddd, $J = 15.1, 8.7, 5.8$ Hz, 1H), 2.92 (ddd, $J = 15.7, 8.6, 6.5$ Hz, 1H), 2.54 – 2.25 (m, 2H). ^{13}C NMR (101 MHz, CDCl_3) δ 174.52, 144.25, 140.83, 127.68, 126.57, 124.94, 124.82, 52.13, 50.25, 31.90, 28.90.

2e: ^1H NMR (400 MHz, CDCl_3) δ 7.35 – 7.21 (m, 5H), 4.12 (qq, $J = 10.9, 7.1$ Hz, 2H), 3.70 (q, $J = 7.2$ Hz, 1H), 1.50 (d, $J = 7.2$ Hz, 3H), 1.20 (t, $J = 7.1$ Hz, 3H). ^{13}C NMR (101 MHz, CDCl_3) δ 174.68, 140.86, 128.71, 127.61, 127.18, 60.84, 45.71, 18.74, 14.25.

2f: ^1H NMR (400 MHz, CDCl_3) δ 7.39 – 7.20 (m, 5H), 4.02 (t, $J = 6.7$ Hz, 2H), 3.72 (q, $J = 7.2$ Hz, 1H), 1.65 – 1.53 (m, 2H), 1.50 (d, $J = 7.2$ Hz, 3H), 0.85 (t, $J = 7.4$ Hz, 3H). ^{13}C NMR (101 MHz, CDCl_3) δ 174.76, 140.88, 128.69, 127.63, 127.18, 66.44, 45.76, 22.07, 18.64, 10.40.

2j: ^1H NMR (400 MHz, CDCl_3) δ 7.24 – 7.19 (m, 2H), 6.90 – 6.83 (m, 2H), 3.79 (s, 3H), 3.72 – 3.63 (m, 4H), 1.47 (d, $J = 7.2$ Hz, 3H). ^{13}C NMR (101 MHz, CDCl_3) δ 175.41, 158.84, 132.81, 128.61, 114.16, 55.40, 52.11, 44.70, 18.80.

2k: ^1H NMR (400 MHz, CDCl_3) δ 7.45 (t, $J = 1.8$ Hz, 1H), 7.39 (dt, $J = 7.5, 1.8$ Hz, 1H), 7.25 – 7.16 (m, 2H), 3.75 – 3.61 (m, 4H), 1.49 (d, $J = 7.2$ Hz, 3H). ^{13}C NMR (101 MHz, CDCl_3) δ 174.47, 142.82, 130.80, 130.45, 130.31, 126.34, 122.78, 52.32, 45.23, 18.60.

2m: ^1H NMR (400 MHz, CDCl_3) δ 7.19 (d, $J = 8.1$ Hz, 2H), 7.13 (d, $J = 8.0$ Hz, 2H), 3.65 (m, 4H), 2.33 (s, 3H), 1.48 (d, $J = 7.2$ Hz, 3H). ^{13}C NMR (101 MHz, CDCl_3) δ 175.30, 137.74, 136.91, 129.47, 127.46, 52.12, 45.15, 21.17, 18.77.

The ^1H and ^{13}C NMR spectra for each product obtained by OYE1 variants-catalyzed reactions are shown in **Figures S68-S81**.

(S)-2a: ^1H NMR (400 MHz, CDCl_3) δ 7.37 – 7.22 (m, 5H), 3.73 (q, $J = 7.2$ Hz, 1H), 3.66 (s, 3H), 1.51 (d, $J = 7.2$ Hz, 3H). ^{13}C NMR (101 MHz, CDCl_3) δ 175.14, 140.72, 128.78, 127.61, 127.28, 52.14, 45.58, 18.74.

(S)-2b: ^1H NMR (400 MHz, CDCl_3) δ 7.22 – 7.16 (m, 2H), 7.11 – 7.06 (m, 2H), 3.70 (q, $J = 7.2$ Hz, 1H), 3.66 (s, 3H), 2.45 (d, $J = 7.2$ Hz, 2H), 1.85 (dp, $J = 13.5, 6.8$ Hz, 1H), 1.49 (d, $J = 7.2$ Hz, 3H), 0.90 (d, $J = 6.6$ Hz, 6H). ^{13}C NMR (101 MHz, CDCl_3) δ 175.38, 140.70, 137.92, 129.50, 127.28, 52.11, 45.20, 30.31, 22.54, 18.76.

(S)-2d: ^1H NMR (400 MHz, CDCl_3) δ 7.39 – 7.35 (m, 1H), 7.26 – 7.15 (m, 3H), 4.07 (dd, $J = 8.4, 6.4$ Hz, 1H), 3.74 (s, 3H), 3.11 (ddd, $J = 15.1, 8.6, 5.8$ Hz, 1H), 2.97 – 2.87 (m, 1H), 2.50 – 2.27 (m, 2H).

^{13}C NMR (101 MHz, CDCl_3) δ 174.53, 144.26, 140.85, 127.69, 126.58, 124.95, 124.83, 52.14, 50.28, 31.91, 28.92.

(*S*)-**2i**: ^1H NMR (400 MHz, CDCl_3) δ 7.24 (t, $J = 8.0$ Hz, 1H), 6.88 (dt, $J = 7.7, 1.3$ Hz, 1H), 6.85 (t, $J = 2.1$ Hz, 1H), 6.80 (ddd, $J = 8.2, 2.6, 0.9$ Hz, 1H), 3.80 (s, 3H), 3.74 – 3.64 (m, 4H), 1.49 (d, $J = 7.2$ Hz, 3H). ^{13}C NMR (101 MHz, CDCl_3) δ 175.01, 159.95, 142.25, 129.75, 120.00, 113.47, 112.62, 55.36, 52.18, 45.60, 18.70.

(*S*)-**2j**: ^1H NMR (400 MHz, CDCl_3) δ 7.25 – 7.19 (m, 2H), 6.88 – 6.83 (m, 2H), 3.79 (s, 3H), 3.72 – 3.64 (m, 4H), 1.48 (d, $J = 7.1$ Hz, 3H). ^{13}C NMR (101 MHz, CDCl_3) δ 175.43, 158.87, 132.84, 128.62, 114.19, 55.42, 52.11, 44.72, 18.80.

(*S*)-**2k**: ^1H NMR (400 MHz, CDCl_3) δ 7.45 (t, $J = 1.8$ Hz, 1H), 7.39 (ddd, $J = 7.5, 2.0, 1.5$ Hz, 1H), 7.25 – 7.16 (m, 2H), 3.72 – 3.63 (m, 4H), 1.49 (d, $J = 7.2$ Hz, 3H). ^{13}C NMR (101 MHz, CDCl_3) δ 174.49, 142.84, 130.82, 130.47, 130.31, 126.35, 122.79, 52.32, 45.25, 18.60.

(*S*)-**2l**: ^1H NMR (400 MHz, CDCl_3) δ 7.47 – 7.41 (m, 2H), 7.21 – 7.13 (m, 2H), 3.73 – 3.63 (m, 4H), 1.48 (d, $J = 7.2$ Hz, 3H). ^{13}C NMR (101 MHz, CDCl_3) δ 174.64, 139.65, 131.89, 129.41, 121.26, 52.28, 45.05, 18.60.

Kinetics assay

Kinetic analyses of OYE1 WT and variants were performed using a microplate spectrophotometer (Epoch, BioTek) to measure the consumption of NADPH [Abs (340 nm), $\epsilon_{340\text{nm}} = 6.2 \text{ mM}^{-1}\text{cm}^{-1}$] including an oxygen consuming system.⁴ The assays were carried out in 200 μL PBS buffer (100 mM, pH 7.0) containing FMN (12.5 μM), NADPH (1.5 mM), glucose oxidase (*ca.* 10 U), glucose (50 mM), at 30 $^\circ\text{C}$ using 5.6 μM to 7.4 μM of the OYEs at substrate concentrations ranging from 0.15 mM to 6.6 mM. All assays were repeated in triplicate. The kinetic parameters were fitted by using Graphpad Prism 6. The protein concentrations of OYEs were measured by the BCA assay using a Micro BCA Protein Assay Kit (Sangon, Shanghai, China).

Homology modeling and molecular simulation

The pre-*S* models for substrates **1a-1d** in the OYE1 variants were manually made based on the structure of (4*R*)-carvone in the OYE1 W116A variant (PDB: 4K7V).⁵ Related structures of substrates were constructed on the structure of (4*R*)-carvone by the “Builder” in PyMOL.⁶ The residue substitutions of

corresponding variants were also constructed in PyMOL.⁶ The constructed models were optimized by molecular dynamic (MD) simulation. Desmond/Maestro (Non-Commercial Distribution, Version 2019.2)⁷ was employed for MD simulation. After protein preparation, each enzyme-substrate system was immersed in an orthorhombic box of SPC waters, while the distances for the orthorhombic box were set to 7.0 Å (a, b, and c) and the ionic strength of the NaCl was set to 0.15 M. In the MD simulations, the enzyme-substrate system was described by the OPLS_2005 force field. An NVT ensemble, a temperature of 300 K, a total simulation time of 50 ns and the trajectory recording interval of 50 ps was used in all MD simulations. During the MD run of 50 ns, the atoms of constructed systems were set as restraints (force constant = 70), except for the residues at positions 37, 39, 74, 82, 85, 116, 118, 196, 250, 296, 375, FMN and the substrates.

The modeled structure of KnOYE1-FMN complex was constructed based on the homology modeling method. The OYE3 in complex with FMN and *p*-hydroxybenzaldehyde (PDB: 5V4P)⁸ was selected as the template for its maximum sequence positives. The model of KnOYE1 was created using SWISS-MODEL server.⁹

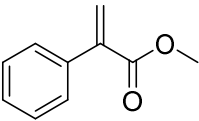
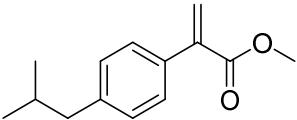
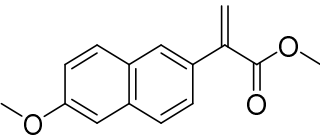
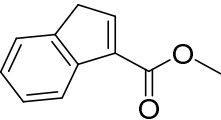
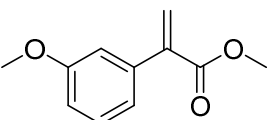
Table S1. Primers used in this study.

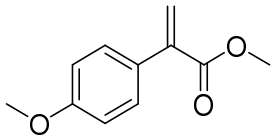
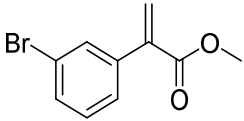
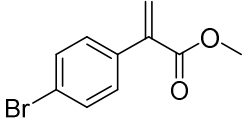
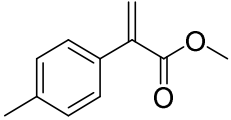
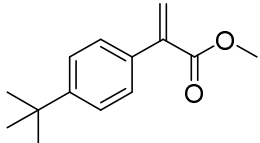
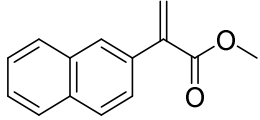
Primer	Sequences (5' to 3')
YqjM-EcoRI-F	CGGAATTCGATGGCCAGAAAATTATTTACACCT
YqjM-XhoI-R	CCGCTCGAGCCAGCCTCTTTTCGTATTGAAC
OYE1-EcoRI-F	CCGGAATTCGATGTCTTTTCGTTAAAGACTTCAA
OYE1-XhoI-R	CCGCTCGAGTTTTTTGTCCCAACCCAGT
OYE1-W116G-F	G TTCAGCTG GGC GTTCTGGGT
OYE1-W116G-R	ACCCAGAAC GCC CAGCTGAAC
OYE1-W116A-F	G TTCAGCTG GCT GTTCTGGGT
OYE1-W116A-R	ACCCAGAAC AGC CAGCTGAAC
OYE1-W116V-F	G TTCAGCTG GTT GTTCTGGGT
OYE1-W116V-R	ACCCAGAAC AAC CAGCTGAAC
OYE1-W116S-F	G TTCAGCTG AGC GTTCTGGGT
OYE1-W116S-R	ACCCAGAAC GCT CAGCTGAAC
OYE1-T37G-F	CCGCCGCTG GGC CGTATGCGT
OYE1-T37G-R	ACGCATACG GCC CAGCGGCGG
OYE1-T37A-F	CCGCCGCTG GCG CGTATGCGT
OYE1-T37A-R	ACGCATACG CGC CAGCGGCGG
OYE1-T37V-F	CCGCCGCTG GTG CGTATGCGT
OYE1-T37V-R	ACGCATACG CAC CAGCGGCGG
OYE1-T37S-F	CCGCCGCTG AGC CGTATGCGT
OYE1-T37S-R	ACGCATACG GCT CAGCGGCGG
OYE1-F74G-F	GAAGGTGCT GGC ATCTCTCCG
OYE1-F74G-R	CGGAGAGAT GCC AGCACCTTC
OYE1-F74A-F	GAAGGTGCT GCG ATCTCTCCG
OYE1-F74A-R	CGGAGAGAT CGC AGCACCTTC
OYE1-F74V-F	GAAGGTGCT GTG ATCTCTCCG
OYE1-F74V-R	CGGAGAGAT CAC AGCACCTTC
OYE1-F74S-F	GAAGGTGCT AGC ATCTCTCCG
OYE1-F74S-R	CGGAGAGAT GCT AGCACCTTC
OYE1-W116A/L118A-F ^a	CTG GCT GTT GCG GGT TGGGCT
OYE1-W116A/L118A-R ^a	AGCCCAACC CGC AAC AGC CAG
OYE1-W116G/L118A-F ^b	G TTCAGCTG GGC GTT GCG GGT
OYE1-W116G/L118A-R ^b	ACC CGC AAC GCC CAGCTGAAC
OYE2.6-EcoRI-F	CCGGAATTCGATGTCTTCTGTTAAAATCTC
OYE2.6-XhoI-R	CCGCTCGAGCAGAGCTTCGATAGCA
OYE2.6-I113A-F	ACCCAGCTG GCG TTCTGGGT
OYE2.6-I113A-R	ACCCAGGAA CGC CAGCTGGGT
OYE2.6-T35A-F	CCGCCGACC GCT CGTTTCCGT
OYE2.6-T35A-R	ACGGAAACG AGC GGTCCGCGG
OYE2.6-N293F-F	GTTTCTGGT TTT GTTGACGTT
OYE2.6-N293F-R	AACGTCAAC AAA ACCAGAAAC

KnOYE1-EcoRI-F	<u>CCGGAATTC</u> GATGTCTACCGGTTTCC
KnOYE1-XhoI-R	CCG <u>CTCGAGG</u> ATTTTCCAACCCAGTT
KnOYE1-R119A-F	GTTCAGCTG <u>GCT</u> AACCTGGGT
KnOYE1-R119A-R	ACCCAGGTT <u>AGC</u> CAGCTGAAC
KnOYE1-T40A-F	GCTCCGCTG <u>GCT</u> CGTTGGCGT
KnOYE1-T40A-R	ACGCCAACG <u>AGC</u> CAGCGGAGC
KnOYE1-S299F-F	GCTAACATC <u>TTT</u> CTGGAAGAA
KnOYE1-S299F-R	TTCTTCCAG <u>AA</u> GATGTTAGC
KnOYE1-W42A-F	CTGACCCGT <u>GCG</u> CGTGCTCTG
KnOYE1-W42A-R	CAGAGCACG <u>GCG</u> ACGGGTCAG

^aUsing OYE1 W116A as the template for overlap PCR; ^bUsing OYE1 W116A/L118A as the template for overlap PCR. The recognition sequences of restriction enzymes were underlined and mutation sites were shown in red.

Table S2. Chiral HPLC methods and retention times for substrates and chiral products.

Substrate	Structure	Method	Rt _(Sub.) min	Rt _{((S)-Prod.)} min	Rt _{((R)-Prod.)} min	Reference ^a
1a		Chiralcel OJ-H, hexane/2-propanol (90 : 10) flowing at 0.8 mL min ⁻¹ , UV 230 nm	31.4±0.2	11.9±0.1	13.7±0.1	1,10-11
1b		Chiralcel OJ-H, hexane/2-propanol (99.5 : 0.5) flowing at 0.8 mL min ⁻¹ , UV 230 nm	33.9±0.2	11.2±0.1	14.0±0.1	10-11
1c		Chiralcel OD-H, hexane/2-propanol (99 : 1) flowing at 0.8 mL min ⁻¹ , UV 254 nm	20.1±0.1	15.9±0.1	12.5±0.1	1,10
1d		Chiralcel OB-H, hexane/2-propanol (99 : 1) flowing at 0.8 mL min ⁻¹ , UV 230 nm	21.4±0.1	15.5±0.2	12.3±0.2	12
1i		Chiralcel OD-H, hexane/2-propanol (99 : 1) flowing at 0.8 mL min ⁻¹ , UV 230 nm	17.9±0.1	12.6±0.1	11.9±0.1	1,10

1j		Chiralcel OJ-H, hexane/2-propanol (80 : 20) flowing at 0.8 mL min ⁻¹ , UV 230nm	44.3±0.2	13.7±0.1	14.9±0.1	1,10
1k		Chiralcel OJ-H, hexane/2-propanol (99 : 1) flowing at 0.8 mL min ⁻¹ , UV 230 nm	27.5±0.2	13.1±0.1	14.1±0.1	11
1l		Chiralcel OJ-H, hexane/2-propanol (90 : 10) flowing at 0.8 mL min ⁻¹ , UV 230 nm	13.0±0.1	9.0±0.1	8.6±0.1	1
1m		Chiralcel OJ-H, hexane/2-propanol (90 : 10) flowing at 0.8 mL min ⁻¹ , UV 230 nm	24.8±0.1	11.5±0.1	10.4±0.1	12
1n		Chiralcel OB-H, hexane/2-propanol (99 : 1) flowing at 0.8 mL min ⁻¹ , UV 230 nm	23.5±0.1	6.3±0.1	7.3±0.1	
1o		Chiralcel OJ-H, hexane/2-propanol (90 : 10) flowing at 0.8 mL min ⁻¹ , UV 254 nm	38.9±0.2	18.4±0.1	19.5±0.1	10

^aThe references used to identify the absolute configurations of the resultant products by comparing their retention times in chiral HPLC.

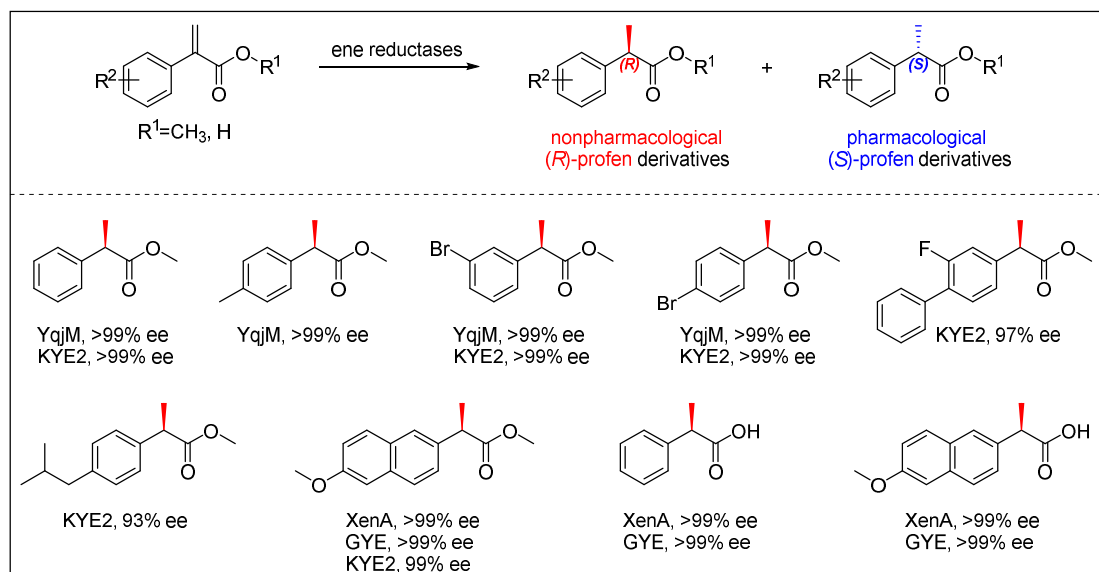


Figure S1. The summary of asymmetric C=C bond bioreduction of 2-arylacrylic acid derivatives (profen precursors) by ene reductases (EREDs). All reported bioreduction of profen precursors by all reported EREDs gave the nonpharmacological (*R*)-enantiomers as the products.^{1,4,13-15}

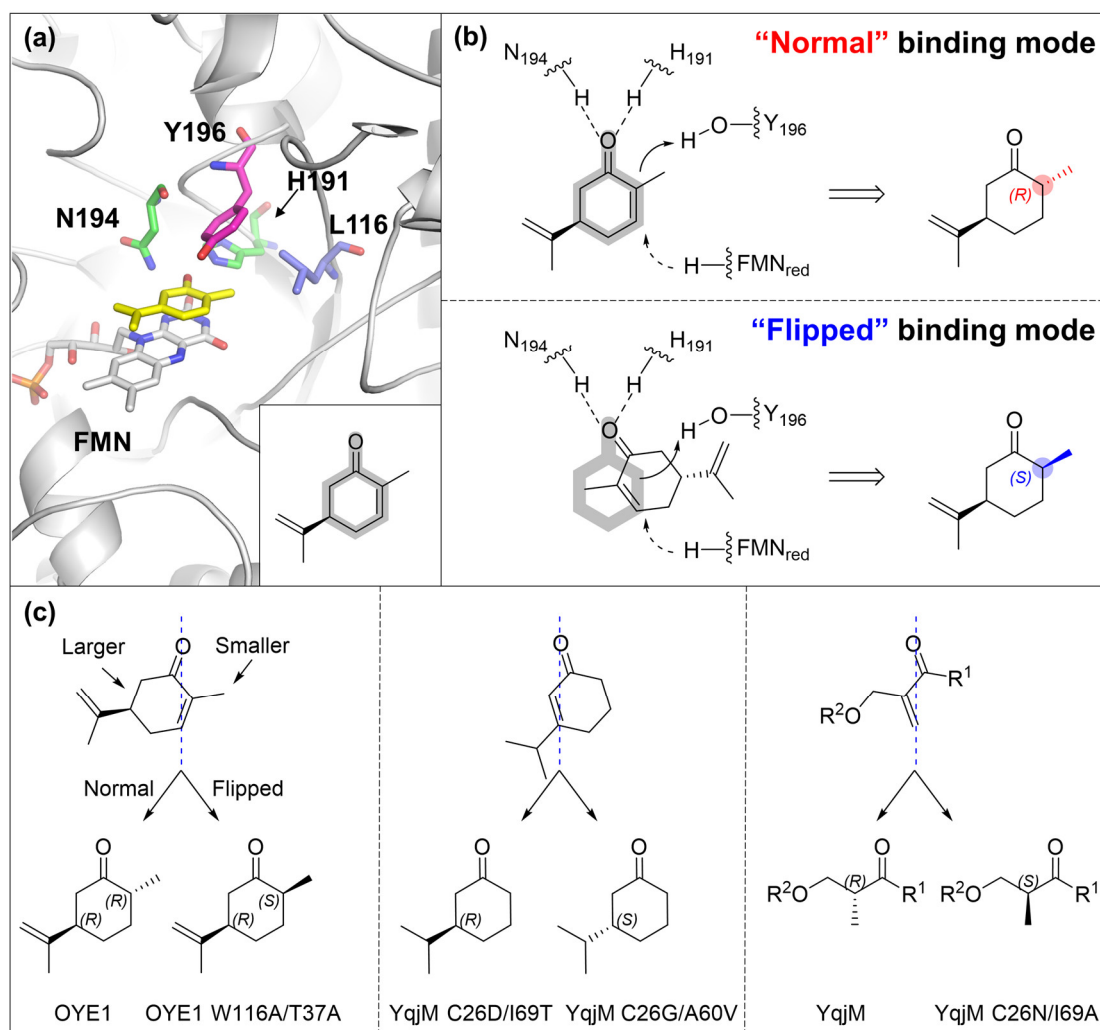


Figure S2. The “Normal” and “flipped” substrate binding modes of EREDs. (a) The typical “normal” binding mode based on the crystal structure of (*R*)-stereopreferred OYE1 W116L variant with (*4R*)-carvone (PDB: 4GWE).^{5,16} (b) Illustration of the “normal” and “flipped” binding mode. The “normal” substrate binding mode would lead to the production of (*1R,4R*)-dihydrocarvone, while the “flipped” substrate binding mode would lead to the production of (*1S,4R*)-dihydrocarvone.¹⁶ (c) Engineering of OYEs to flip the binding mode. Most wildtype OYEs share the “normal” substrate binding mode. Protein engineering of OYEs can potentially flip the substrate binding mode and the cases are rarely reported in contrast to other enzymes (e.g. ketoreductases).^{2,4-5,16-17}

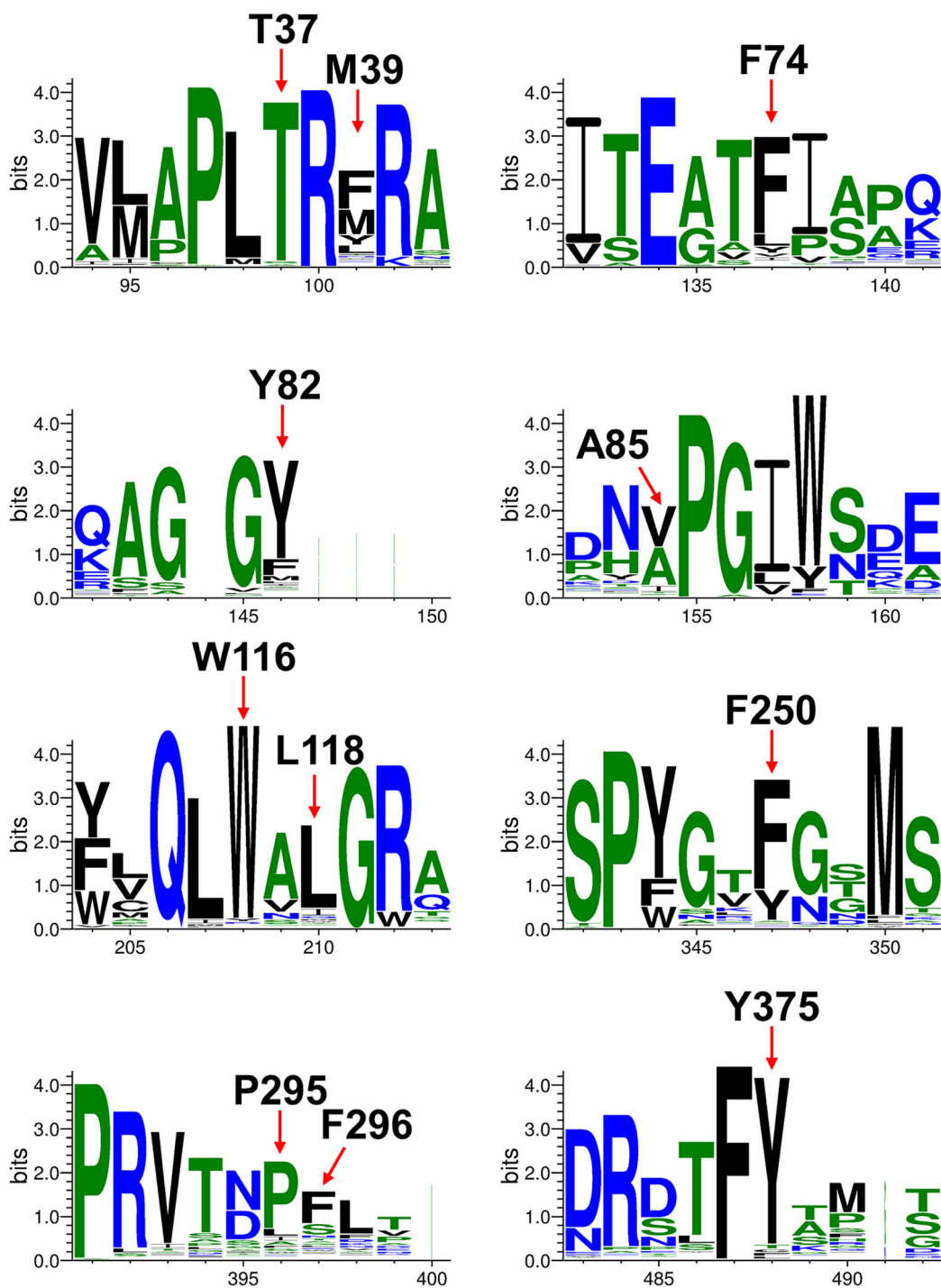


Figure S3. The sequence logo analyses of the key residues surrounding the active site of OYE1 and homologs created by the WebLogo 3.0 tool.¹⁸ The residue numbering follows that of OYE1. The positions of T37, M39, F74, Y82, A85, W116, and L118 were analyzed from 500 homologs of OYE1. The positions of F250, P295, F296, and Y375 were analyzed from 200 homologs of OYE1, since the C-terminal of these enzymes has lower conservation than that of the N-terminal.

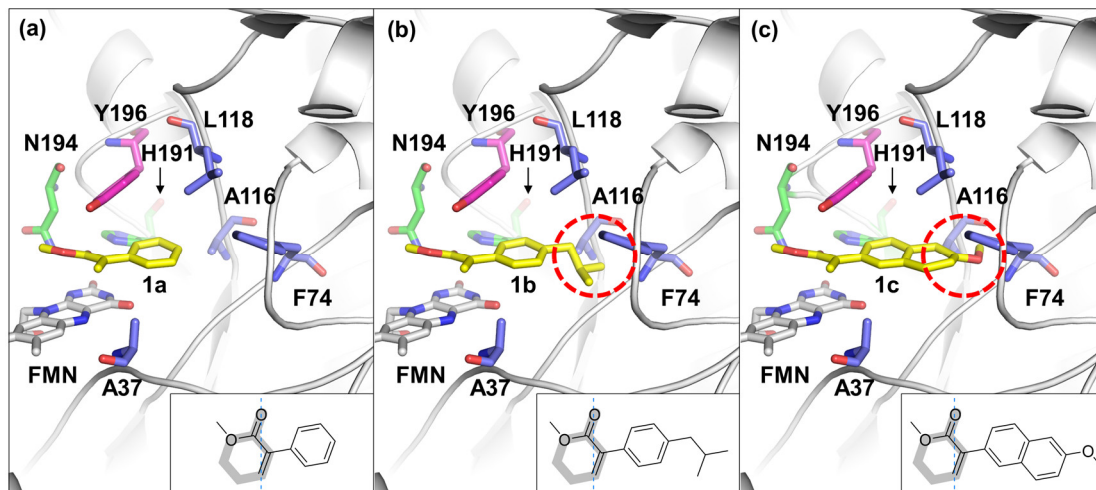


Figure S4. The pro-*S* models of the OYE1 W116A/T37A variant with **1a**, **1b**, and **1c**, respectively. (a) The pro-*S* model of the OYE1 W116A/T37A variant with **1a**. The model was manually constructed by modification the structure of (4*R*)-carvone in the OYE1 W116A variant⁵ and then optimized by molecular dynamic simulation. (b,c) The pro-*S* models of OYE1 the W116A/T37A with **1b** and **1c**, respectively. The models were manually constructed by modification of the structure of **1a** in the model of the W116A/T37A variant with **1a** and not optimized. The bulky residue F74 blocks the location of 4-isobutylphenyl group of **1b** and 6-methoxynaphthyl group of **1c**. The bottom right corner of each panel shows a simplified (flipped) model of substrate recognition, with the 2-cyclohexenone skeleton superimposed in gray as a comparison.

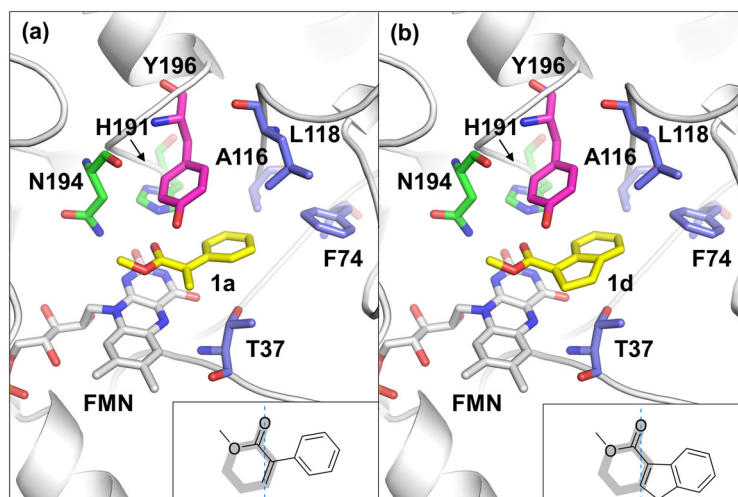


Figure S5. The pro-*S* models of the OYE1 W116A variant with **1a** and **1d**. (a) The pro-*S* model of the OYE1 W116A variant with **1a**. The model was manually constructed by modifying the structure of (4*R*)-carvone in the OYE1 W116A variant⁵ and then optimized by molecular dynamic simulation. (b) The pro-*S* model of OYE1 the W116A variant with **1d**. The model was manually constructed by modification of the structure of **1a** in the model of W116A with **1a** and not optimized. The binding model of **1d** in OYE1 W116A variant was similar as that of **1a**. The bottom right corner of each panel shows a simplified (flipped) model of substrate recognition, with the 2-cyclohexenone skeleton superimposed in gray as a comparison.

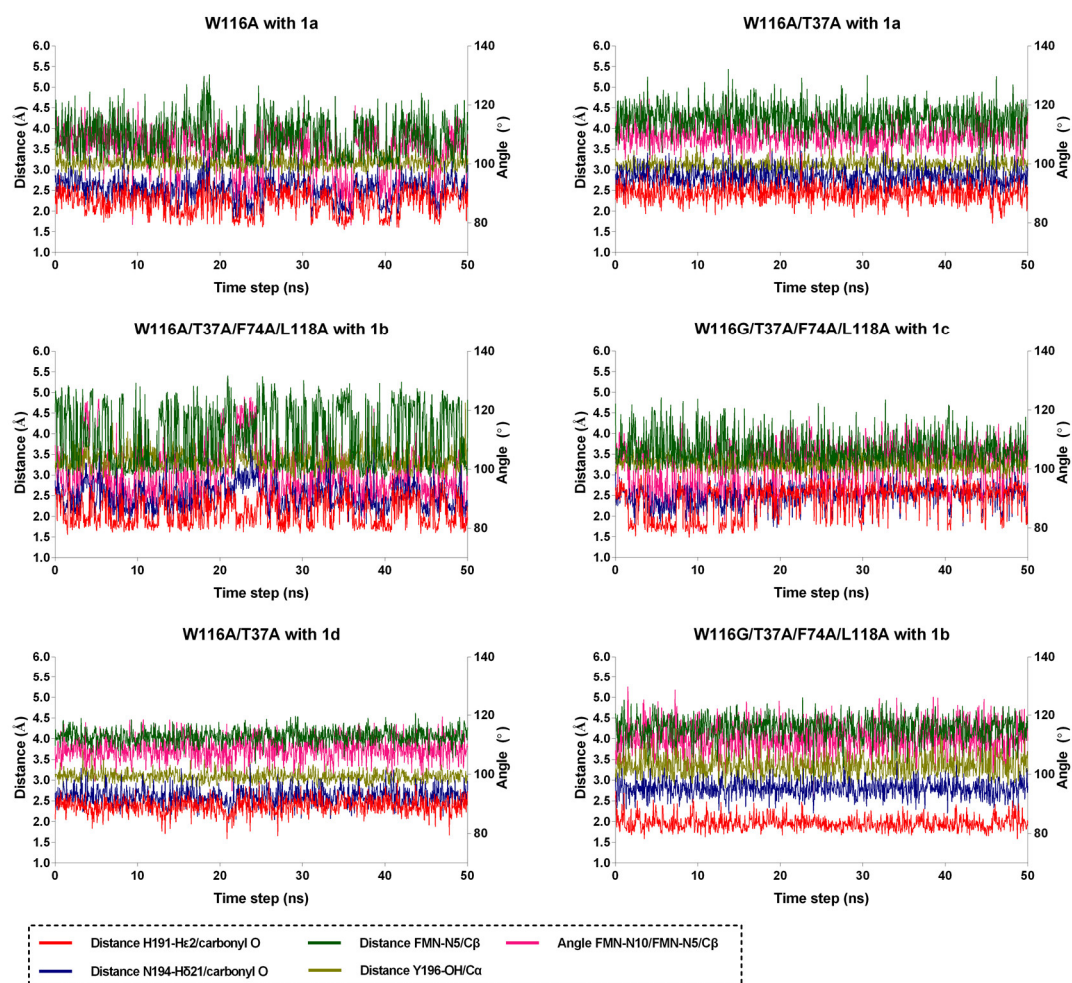
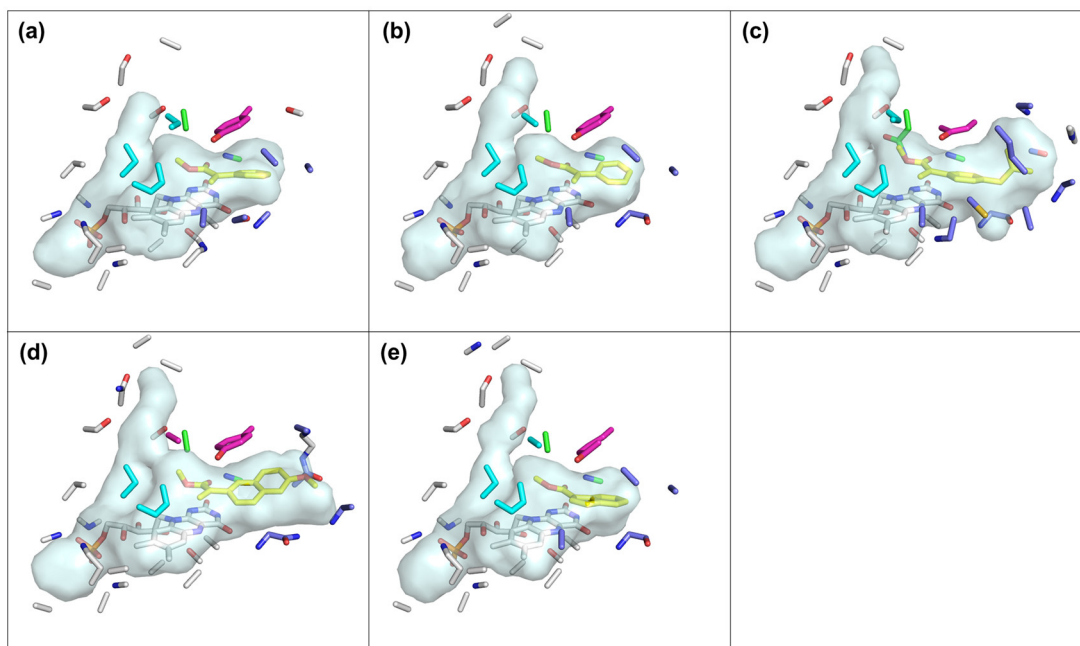


Figure S6. The distances and angles measured over 50 ns MD trajectory. The distances between carbonyl oxygen of the substrates (**1a-1d**) and the side chains of H191/N194, the distances between $C\beta/C\alpha$ of the substrates (**1a-1d**) and FMN-N5/Y196, and the angles between FMN and the substrates (N10-N5- $C\beta$) were measured.



(f)

	Area (Å ²)	Volume (Å ³)
(a) W116A with 1a	429.4	219.6
(b) W116A/T37A with 1a	448.7	231.0
(c) W116A/T37A/F74A/L118A with 1b	540.3	260.3
(d) W116G/T37A/F74A/L118A with 1c	515.1	275.9
(e) W116A/T37A with 1d	438.7	225.8

Figure S7. The substrate binding pockets of related OYE1 variants. (a) The substrate binding pocket of the OYE1 W116A variant with **1a**. (b) The substrate binding pocket of the OYE1 W116A/T37A variant with **1a**. (c) The substrate binding pocket of the OYE1 W116A/T37A/F74A/L118A variant with **1b**. (d) The substrate binding pocket of the OYE1 W116G/T37A/F74A/L118A variant with **1c**. (e) The substrate binding pocket of the OYE1 W116A/T37A variant with **1d**. (f) The calculated area and volume of the substrate binding pockets in related OYE1 variants. The substrate binding pockets were calculated by using CASTp 3.0 analysis¹⁹ and the figures were prepared using PyMOL⁶.

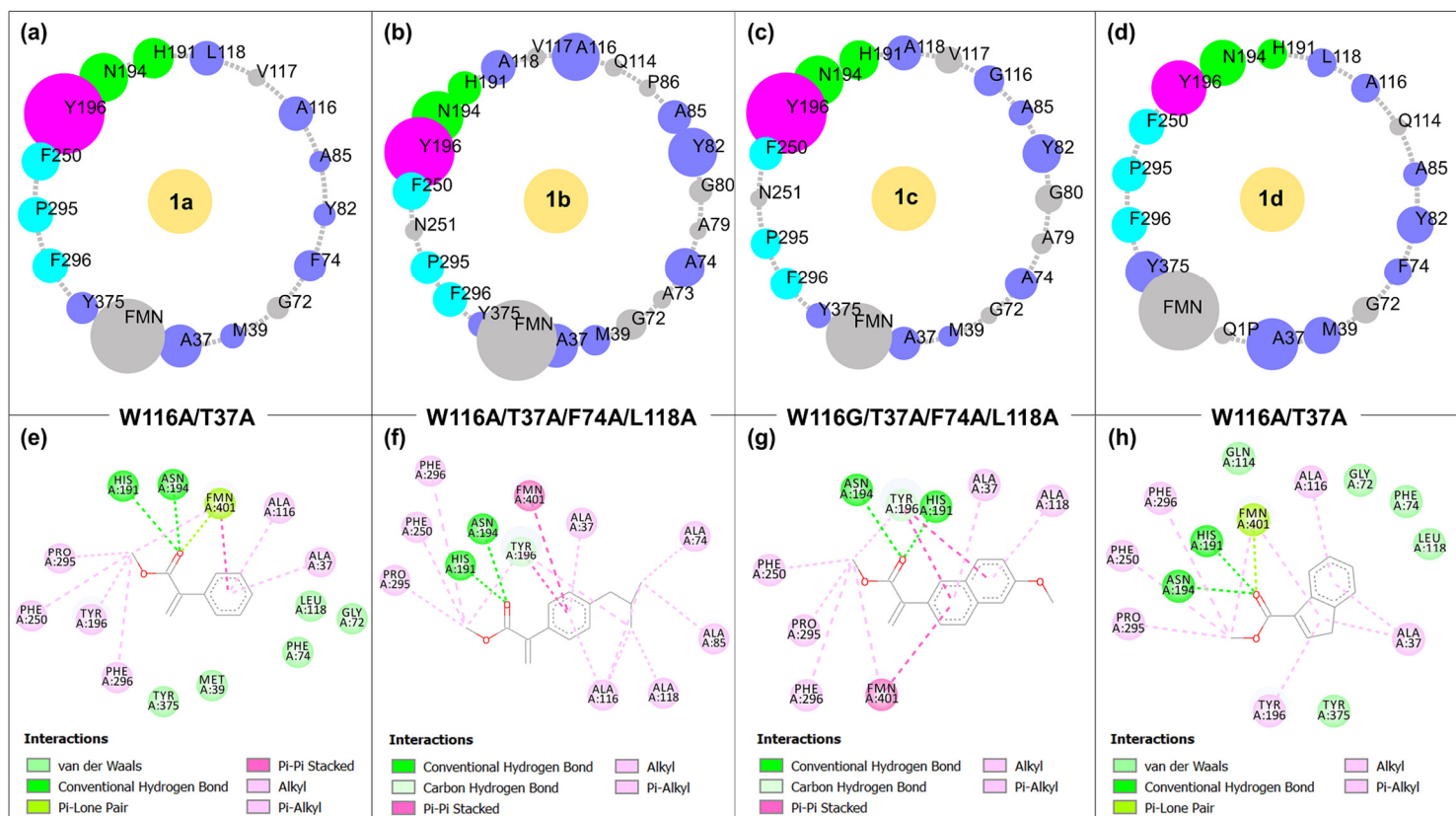


Figure S8. The interactions between OYE1 variants and related substrates. The interactions of the OYE1 W116A/T37A variant with **1a** (a, e), the W116A/T37A/F74A/L118A variant with **1b** (b, f), the W116G/T37A/F74A/L118A variant with **1c** (c, g), and the W116A/T37A variant with **1d** (d, h) were analyzed and visualized by the Protein Contacts Atlas online tool (a-d)²⁰ and Discovery Studio Visualizer (e-h), respectively.

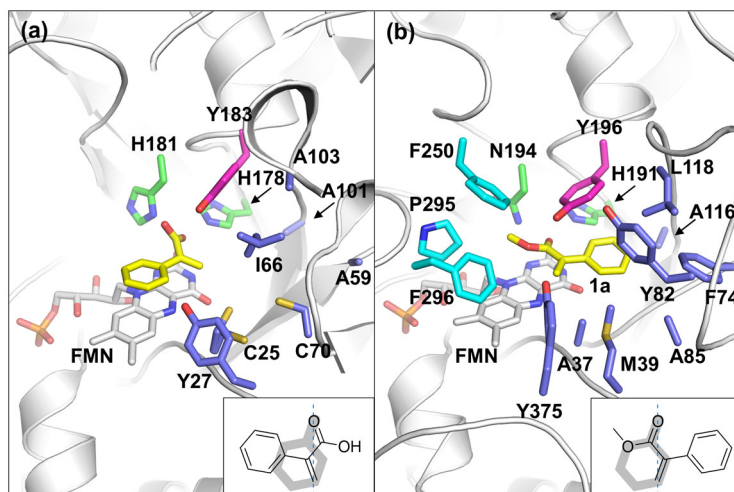


Figure S9. Comparison of the substrate binding pockets of XenA and OYE1. (a) The substrate binding pocket of the (*R*)-stereopreferred XenA with 2-phenylacrylic acid (PDB: 5N6Q).¹⁵ The residues that create the right binding pocket of XenA are shown in blue. The catalytic residues H178 and H181 are shown in green, while Y183 is shown in magenta. The substrate 2-phenylacrylic acid is shown in yellow and FMN in shown in white. (b) The substrate binding pocket of the (*S*)-stereopreferred OYE1 W116A/T37A variant with **1a**. The residues that create the left and right binding pockets of OYE1 are shown in cyan and blue, respectively. The catalytic residues H191 and N194 are shown in green, while Y196 is shown in magenta. The substrate **1a** and FMN are shown in yellow and white, respectively. The residues C25, A59, A101, and A103 of XenA correspond to T37A, F74, W116A, L118 of OYE1 W116A/T37A variant, respectively. The bottom right corner of each panel shows a simplified (flipped) model of substrate recognition, with the 2-cyclohexenone skeleton superimposed in gray as a comparison.

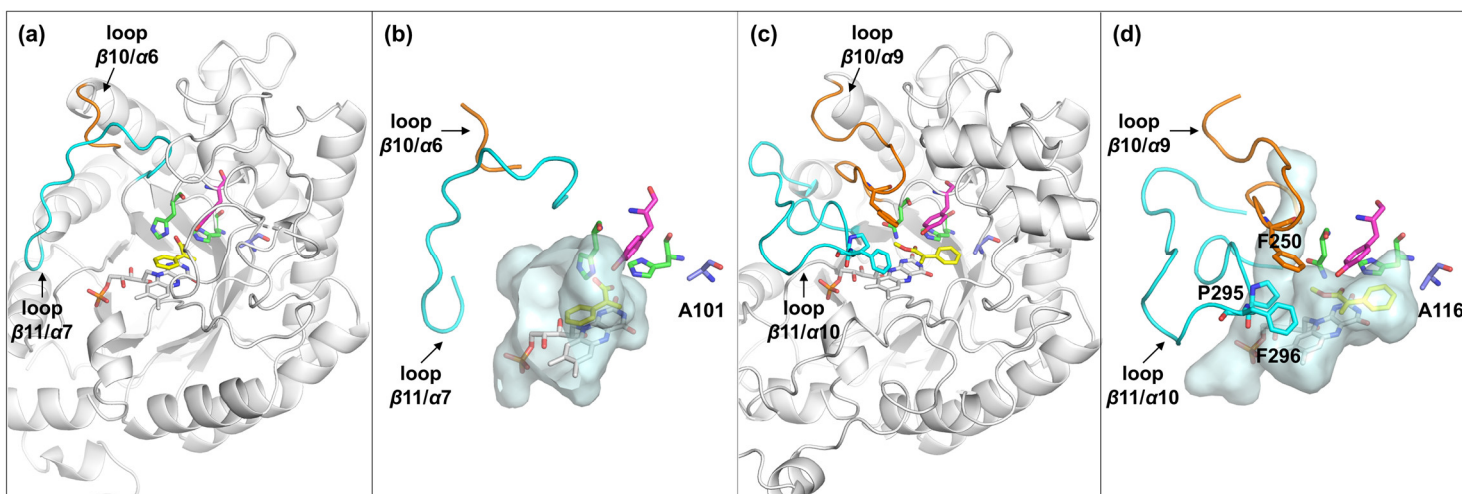


Figure S10. Structural comparison of XenA and OYE1. (a) The (*R*)-stereopreferred XenA with 2-phenylacrylic acid (PDB: 5N6Q).¹⁵ The catalytic residues H178 and H181 are shown in green, while Y183 is shown in magenta. The residue A101 corresponding to W116 of OYE1 is shown in blue. The substrate 2-phenylacrylic acid is shown in yellow and FMN is shown in white. The loops β_{11}/α_7 and β_{10}/α_6 are shown in cyan and orange, respectively. (b) The calculated substrate binding pocket (by CASTp 3.0¹⁹) of XenA with 2-phenylacrylic acid. The loops β_{11}/α_7 and β_{10}/α_6 of XenA were slightly away from the substrate binding pocket, resulting in an open pocket. (c) The (*S*)-stereopreferred OYE1 W116A/T37A with **1a** (optimized model). The catalytic residues H191, N194, and Y196 are shown in green and magenta, respectively. The key residue W116A is shown in blue. The substrate **1a** and FMN are shown in yellow and white, respectively. The loops β_{11}/α_{10} and β_{10}/α_9 are shown in cyan and orange, respectively, while F250, P295, and F296 on the loops are shown as sticks. (d) The calculated substrate binding pocket (by CASTp 3.0) of OYE1 W116A/T37A variant with **1a**. The loops β_{11}/α_{10} and β_{10}/α_9 are closer around the substrate binding pocket.

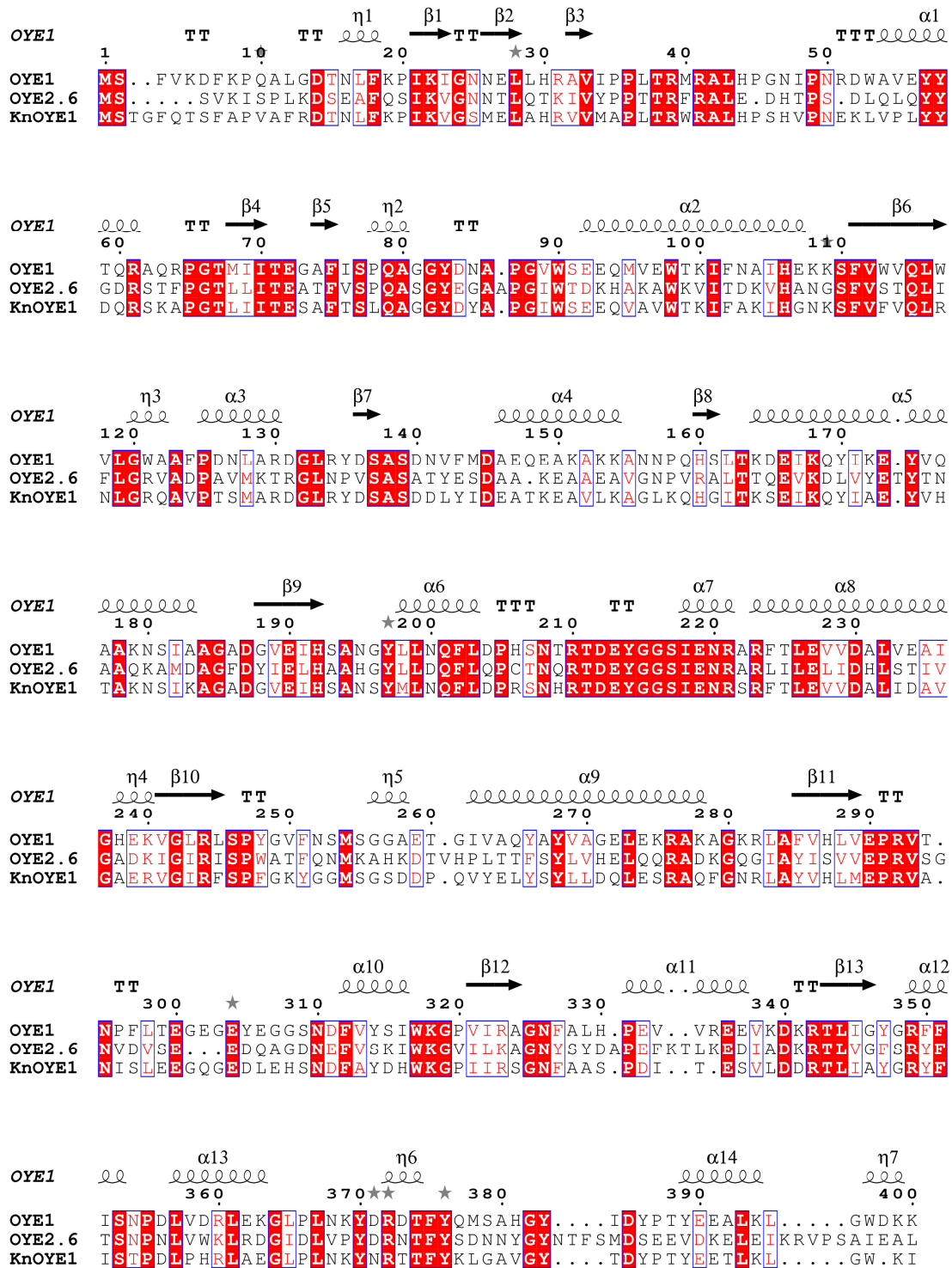


Figure S11. Multiple-sequence alignment of EREDs. The alignment was created by CLC sequence viewer 7 and visualized by ESPript 3.0.²¹ Crystal structure of OYE1 with *p*-hydroxybenzaldehyde (PDB: 1OYB)²² was uploaded to ESPript 3.0 for depiction of the secondary structure of OYE1.

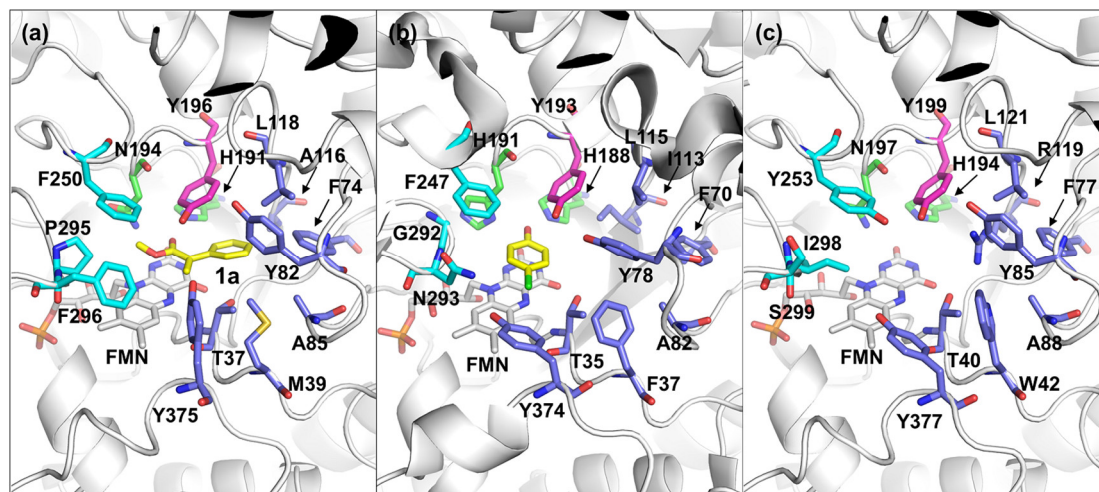


Figure S12. Structural comparison of OYE1, OYE2.6 and KnOYE1. (a) The pro-*S* model of OYE W116A variant with **1a**. (b) The structure of OYE2.6 with *p*-chlorophenol (PDB: 4DF2)²³. (c) The modeled structure of KnOYE1. OYE3 WT (PDB: 5V4P)⁸ was used as the template for homology modeling of KnOYE1 by SWISS-MODEL.⁹ The residues that create the left and right binding pockets of these models are shown in cyan and blue, respectively.

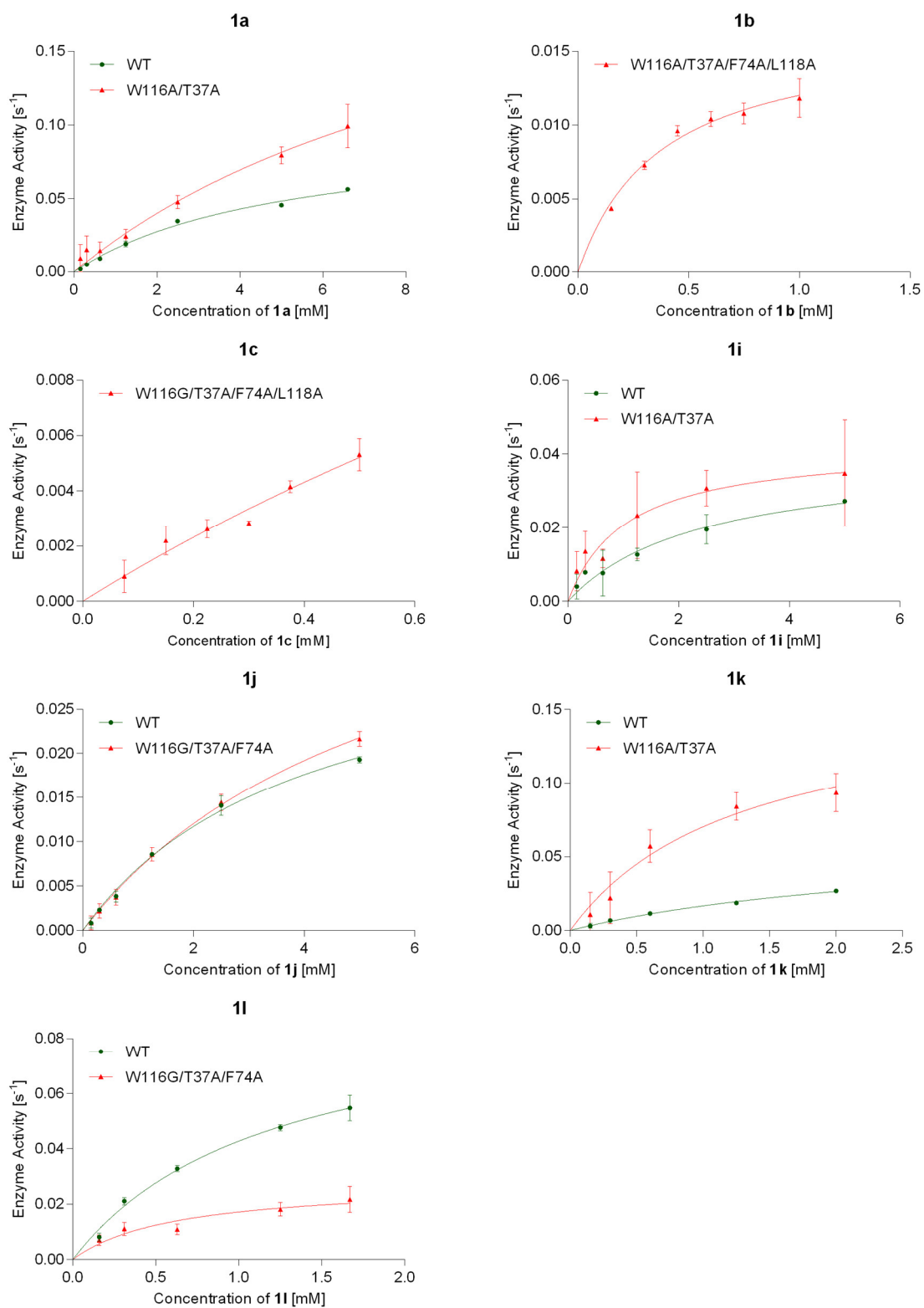


Figure S13. Kinetic analysis of OYE1 WT and variants for 2-arylacrylic acid derivatives. The enzyme activity of each panel was calculated by NADPH consumption monitored at A340 absorbance with three individual assays.

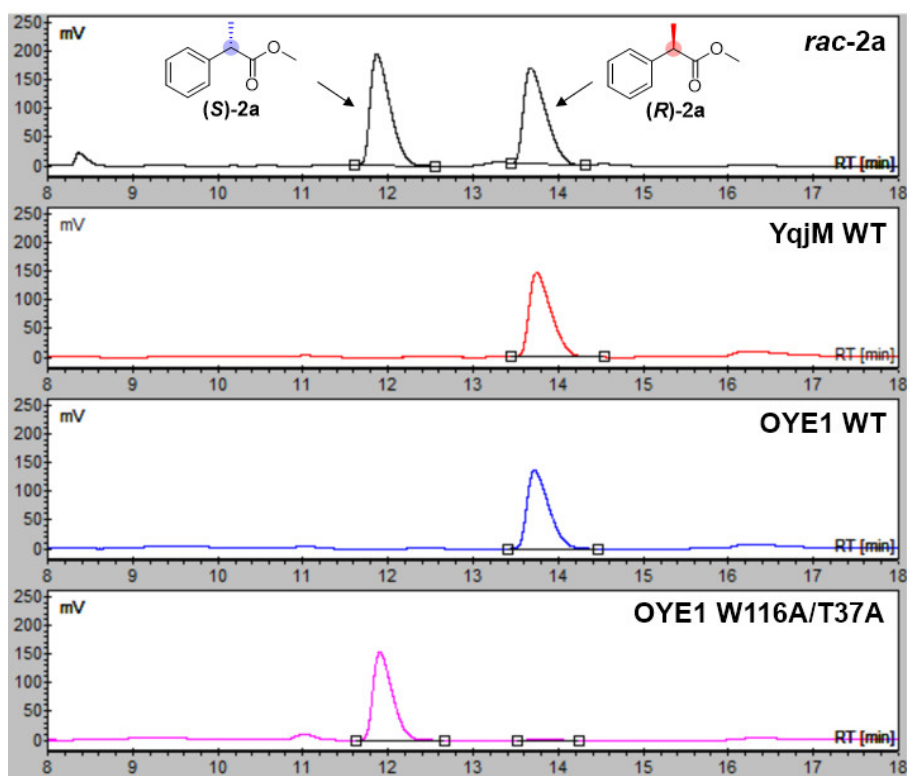


Figure S14. HPLC traces for the product of **2a** by EREDs catalyzed reactions. The racemic mixture of **2a** contains authenticated standards.

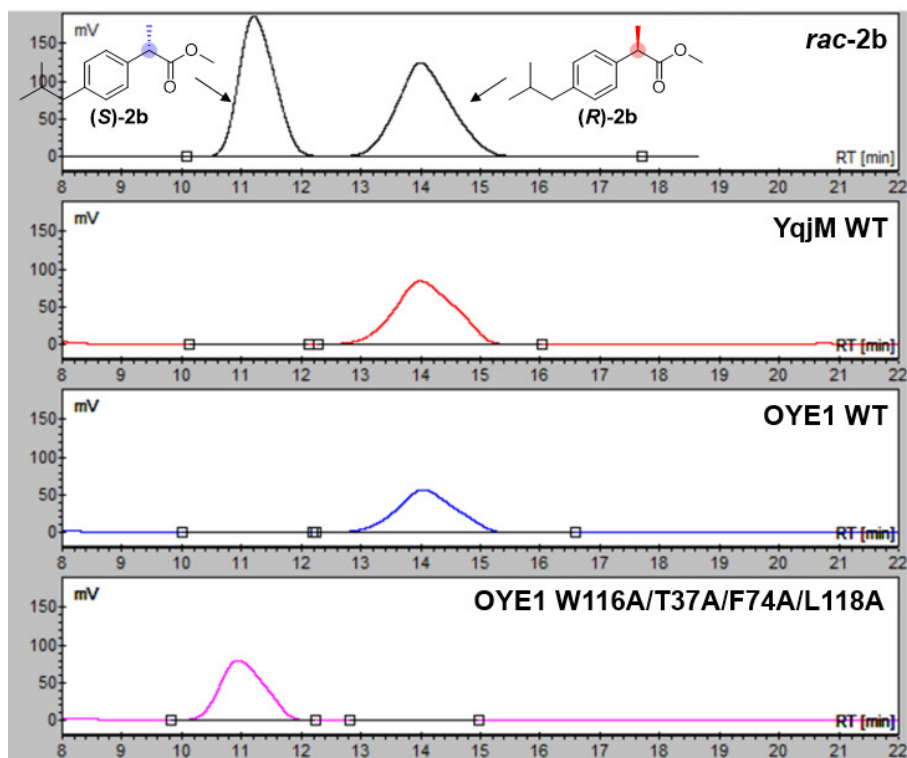


Figure S15. HPLC traces for the product of **2b** by EREDs catalyzed reactions. The racemic mixture of **2b** contains authenticated standards.

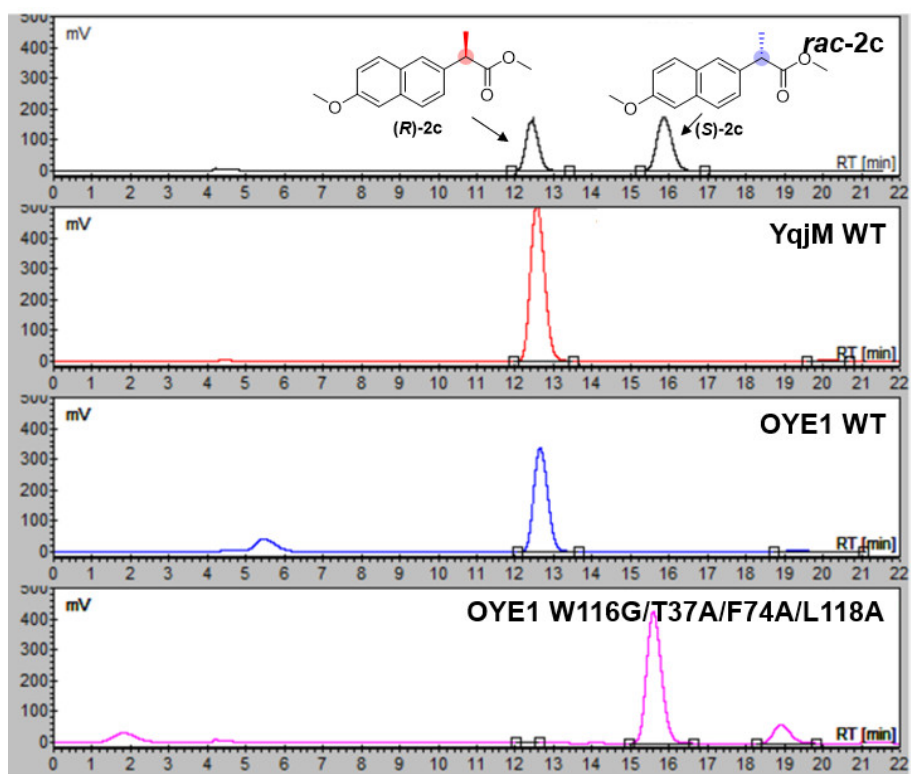


Figure S16. HPLC traces for the product of **2c** by EREDs catalyzed reactions. The racemic mixture of **2c** contains authenticated standards.

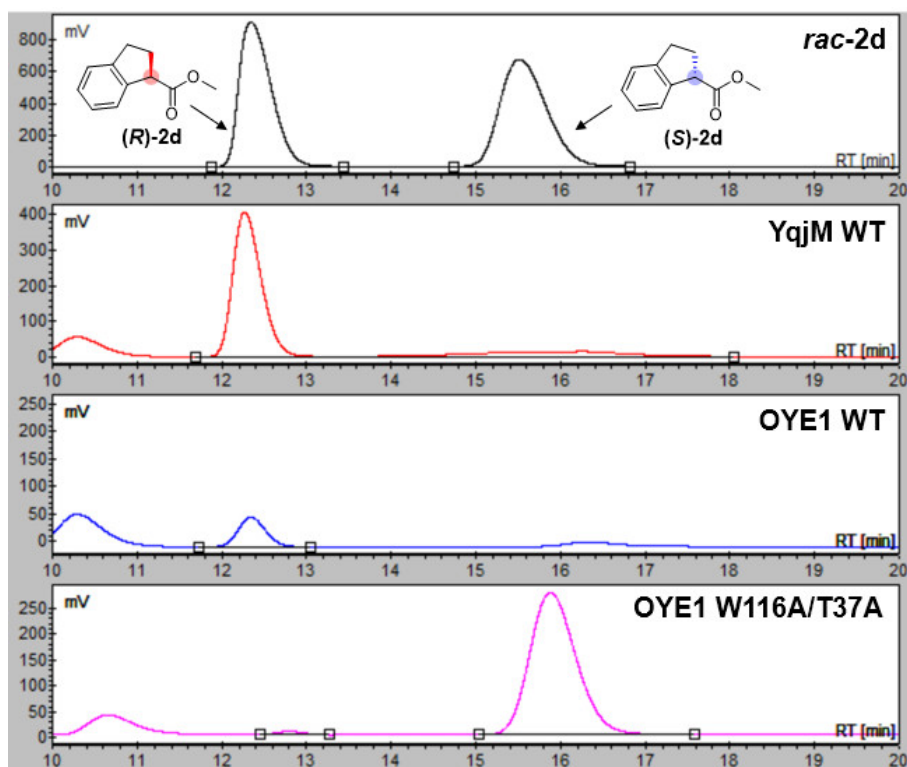


Figure S17. HPLC traces for the product of **2d** by EREDs catalyzed reactions. The racemic mixture of **2d** contains authenticated standards.

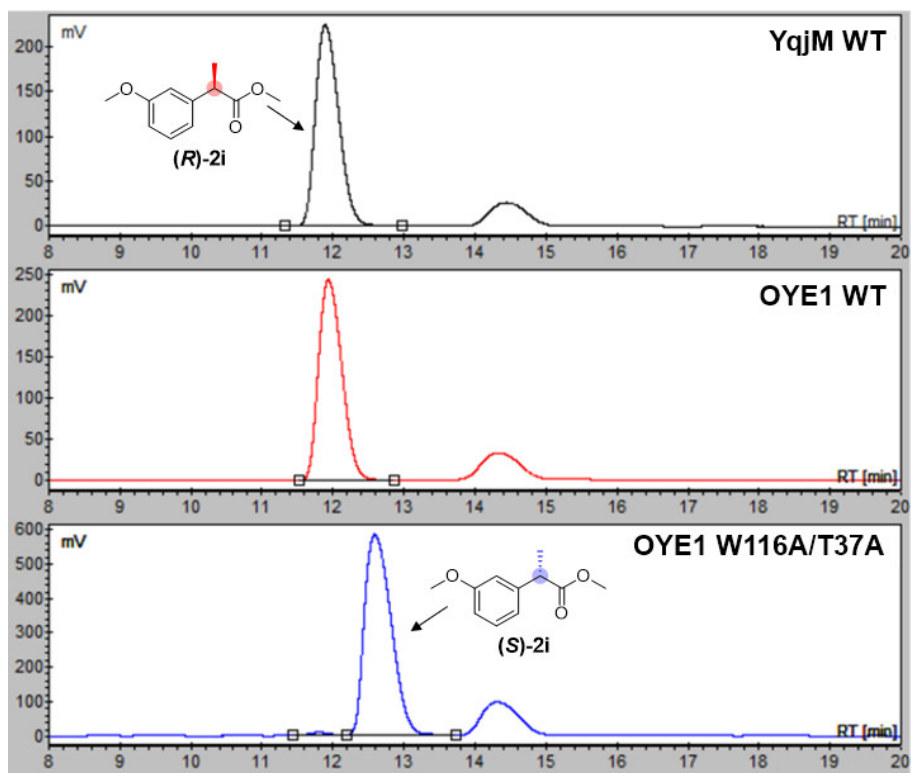


Figure S18. HPLC traces for the product of **2i** by EREDs catalyzed reactions.

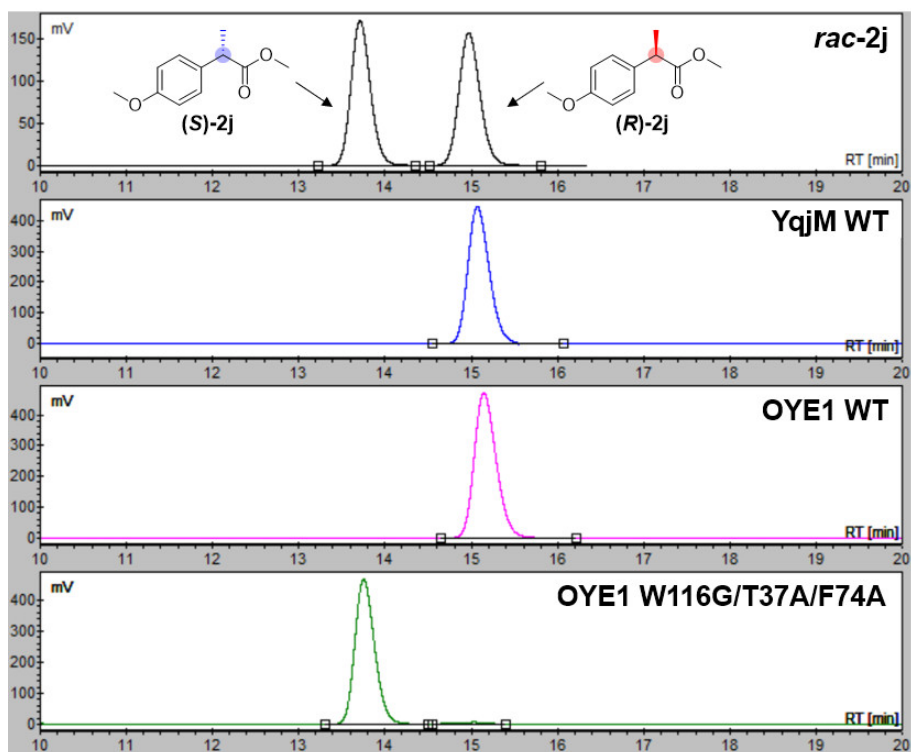


Figure S19. HPLC traces for the product of **2j** by EREDs catalyzed reactions.

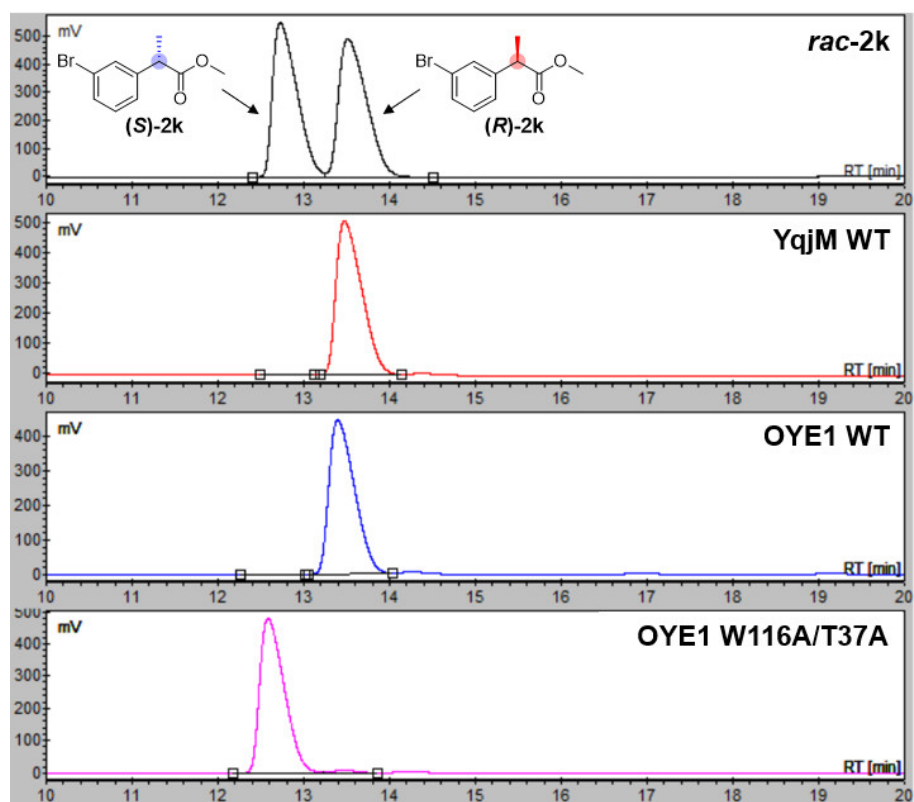


Figure S20. HPLC traces for the product of **2k** by EREDs catalyzed reactions. The racemic mixture of **2k** contains authenticated standards.

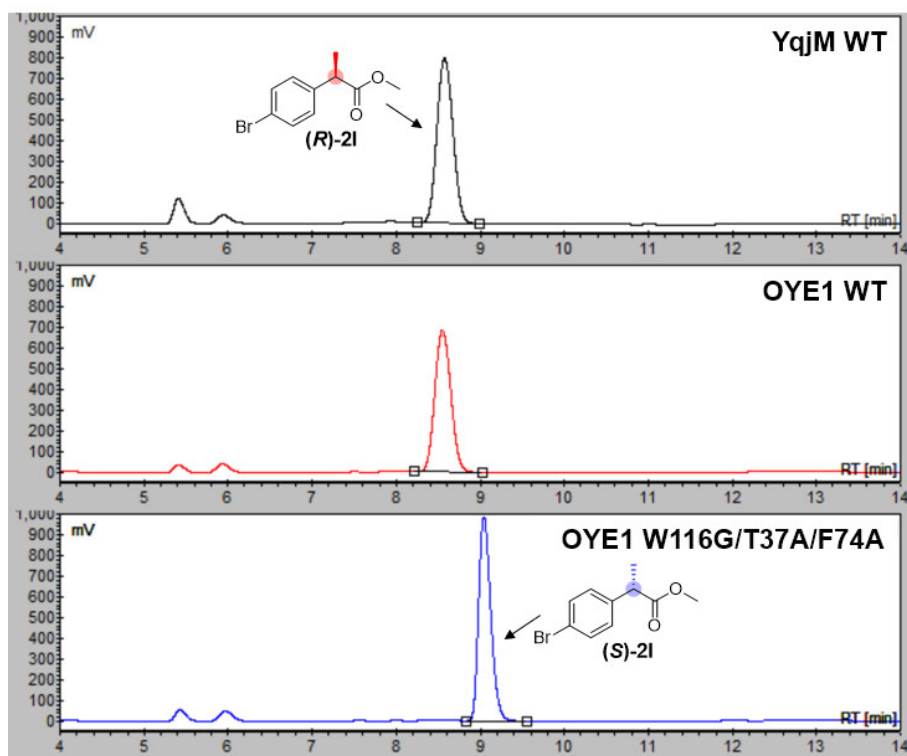


Figure S21. HPLC traces for the product of **21** by EREDs catalyzed reactions.

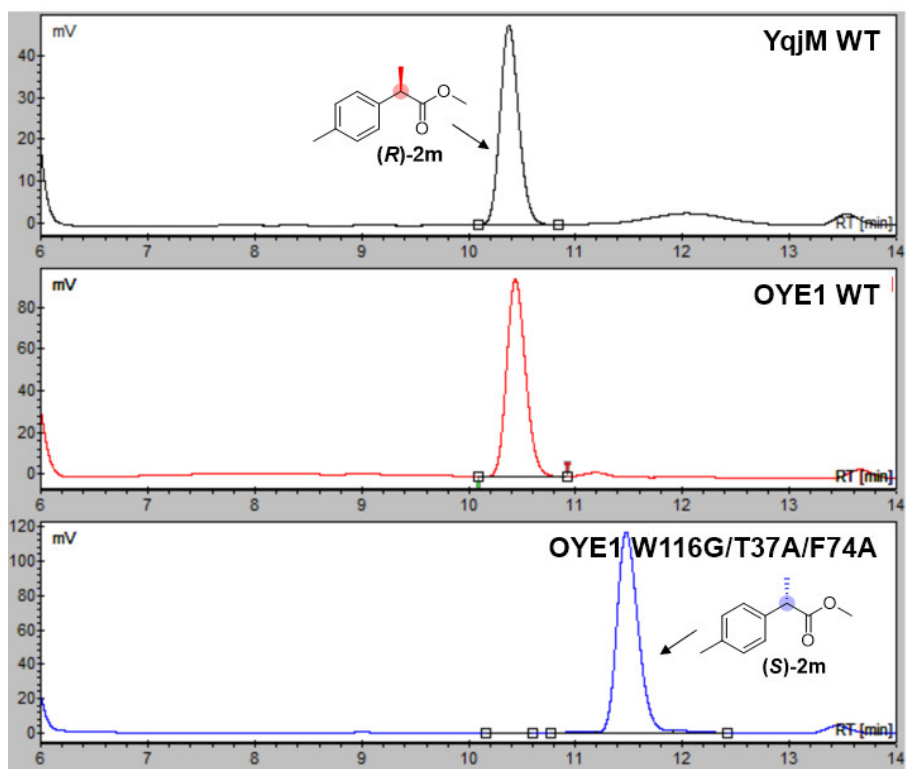


Figure S22. HPLC traces for the product of **2m** by EREDs catalyzed reactions.

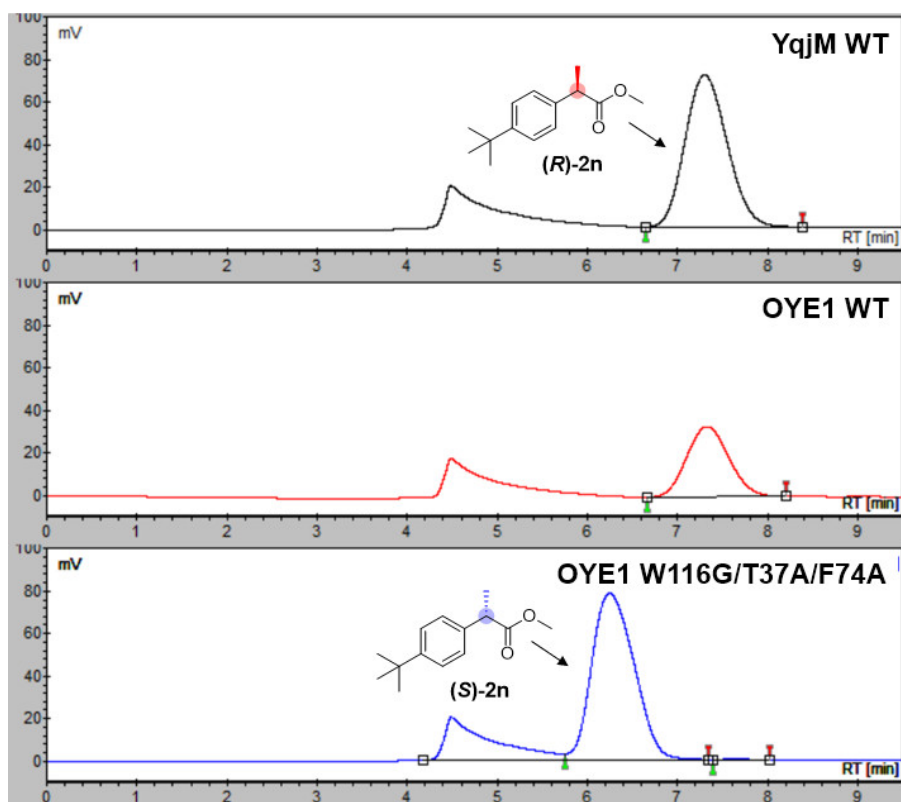


Figure S23. HPLC traces for the product of **2n** by EREDs catalyzed reactions.

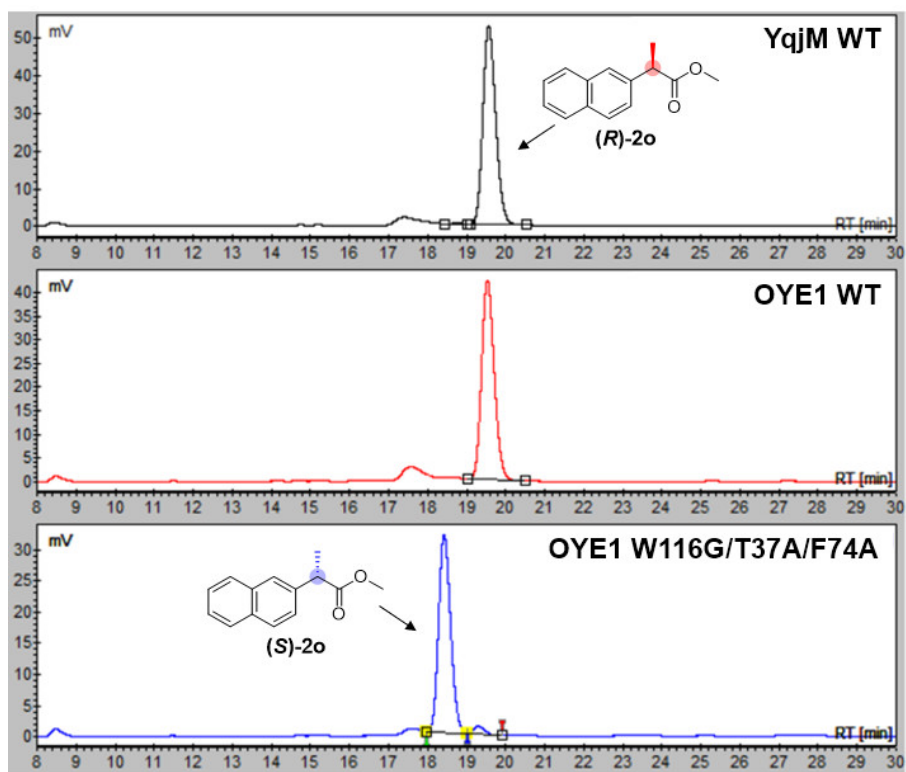


Figure S24. HPLC traces for the product of **2o** by EREDs catalyzed reactions.

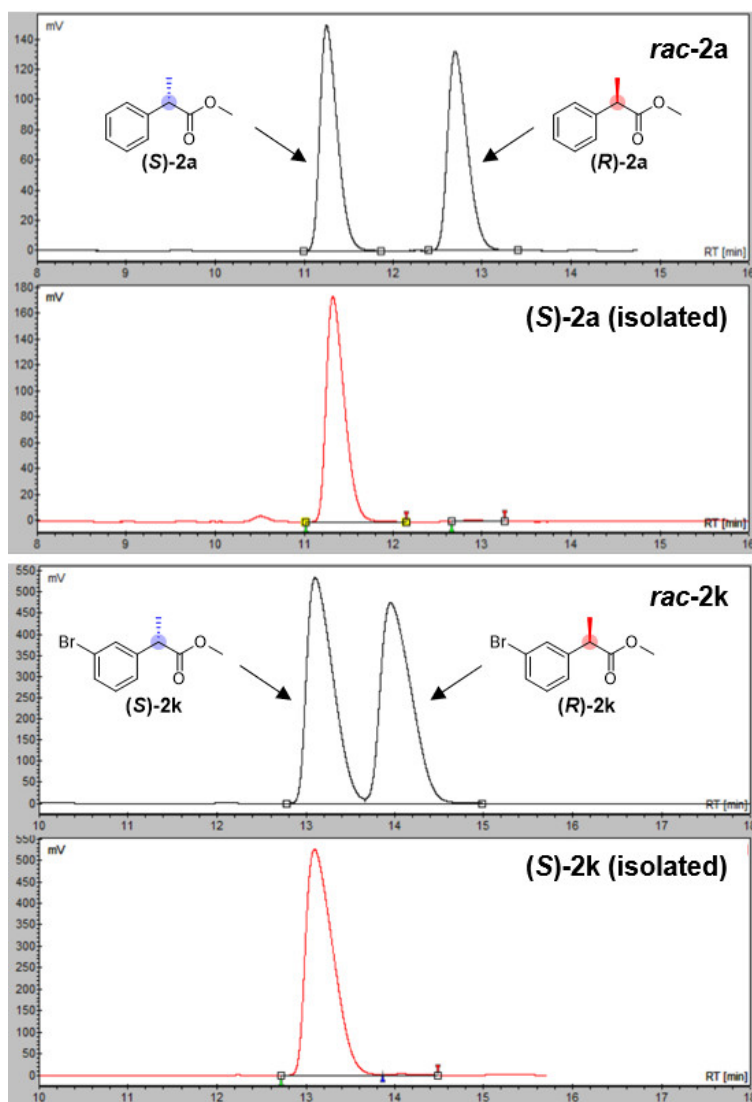


Figure S25. HPLC traces for the isolated (*S*)-**2a** and (*S*)-**2k** by OYE1 variants catalyzed reactions. The (*S*)-**2a** (98% *ee*) was isolated from bio-reduction of **1a** catalyzed by OYE1 W116A/T37A variant. The (*S*)-**2k** (99% *ee*) was isolated from bio-reduction of **1k** catalyzed by OYE1 W116A/T37A variant. The racemic mixtures of **2a** and **2k** contain authenticated standards.

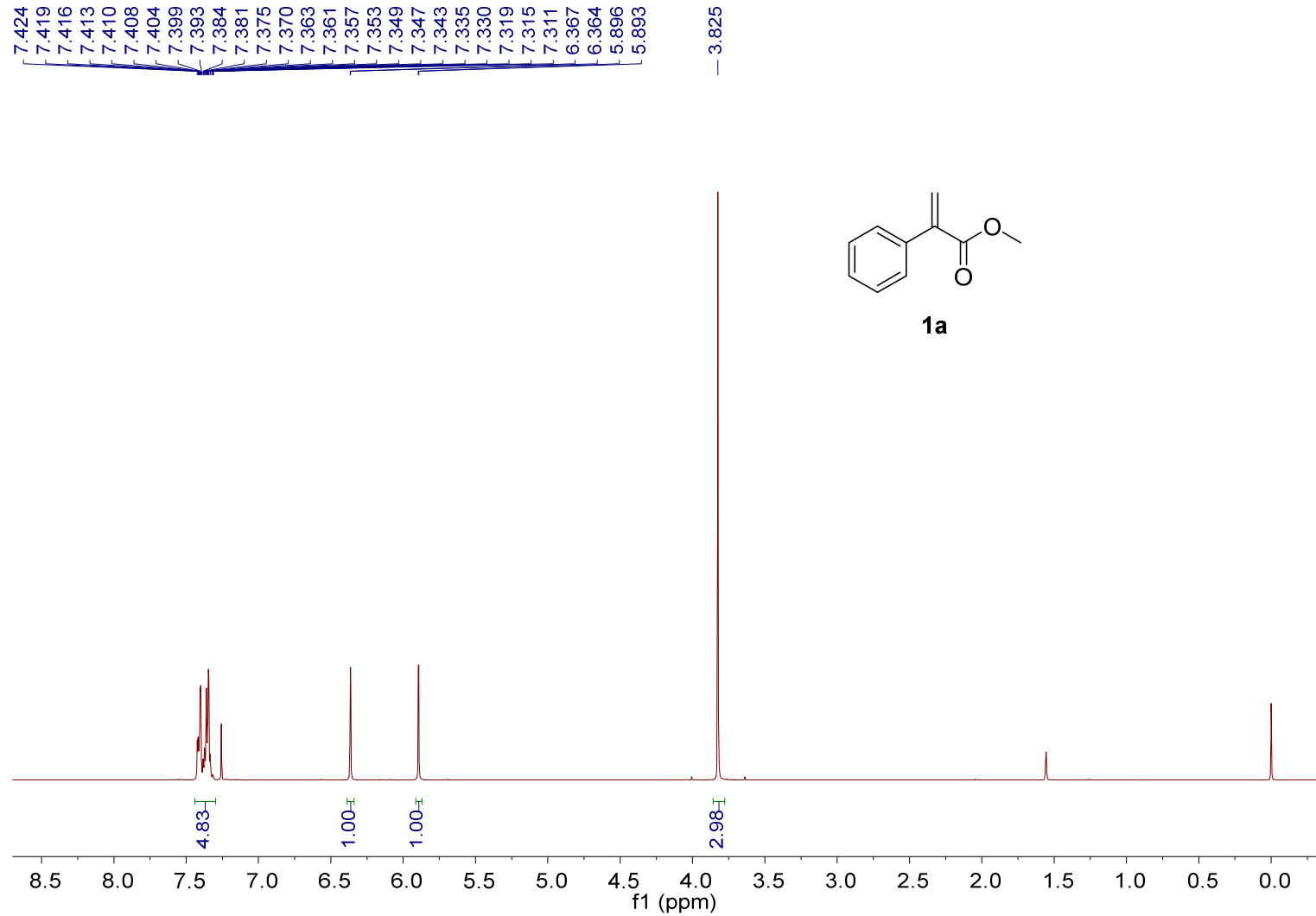


Figure S26. ^1H NMR spectrum of **1a** (400 MHz, in CDCl_3).

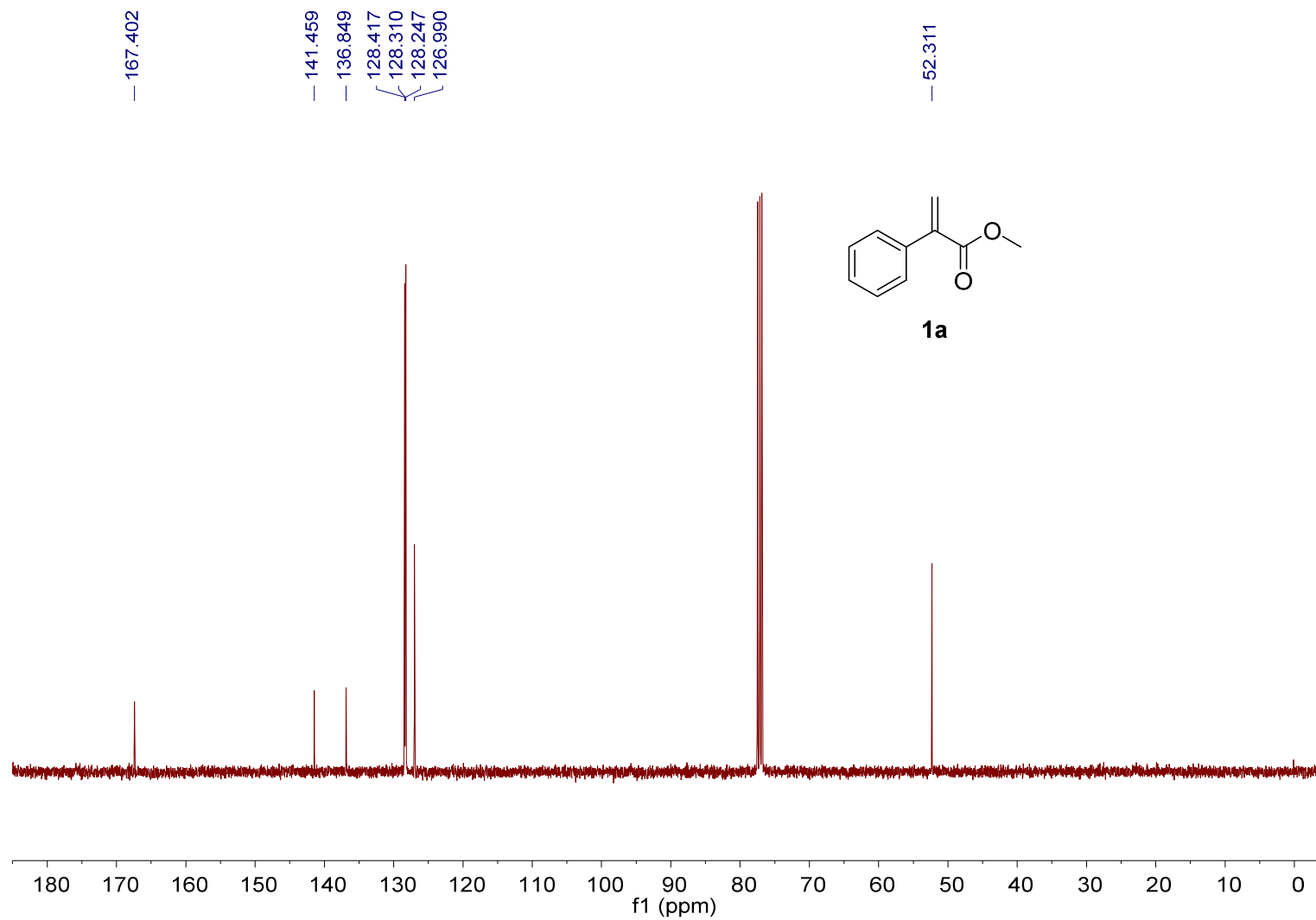


Figure S27. ^{13}C NMR spectrum of **1a** (101 MHz, in CDCl_3).

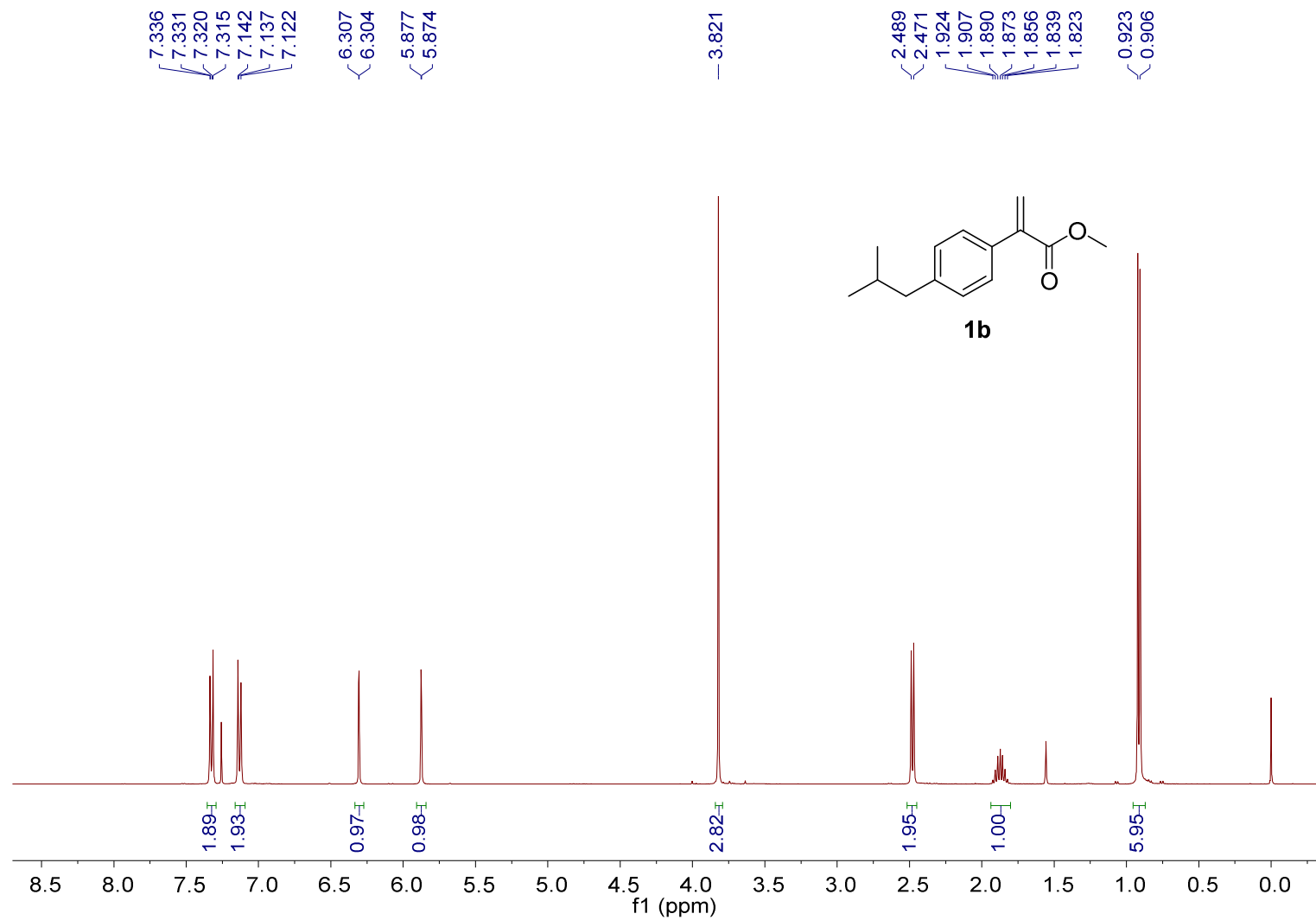


Figure S28. ¹H NMR spectrum of **1b** (400 MHz, in CDCl₃).

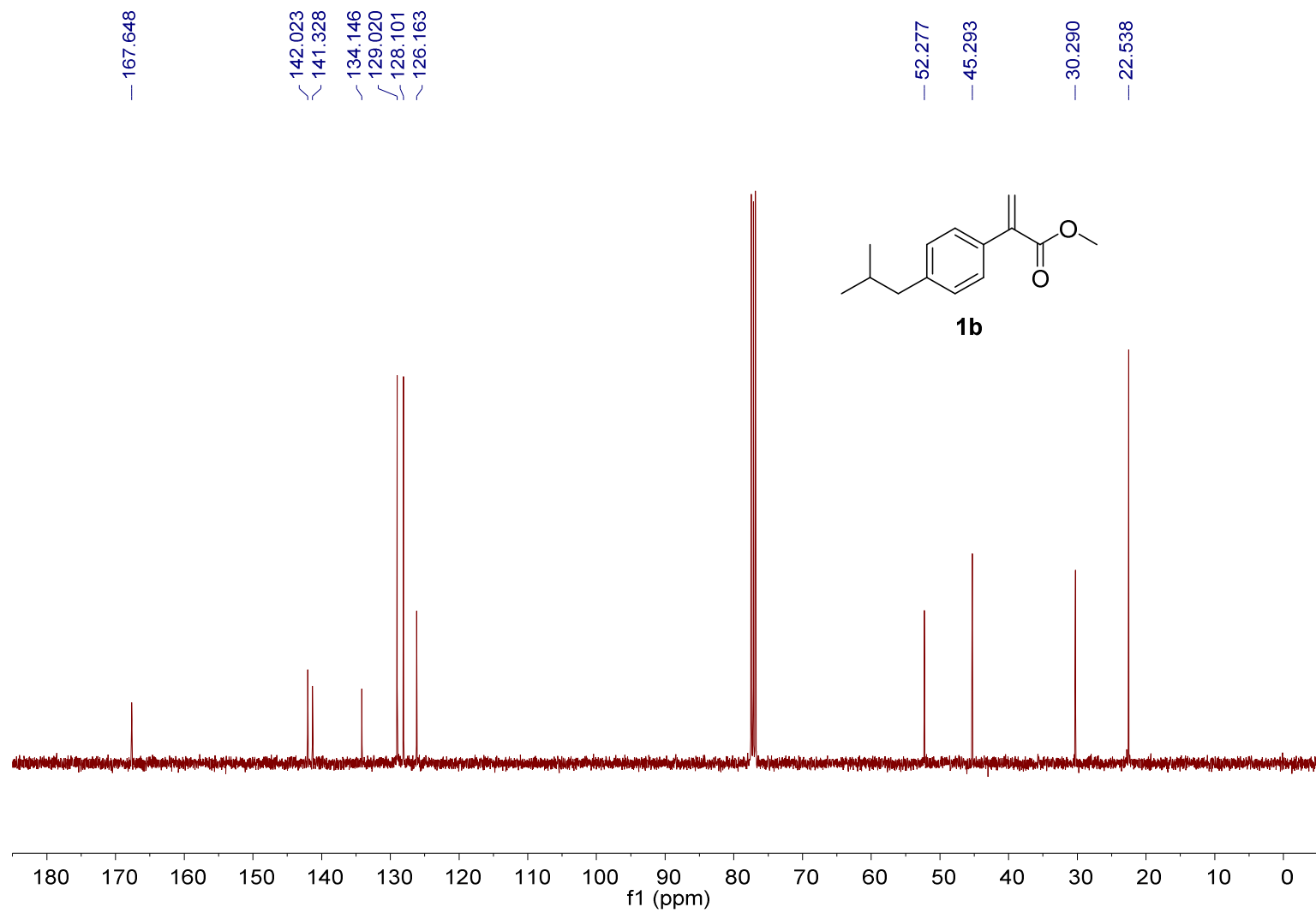


Figure S29. ^{13}C NMR spectrum of **1b** (101 MHz, in CDCl_3).

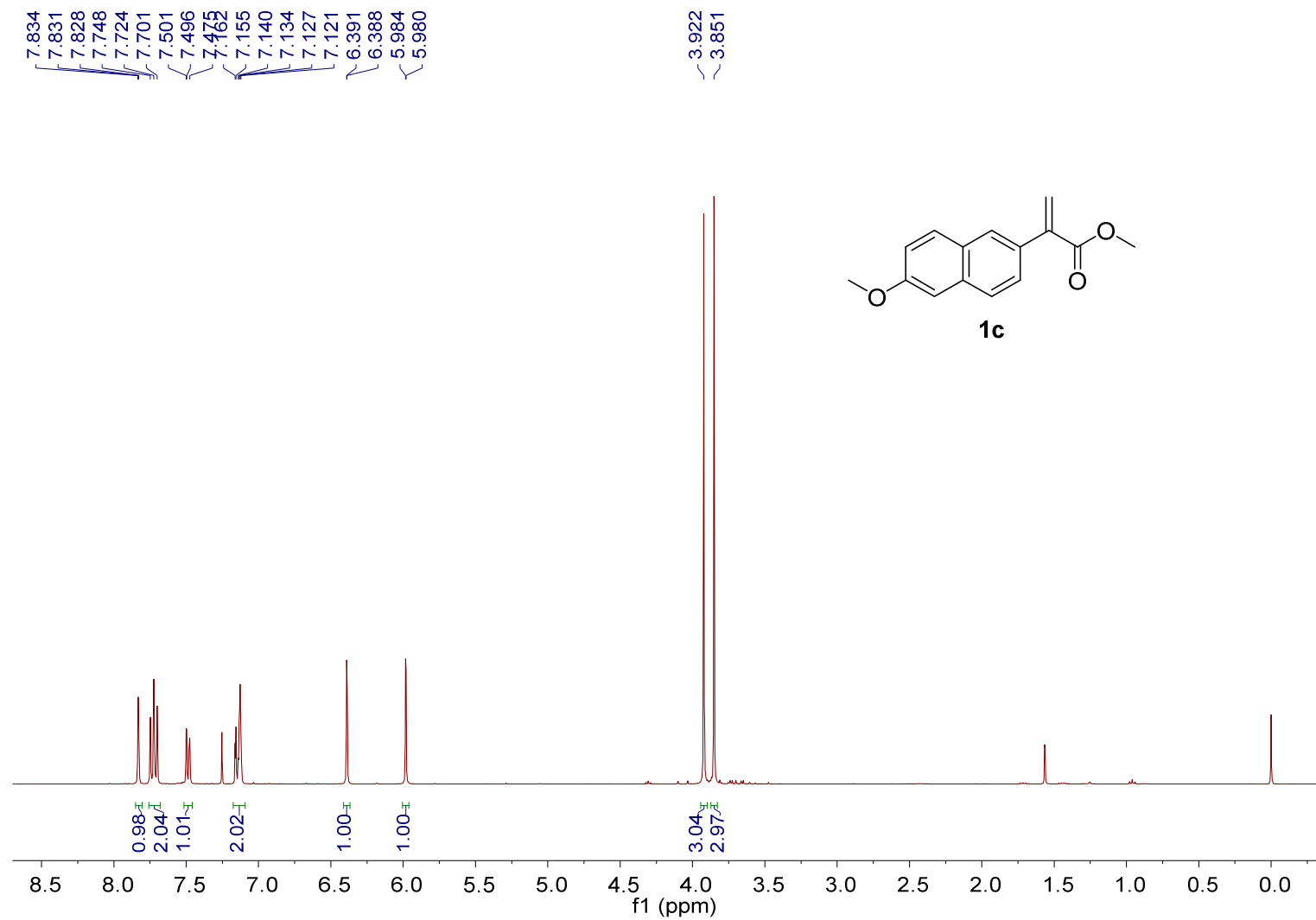
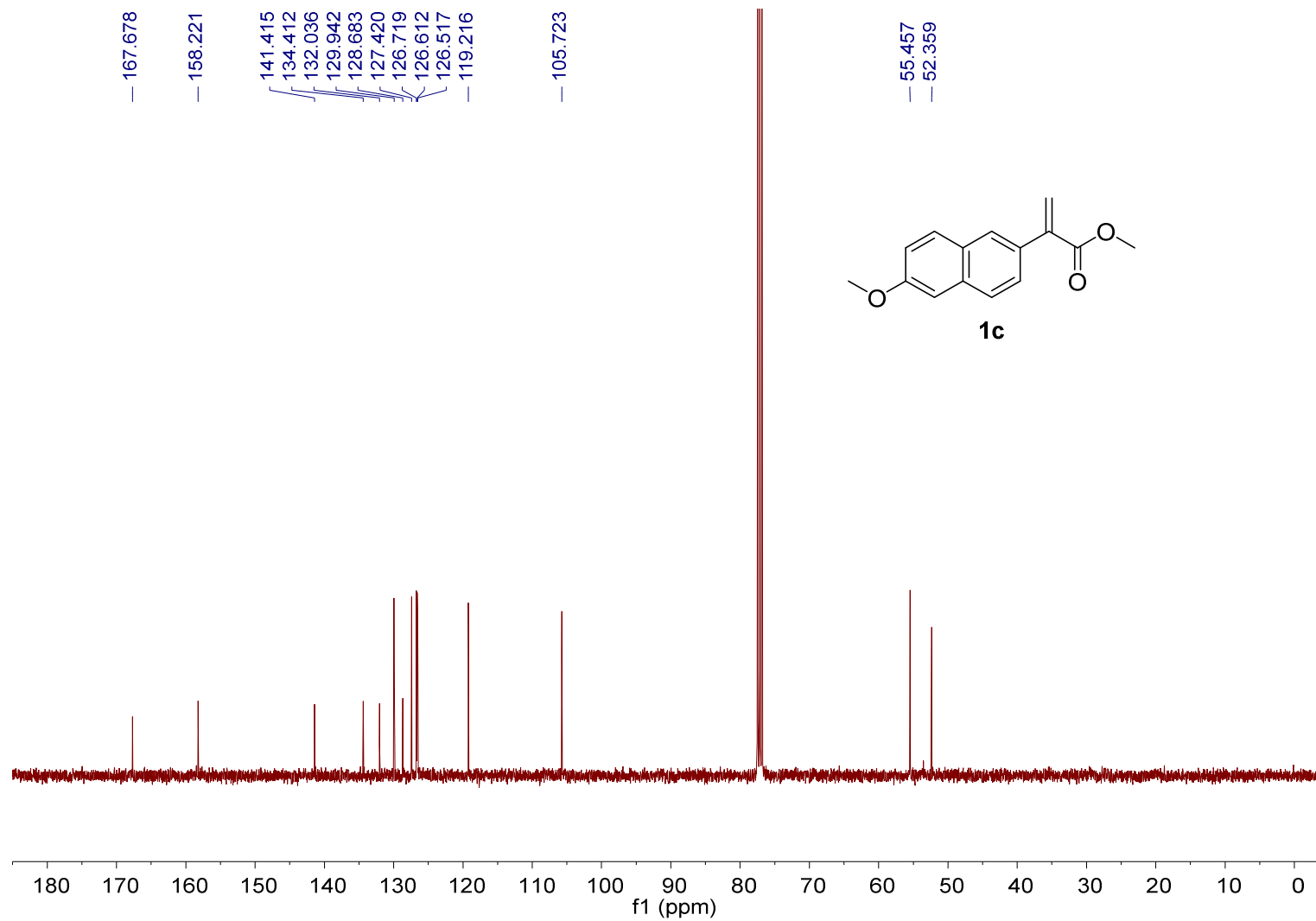


Figure S30. ¹H NMR spectrum of **1c** (400 MHz, in CDCl₃).



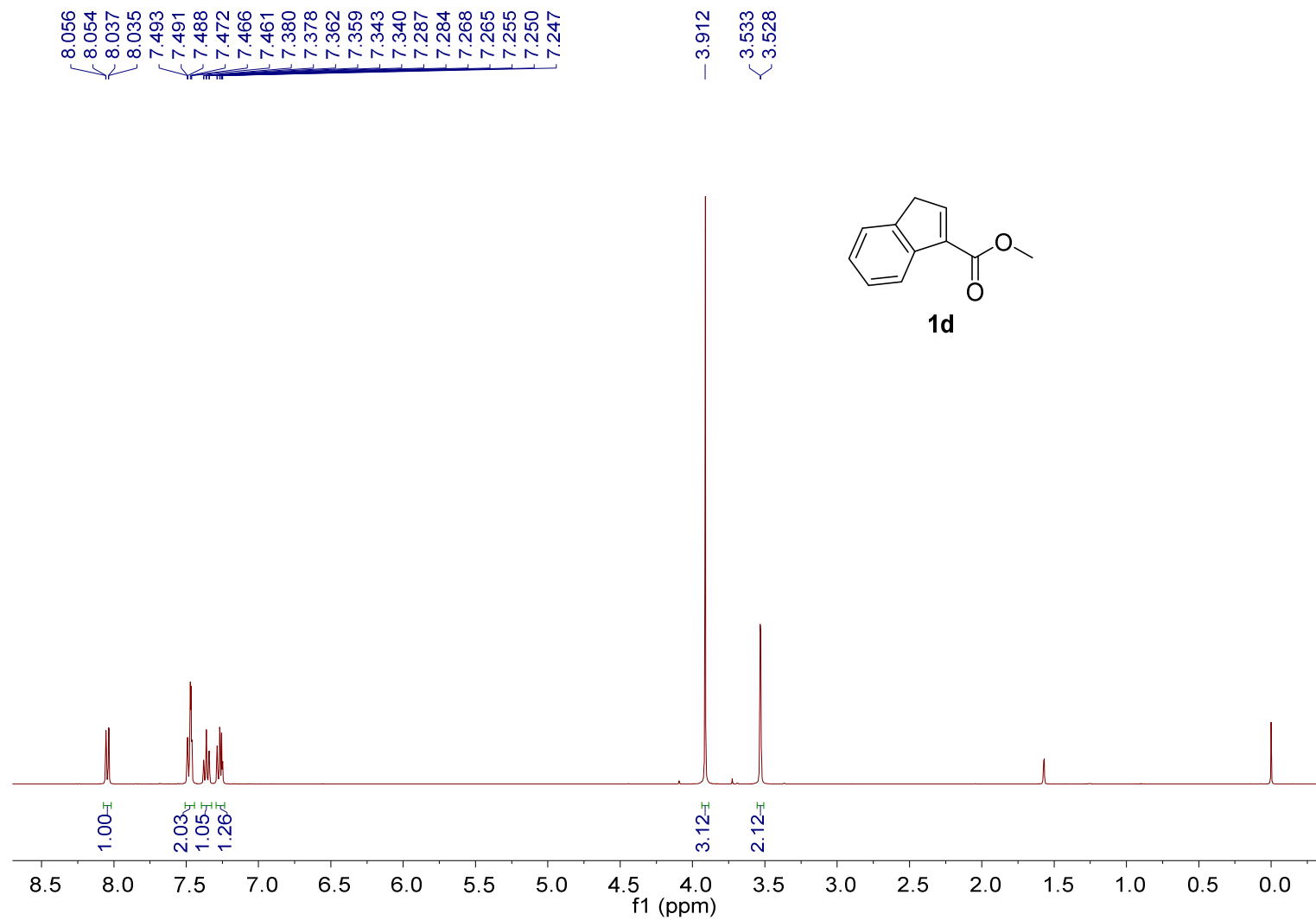


Figure S32. ^1H NMR spectrum of **1d** (400 MHz, in CDCl_3).

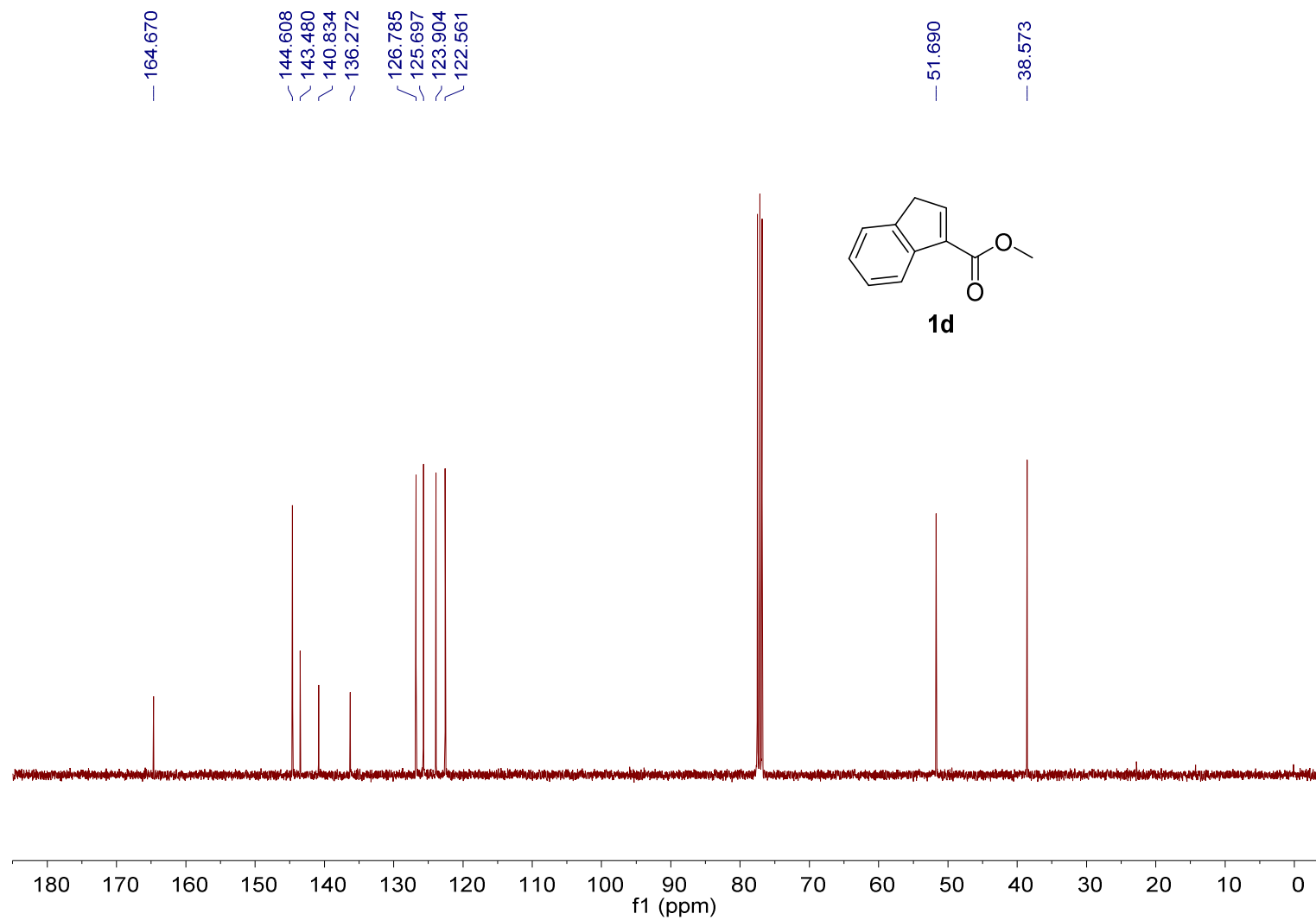


Figure S33. ^{13}C NMR spectrum of **1d** (101 MHz, in CDCl_3).

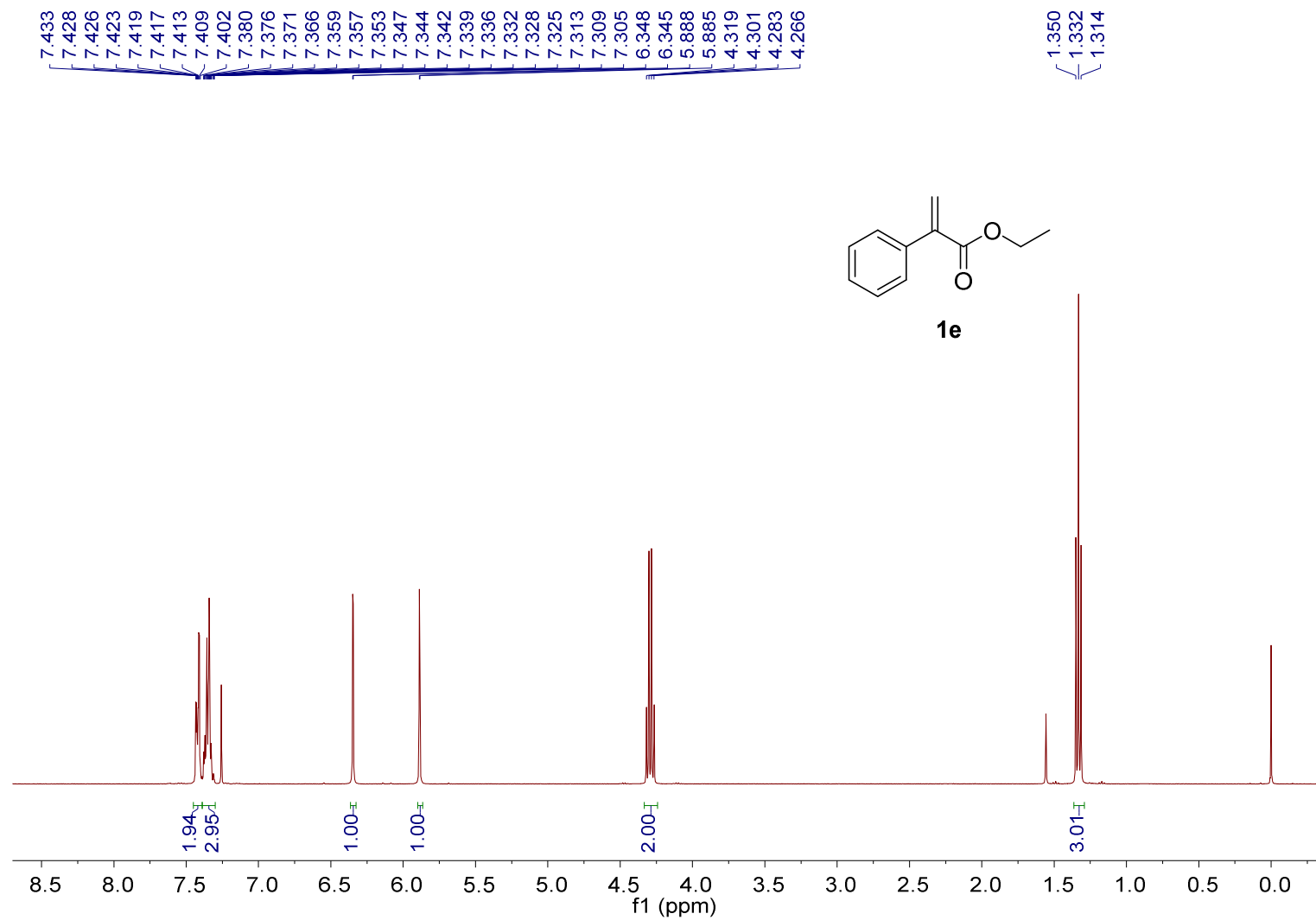


Figure S34. ¹H NMR spectrum of **1e** (400 MHz, in CDCl₃).

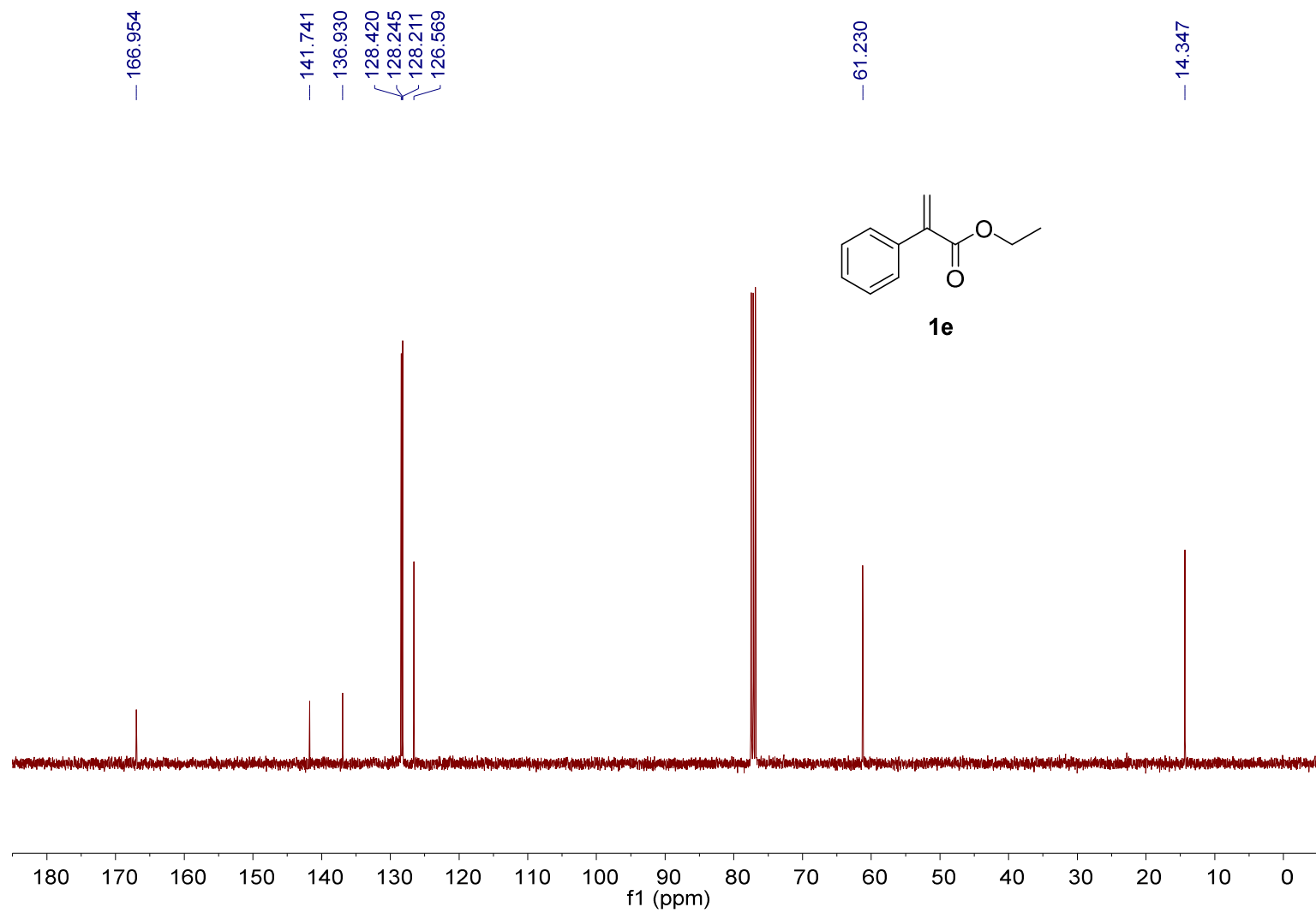


Figure S35. ^{13}C NMR spectrum of **1e** (101 MHz, in CDCl_3).

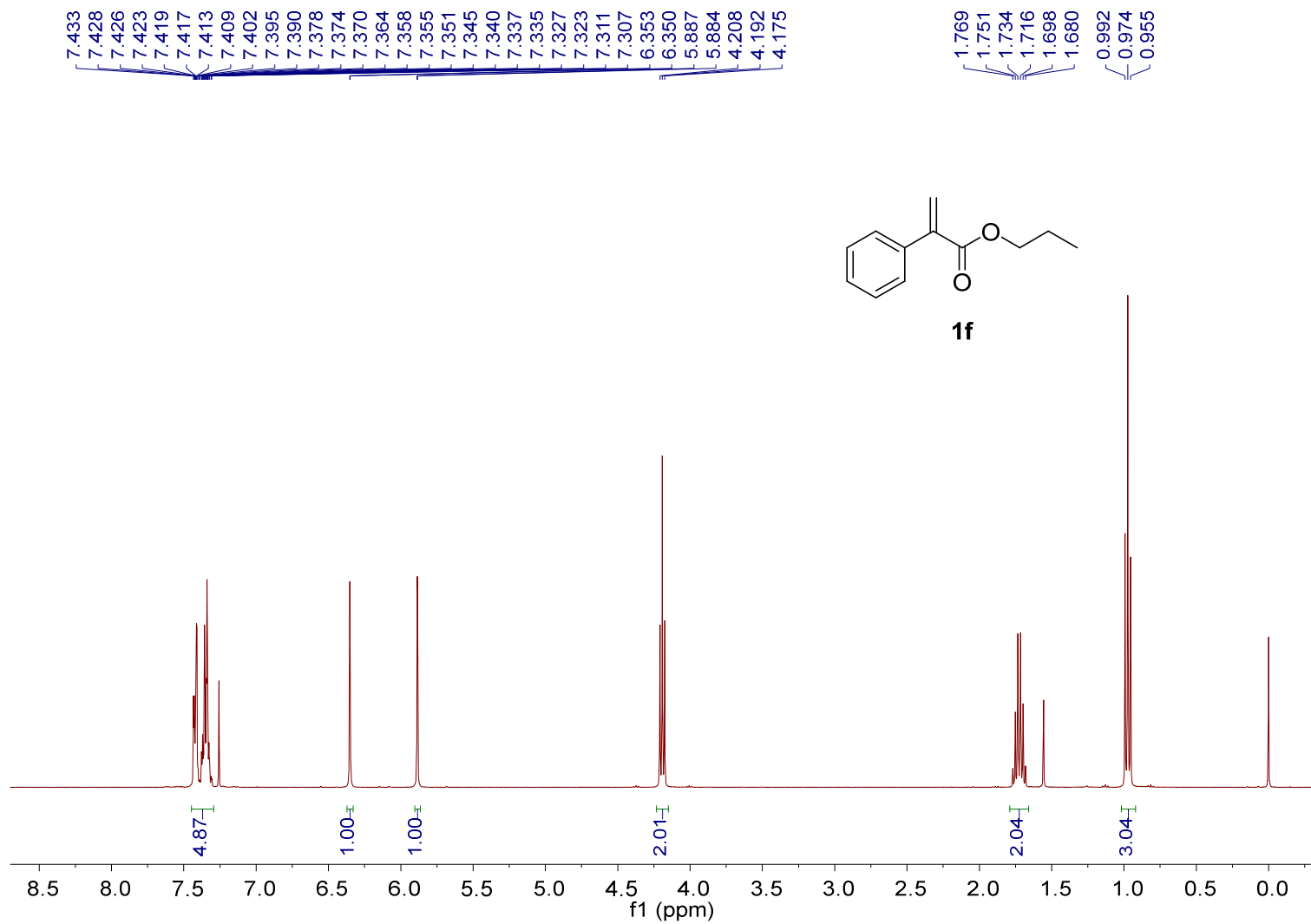


Figure S36. ¹H NMR spectrum of **1f** (400 MHz, in CDCl₃).

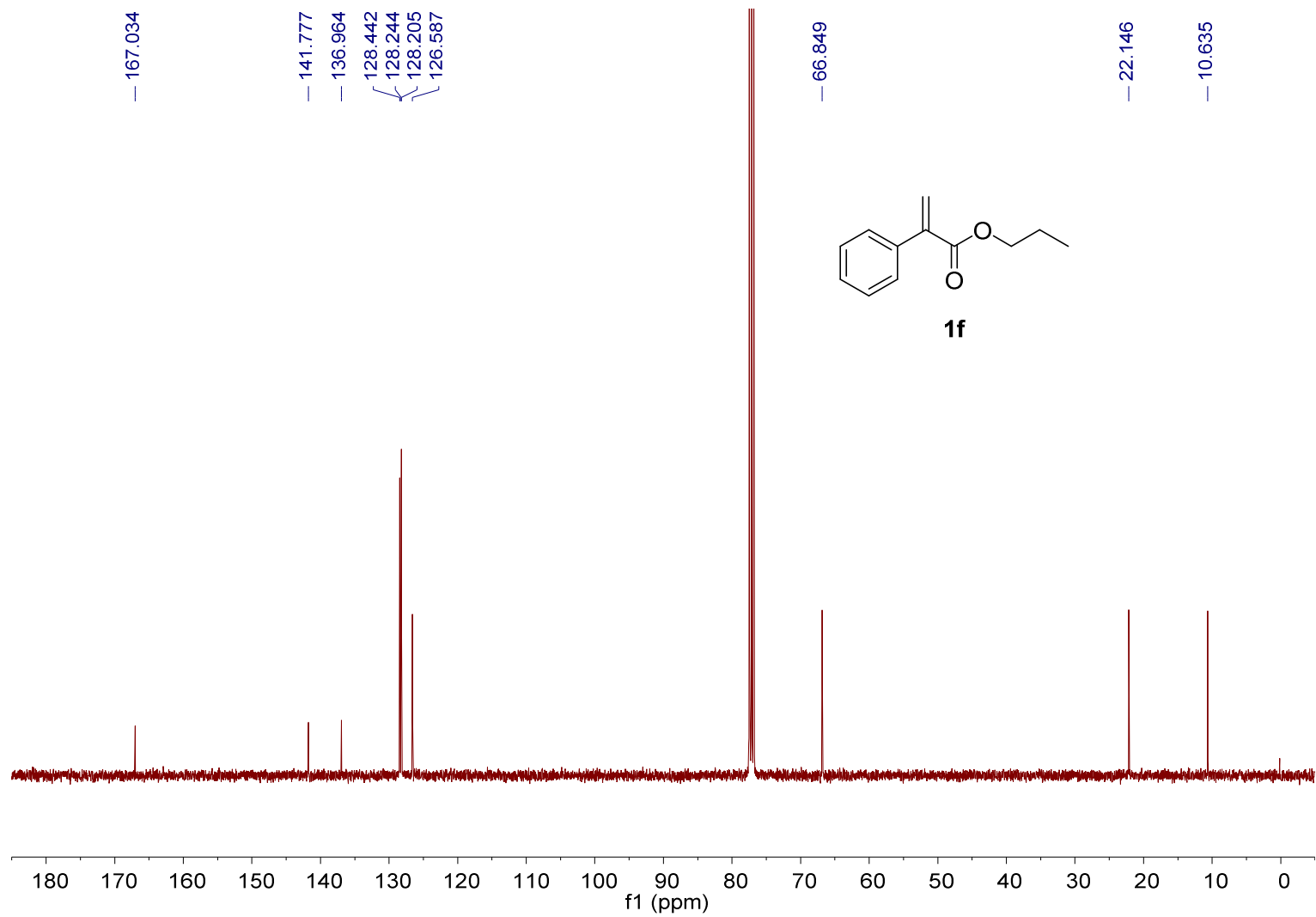


Figure S37. ^{13}C NMR spectrum of **1f** (101 MHz, in CDCl_3).

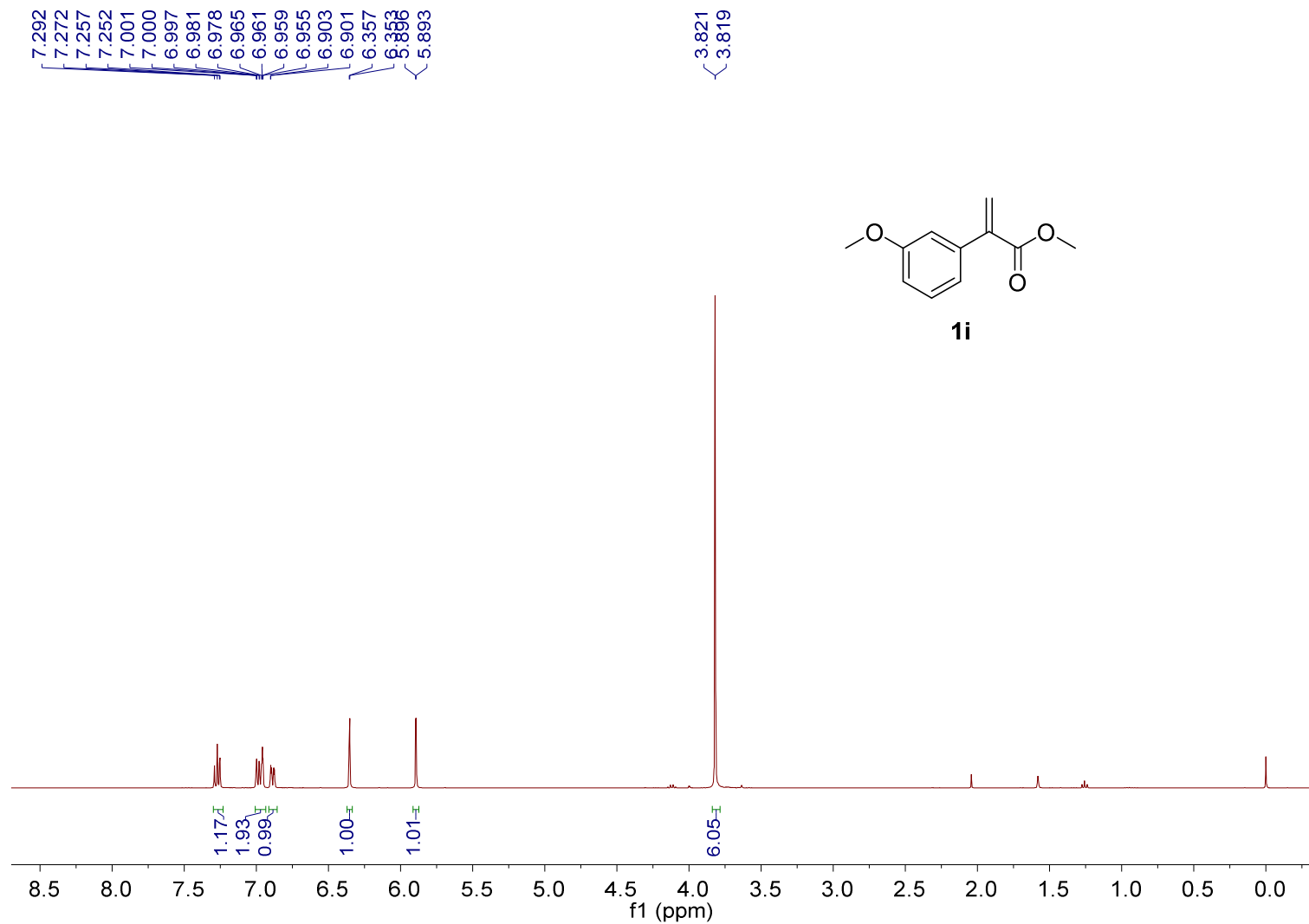
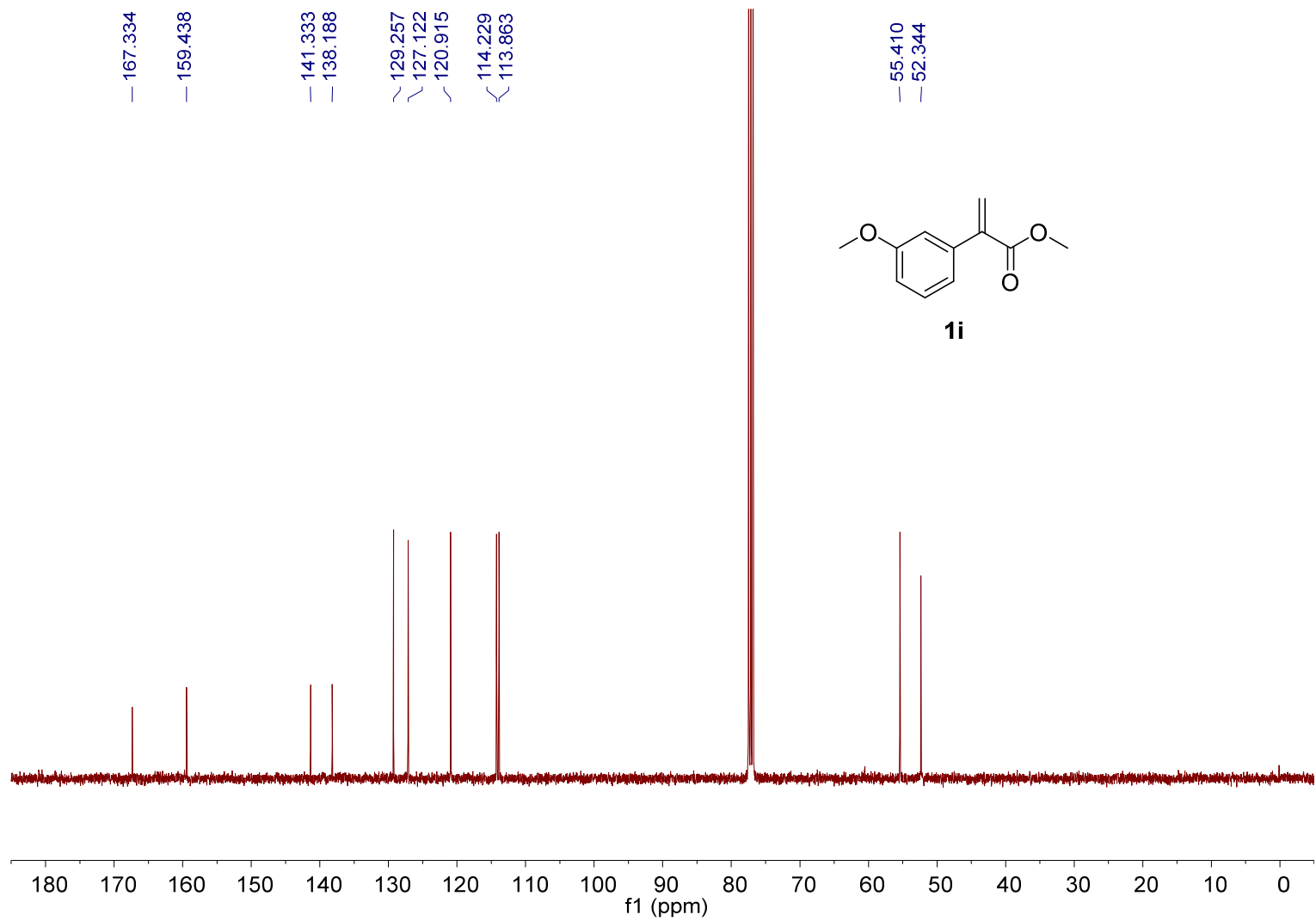


Figure S38. ¹H NMR spectrum of **1i** (400 MHz, in CDCl₃).



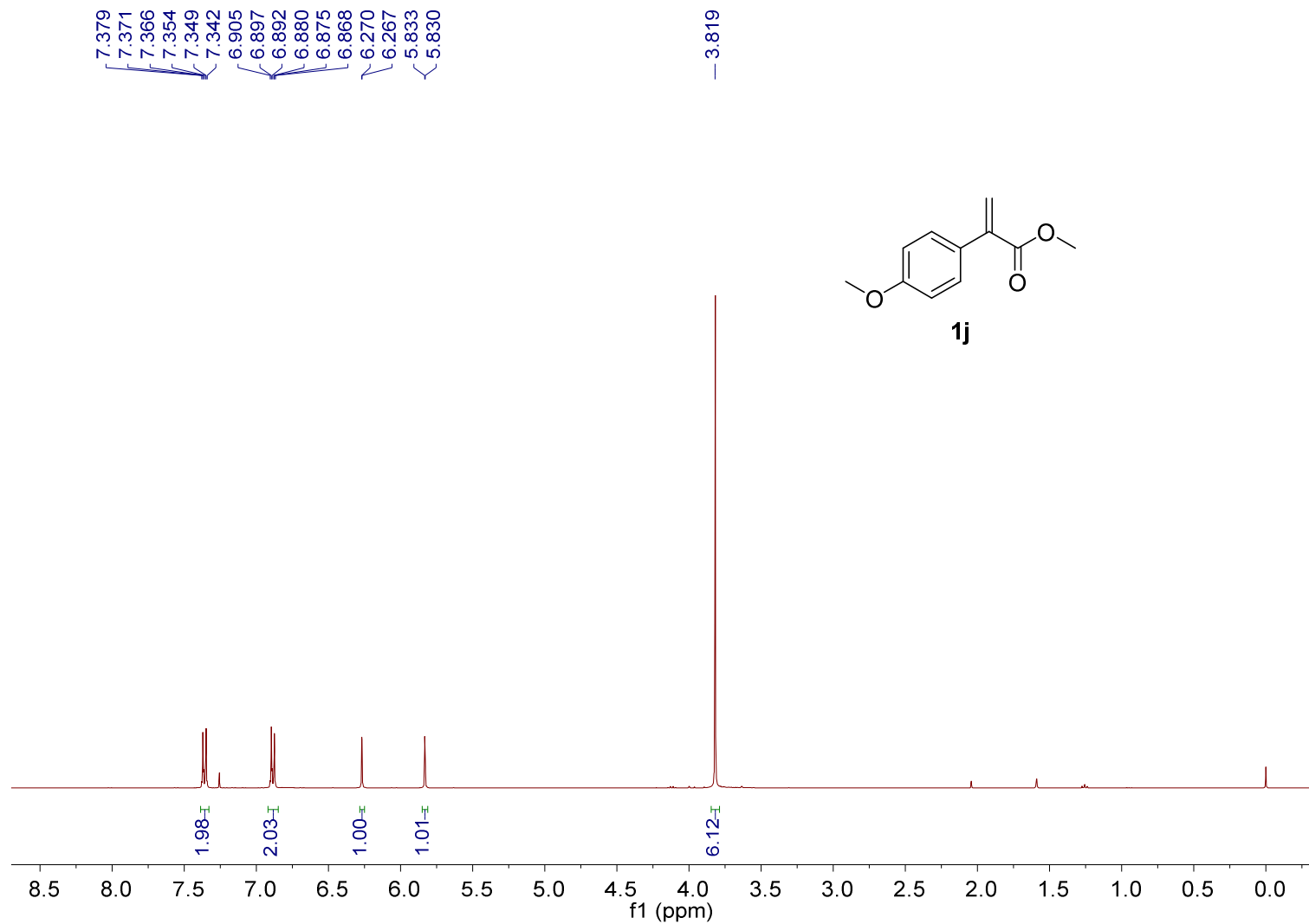


Figure S40. ^1H NMR spectrum of **1j** (400 MHz, in CDCl_3).

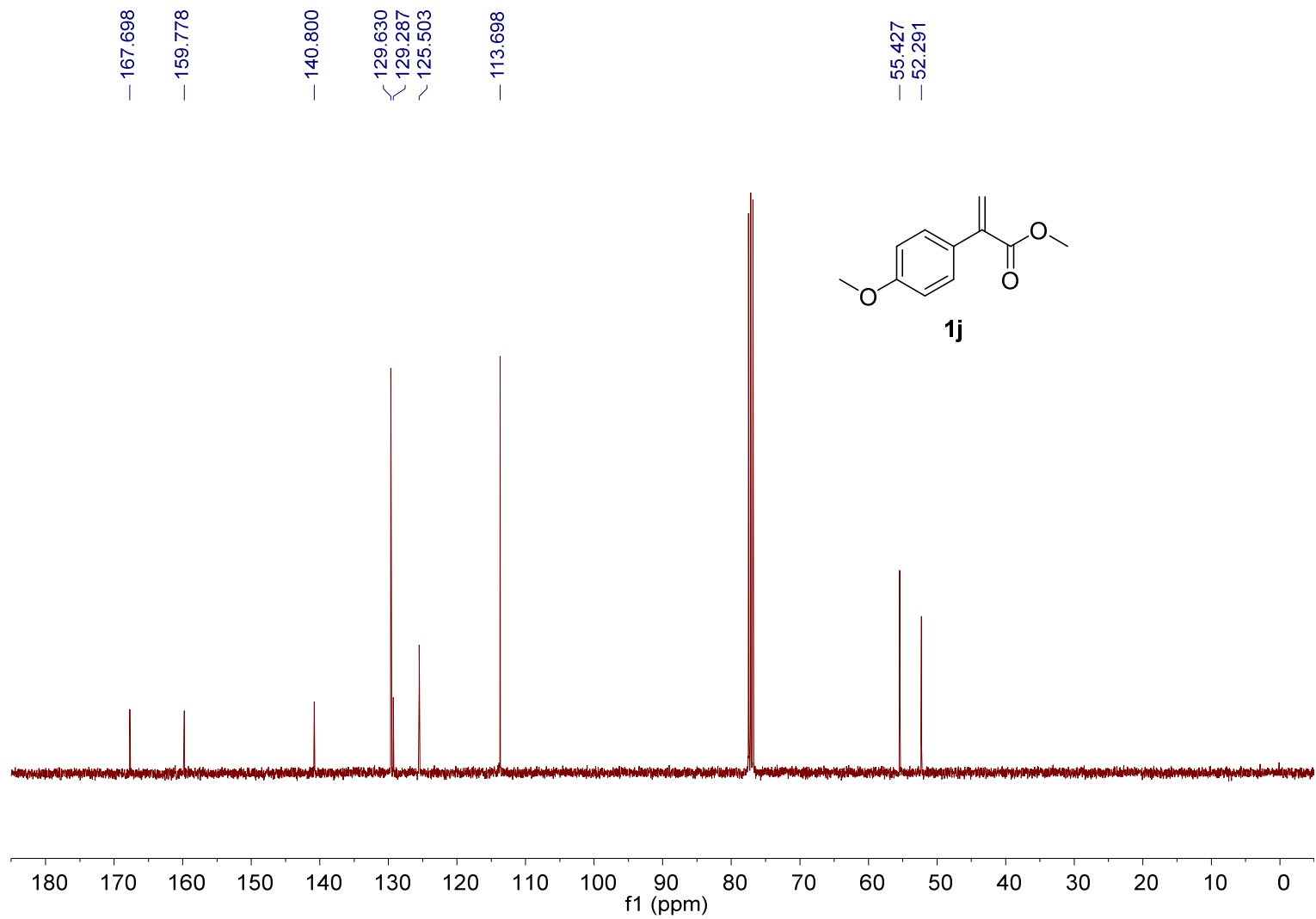


Figure S41. ¹³C NMR spectrum of **1j** (101 MHz, in CDCl₃).

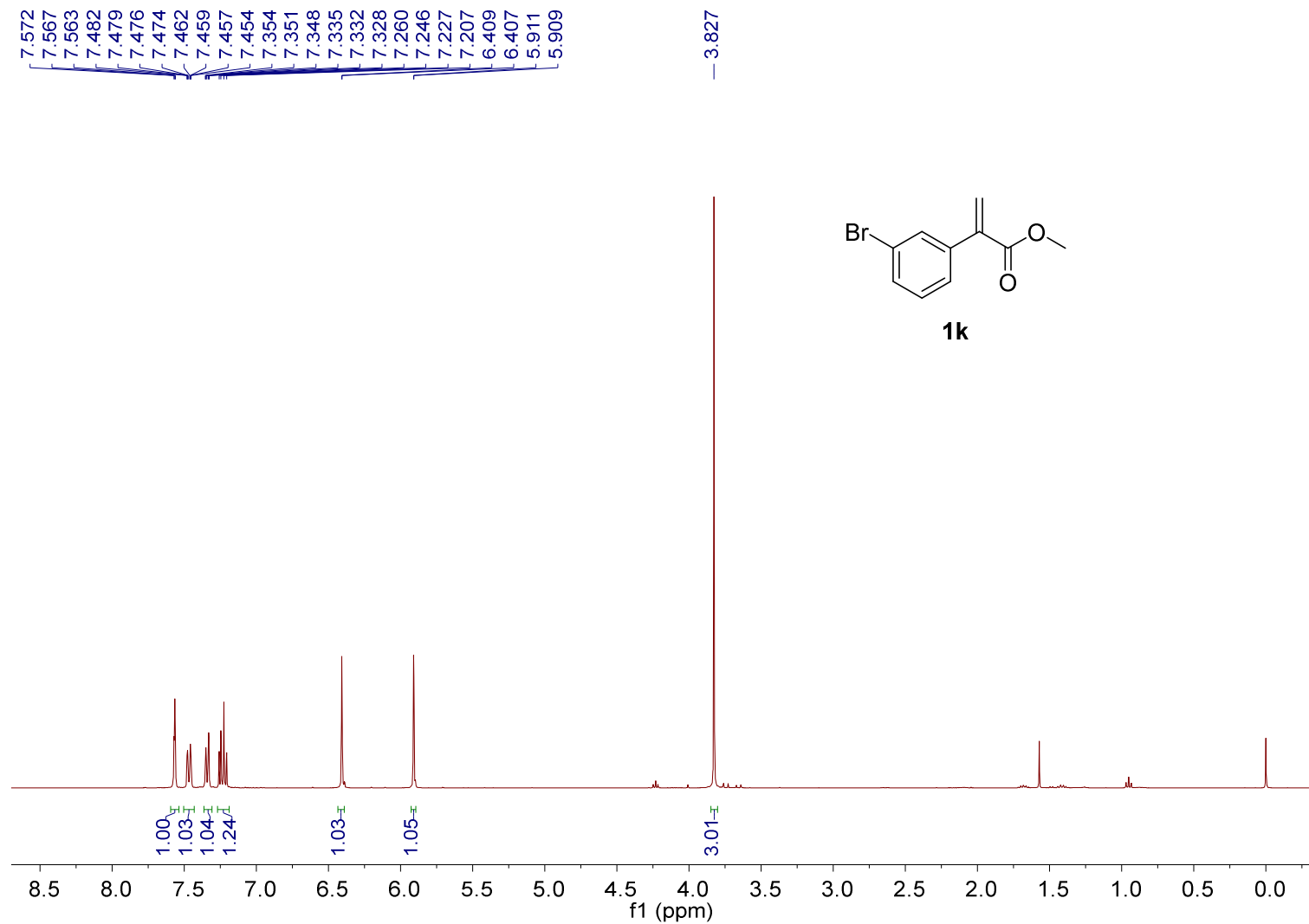


Figure S42. ^1H NMR spectrum of **1k** (400 MHz, in CDCl_3).

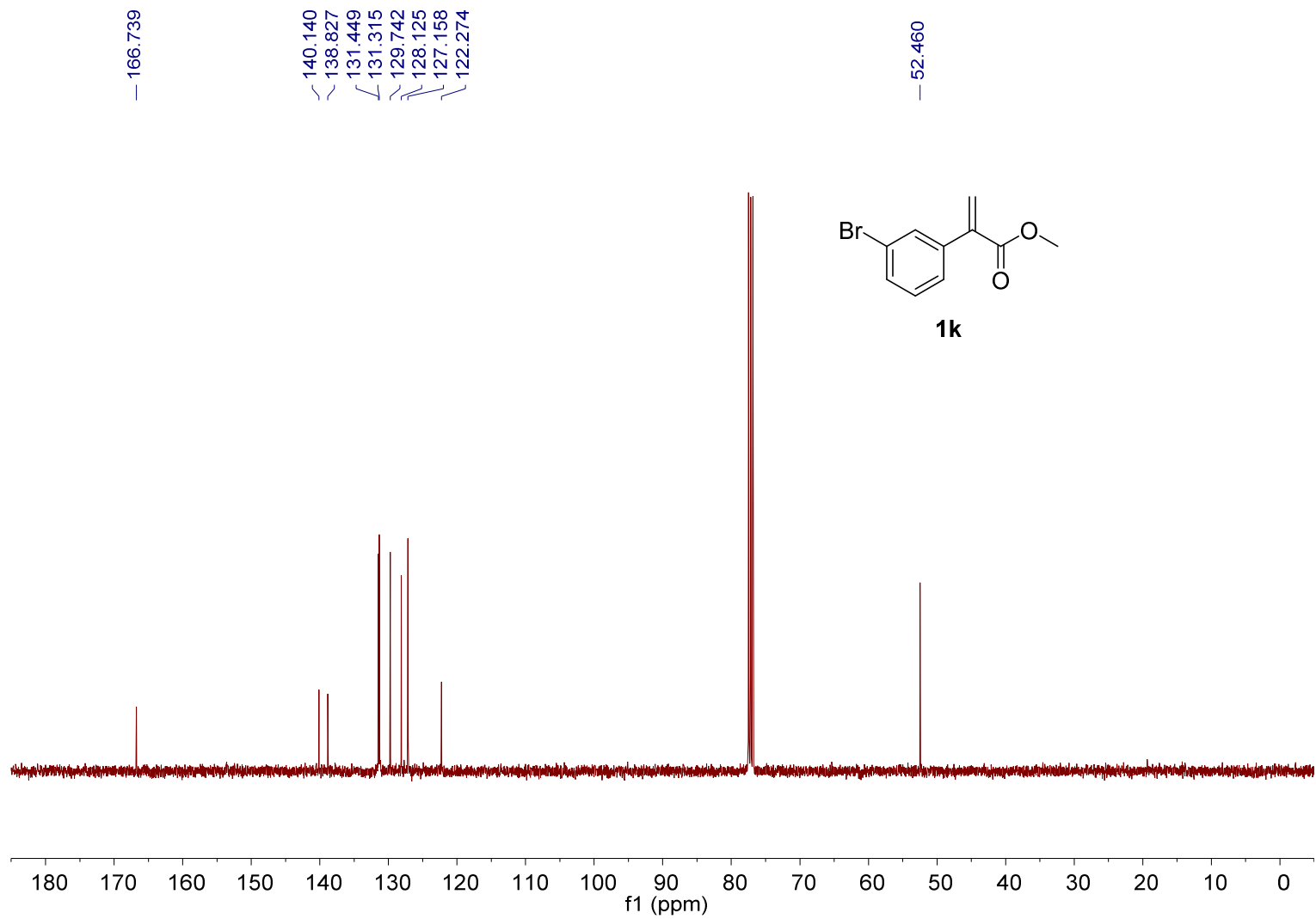


Figure S43. ¹³C NMR spectrum of **1k** (101 MHz, in CDCl₃).

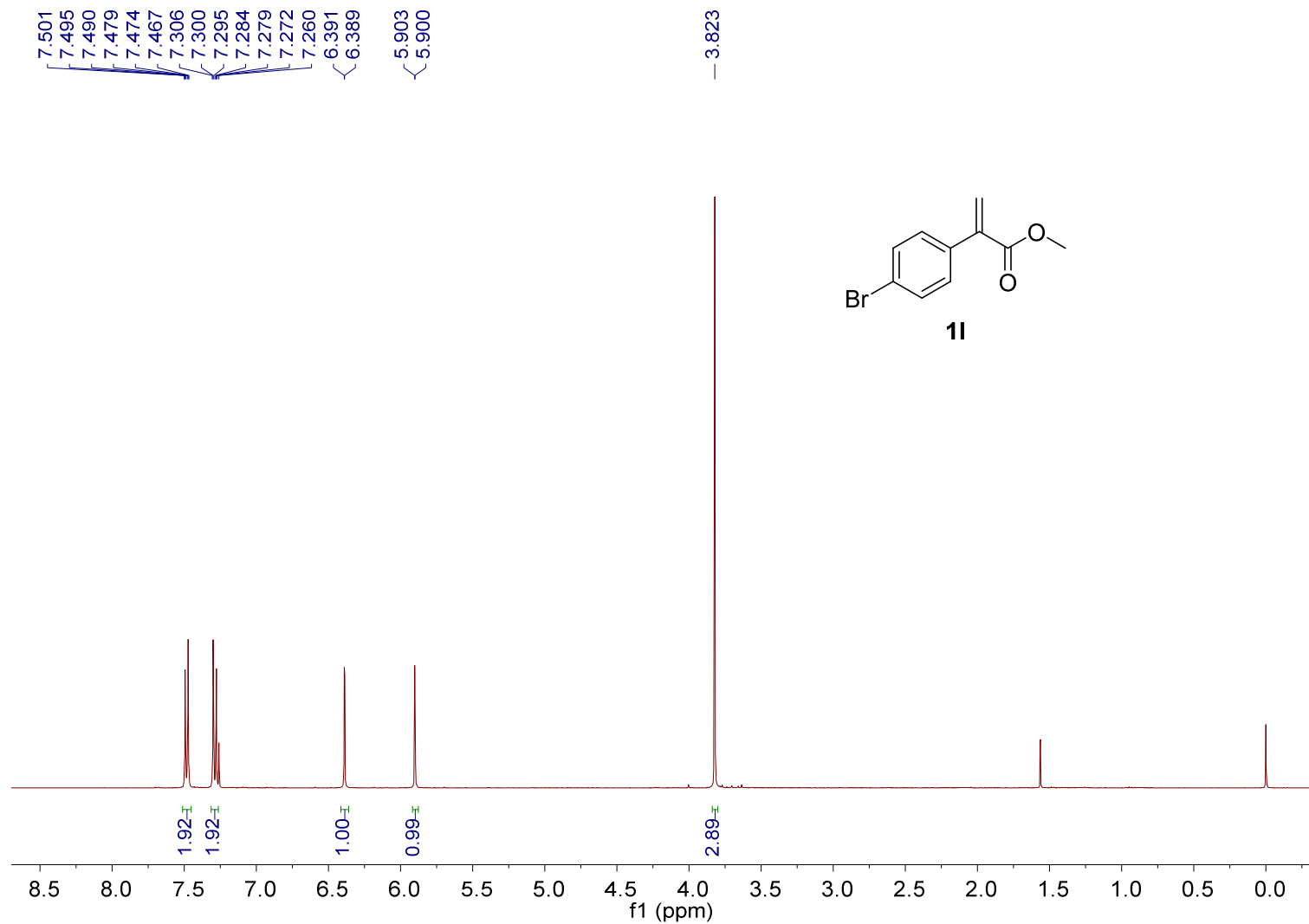


Figure S44. ^1H NMR spectrum of **11** (400 MHz, in CDCl_3).

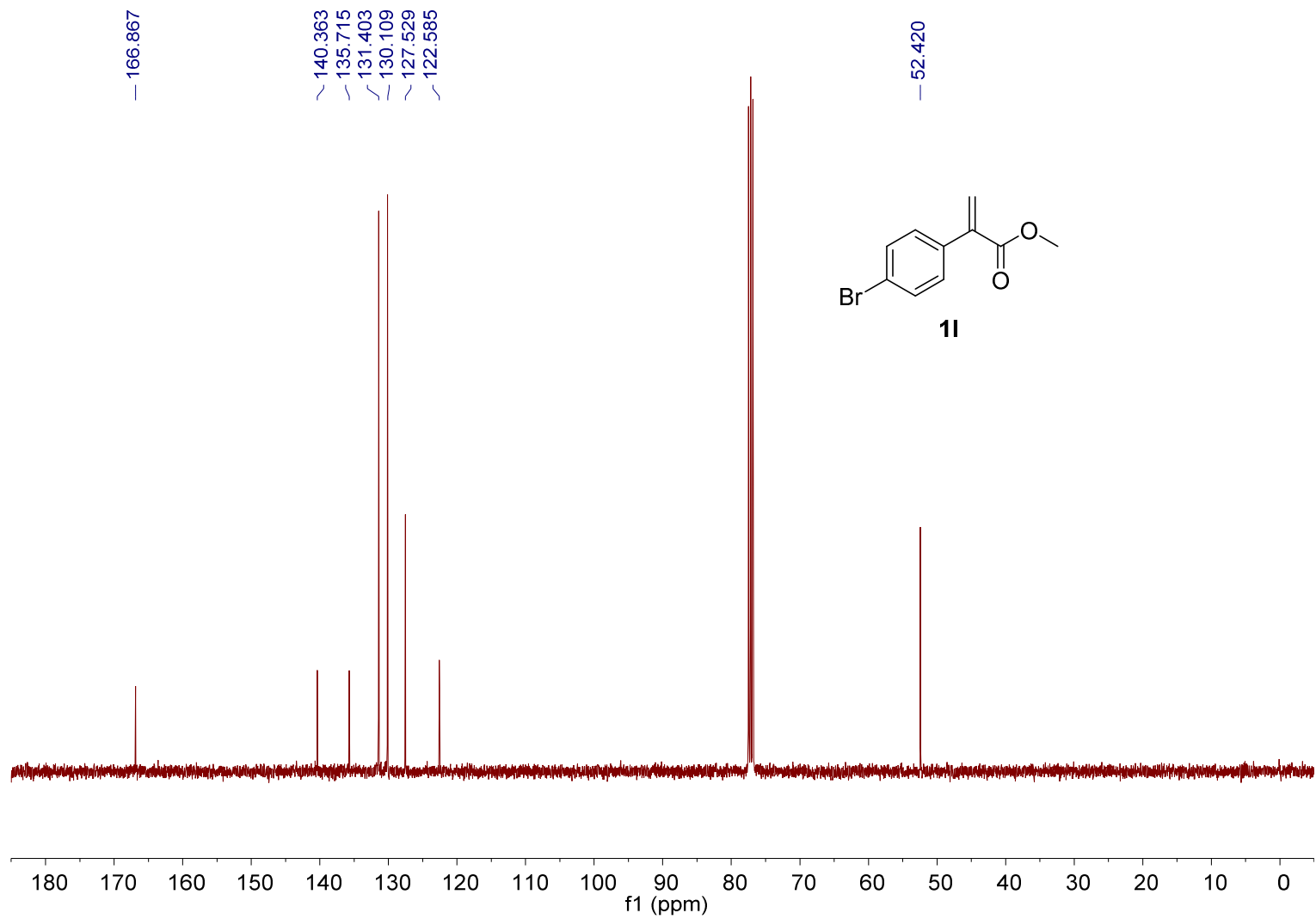


Figure S45. ¹³C NMR spectrum of **11** (101 MHz, in CDCl₃).

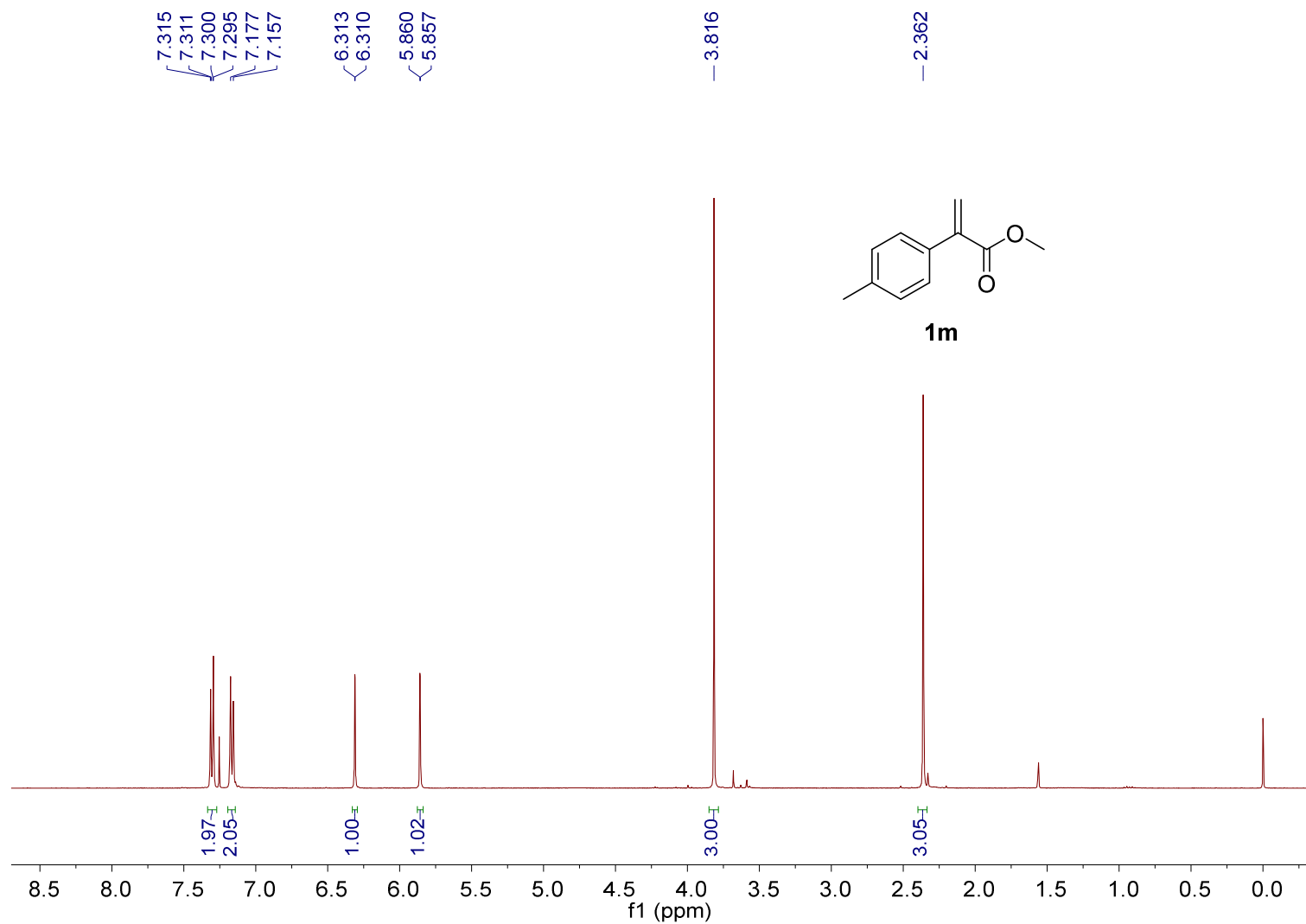


Figure S46. ^1H NMR spectrum of **1m** (400 MHz, in CDCl_3).

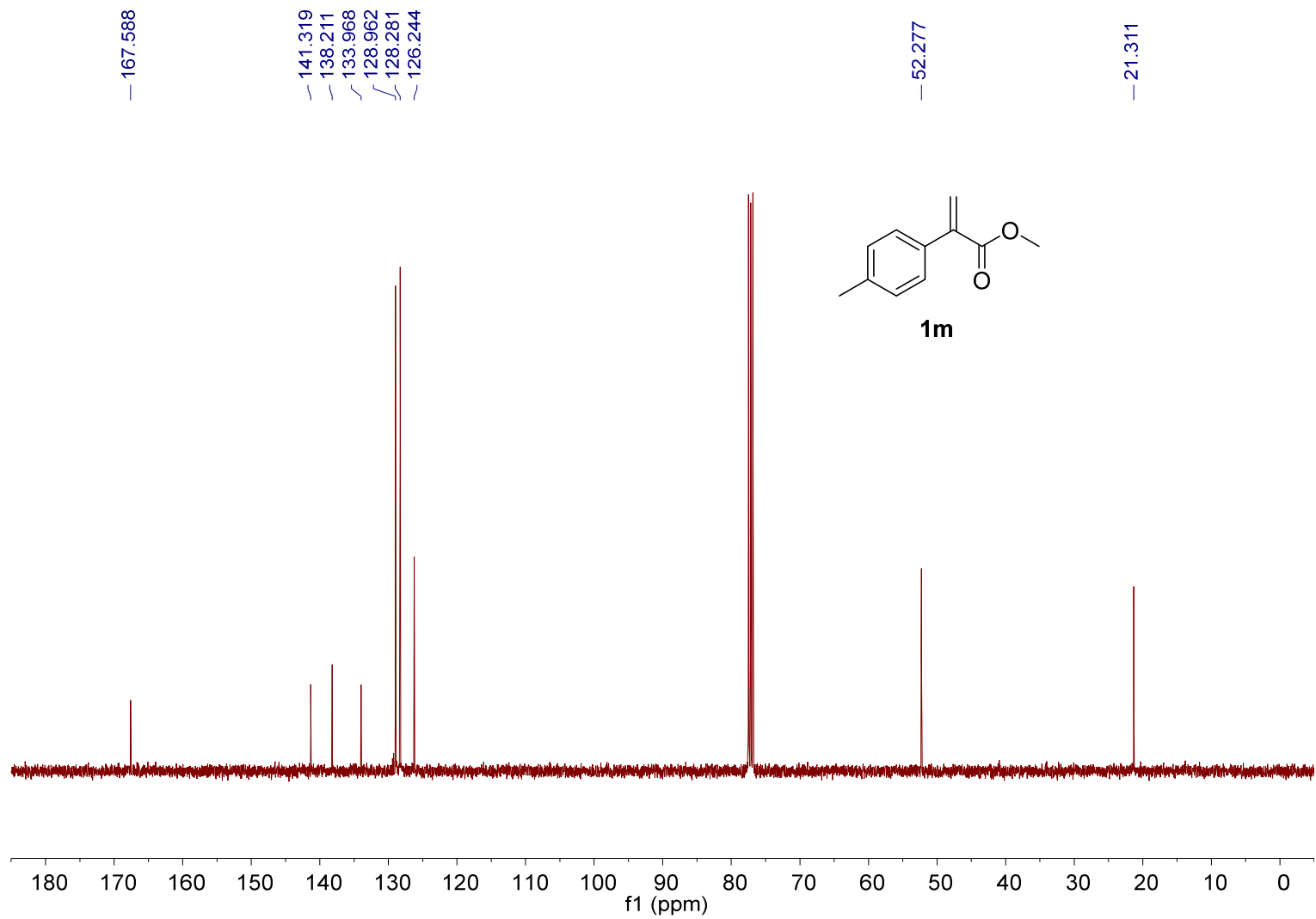


Figure S47. ¹³C NMR spectrum of **1m** (101 MHz, in CDCl₃).

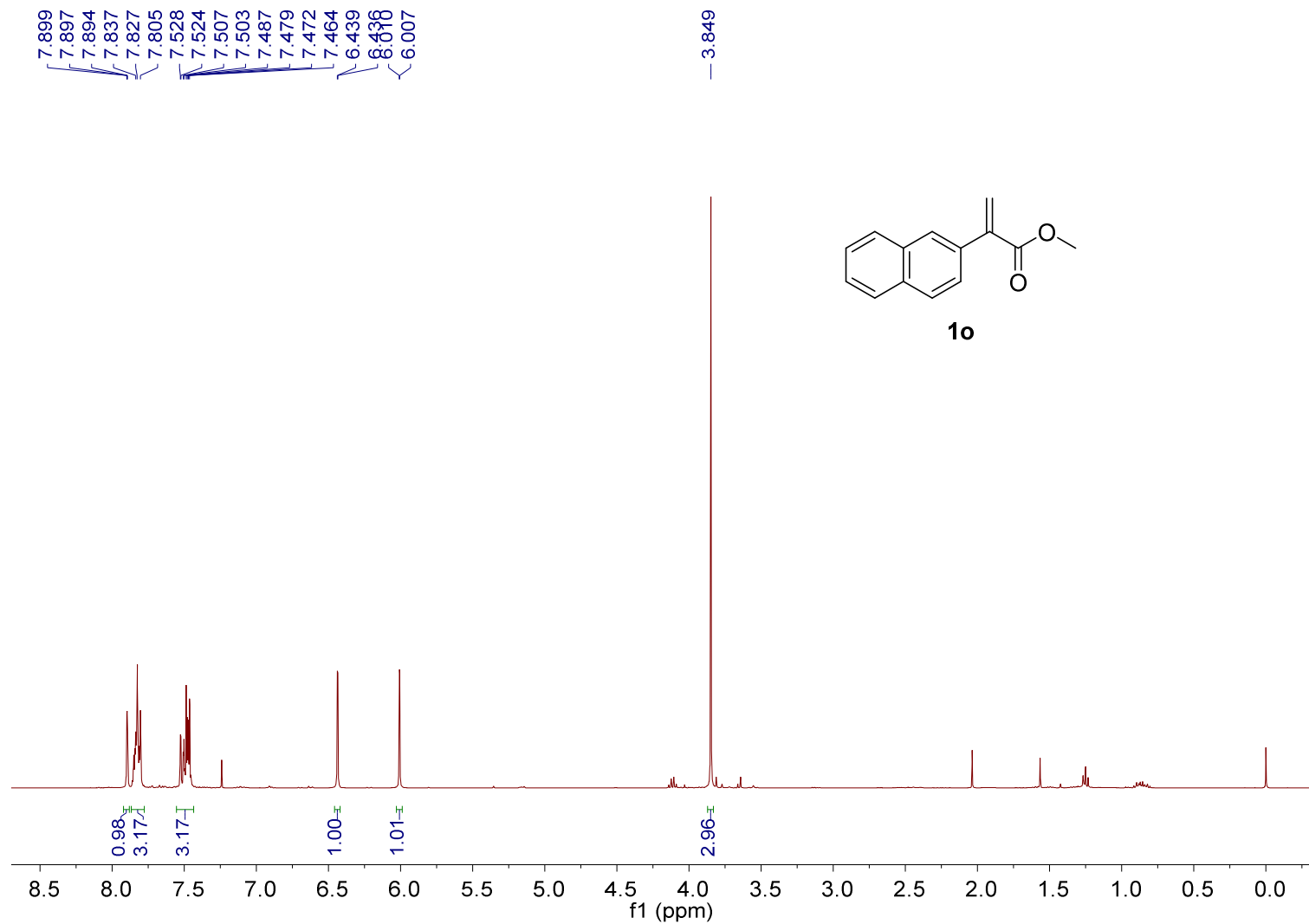


Figure S48. ¹H NMR spectrum of **1o** (400 MHz, in CDCl₃).

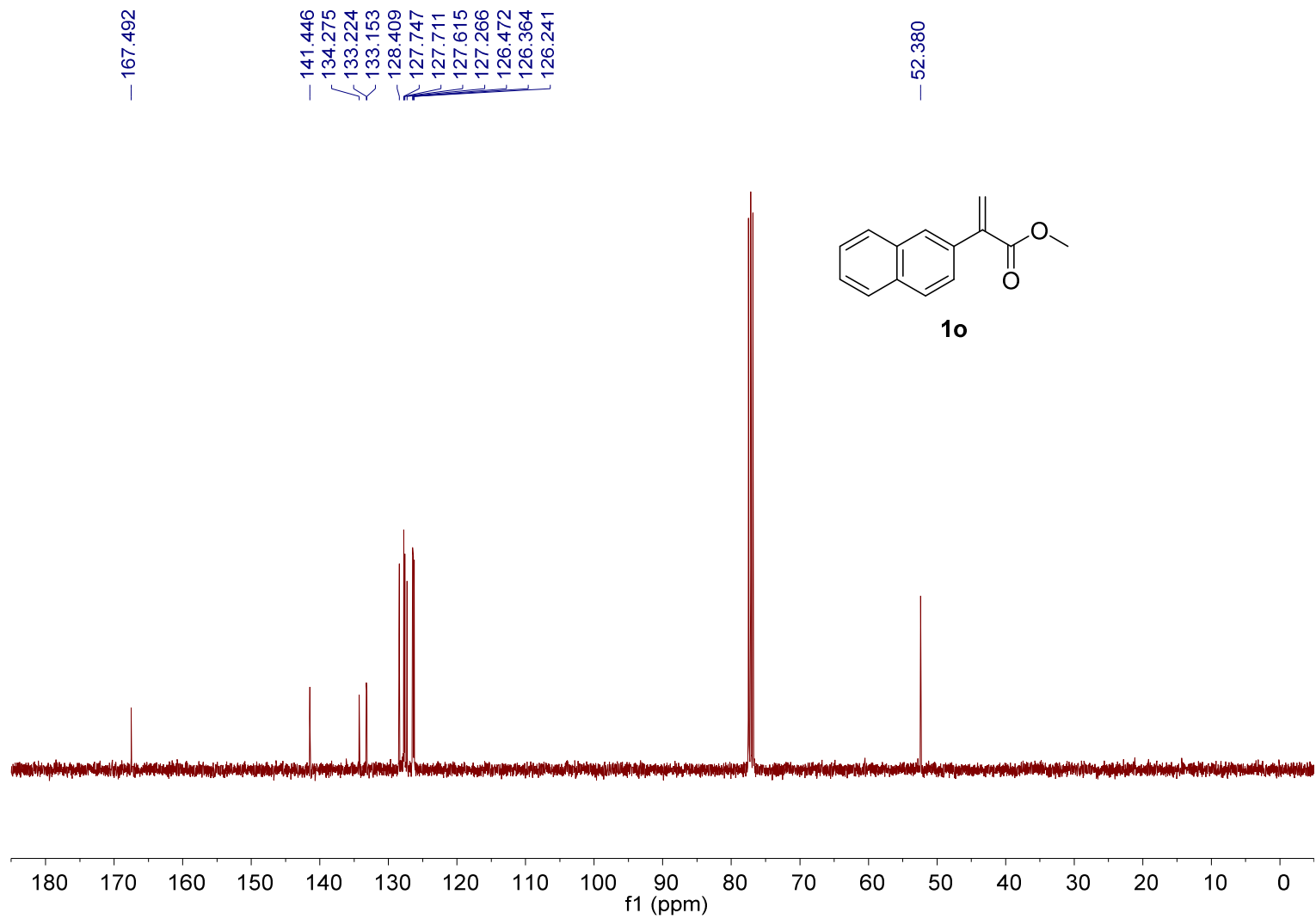


Figure S49. ¹³C NMR spectrum of **1o** (101 MHz, in CDCl₃).

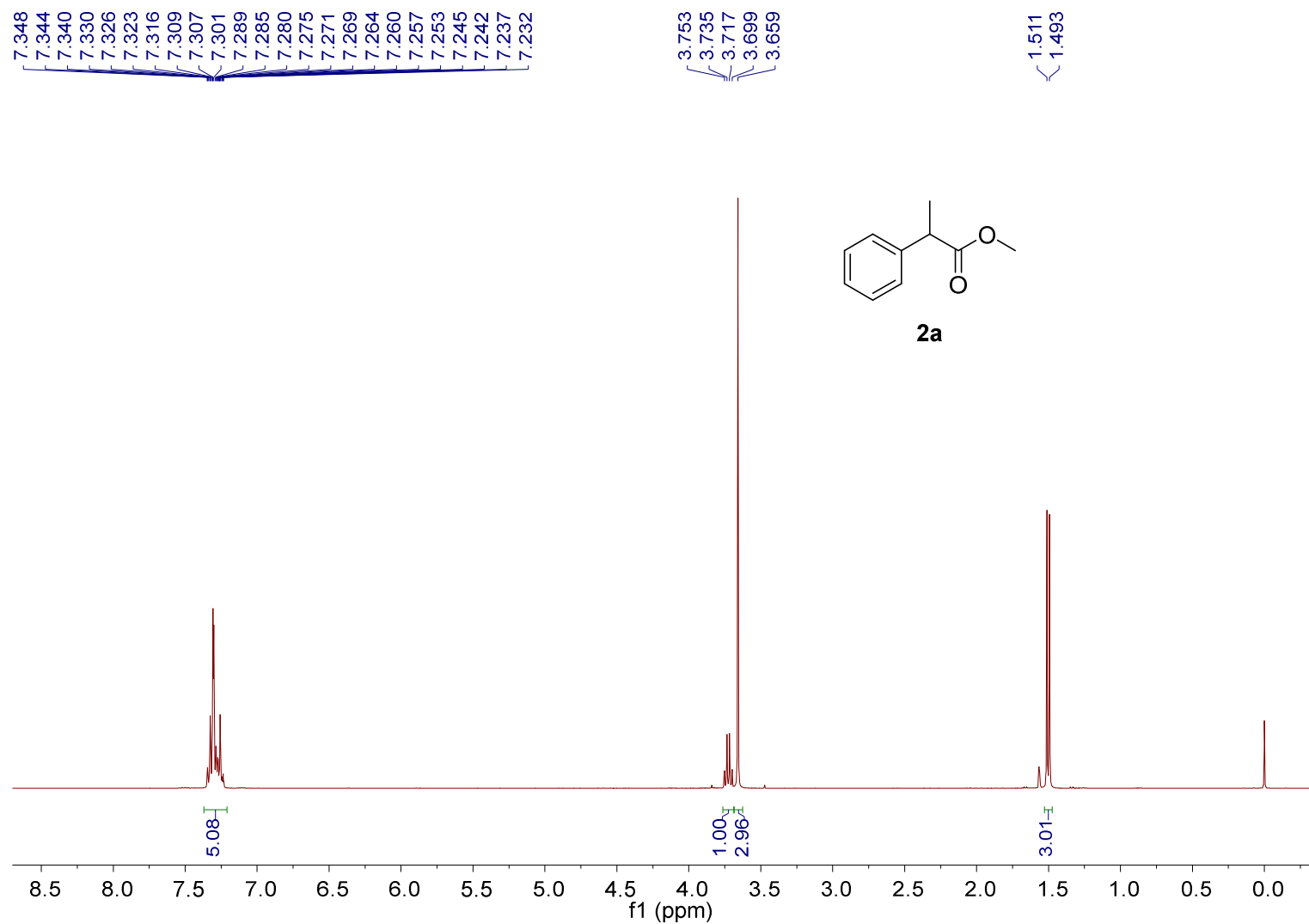


Figure S50. ¹H NMR spectrum of **2a** (400 MHz, in CDCl₃).

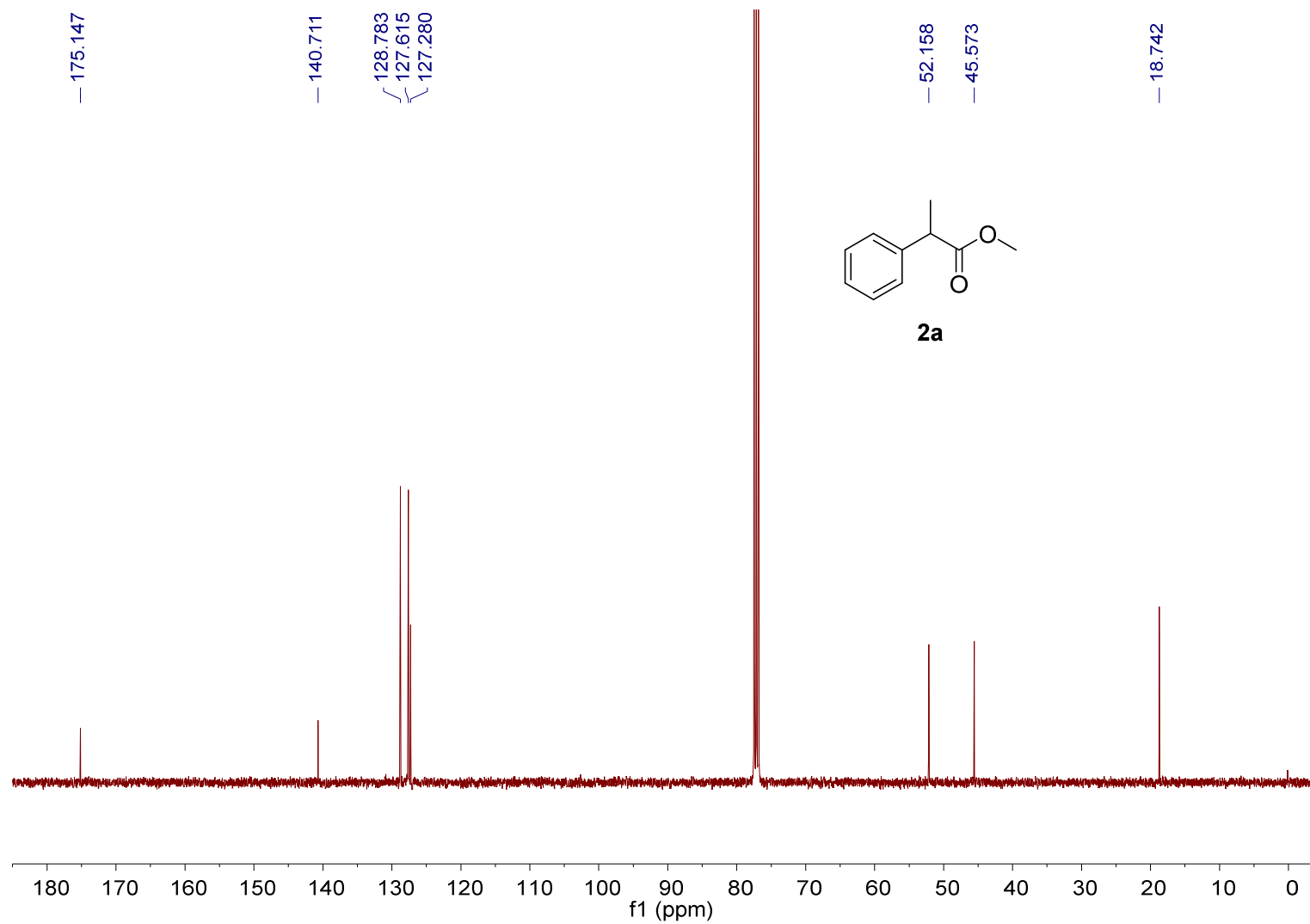


Figure S51. ¹³C NMR spectrum of **2a** (101 MHz, in CDCl₃).

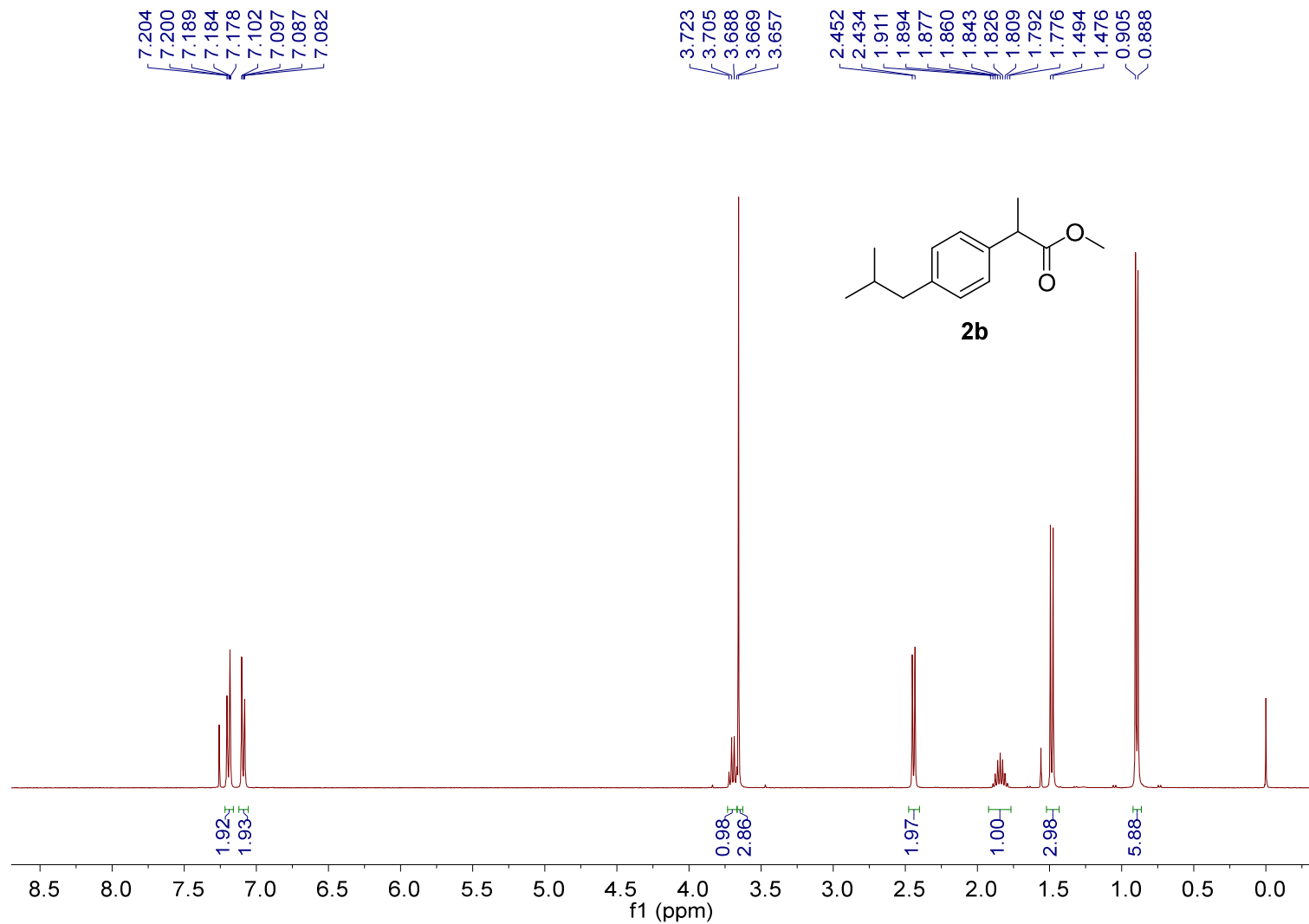


Figure S52. ¹H NMR spectrum of **2b** (400 MHz, in CDCl₃).

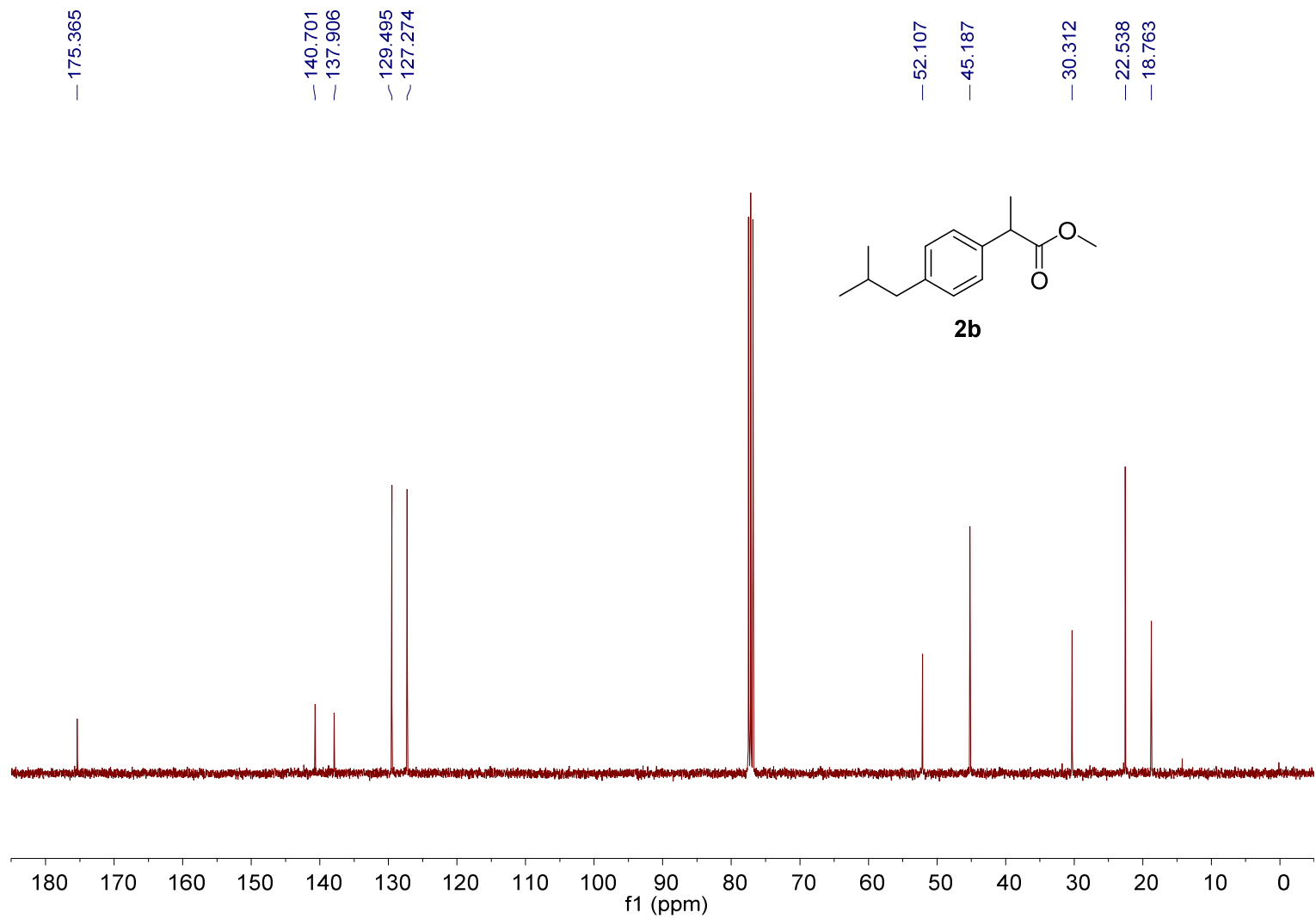


Figure S53. ^{13}C NMR spectrum of **2b** (101 MHz, in CDCl_3).

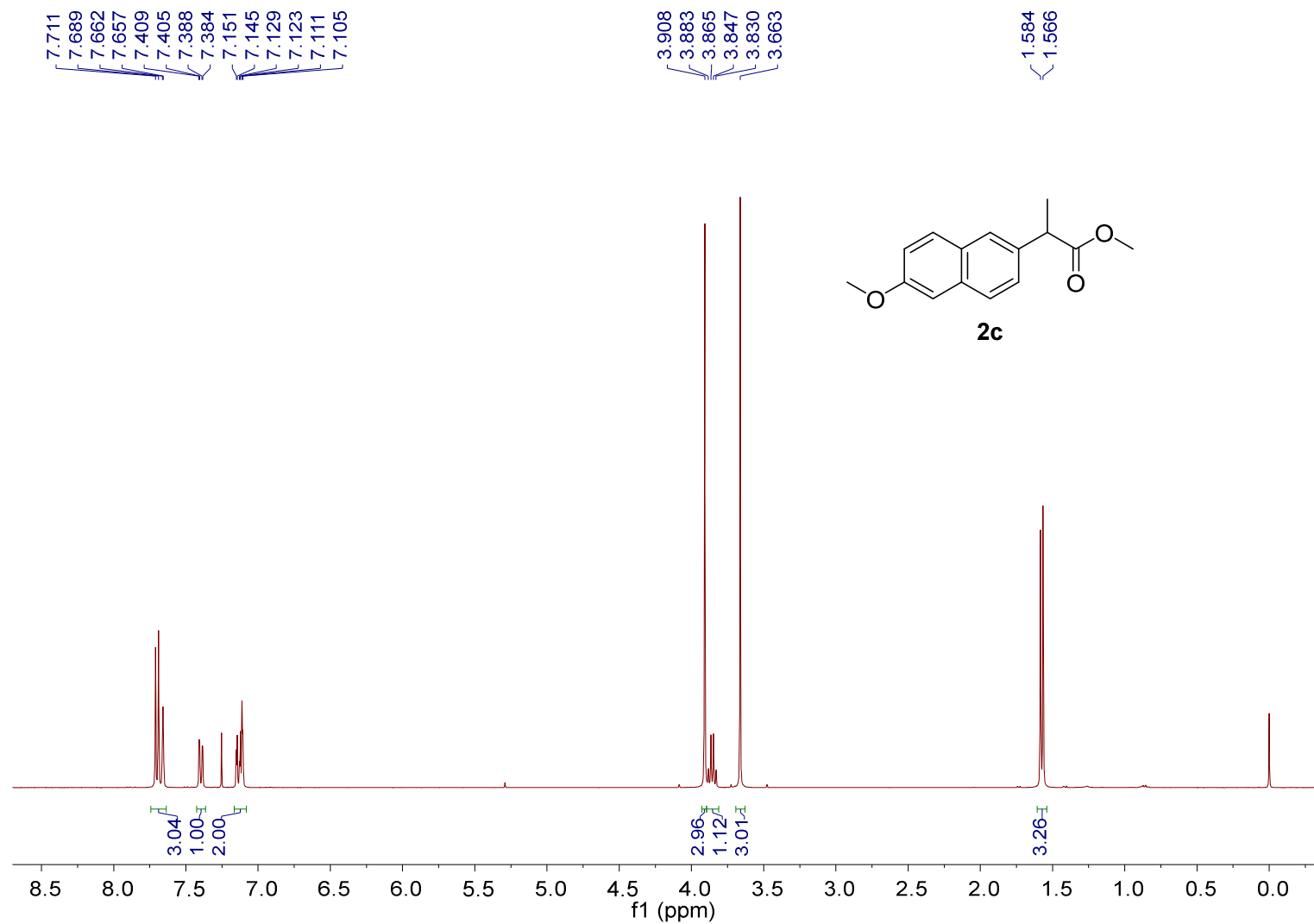


Figure S54. ^1H NMR spectrum of **2c** (400 MHz, in CDCl_3).

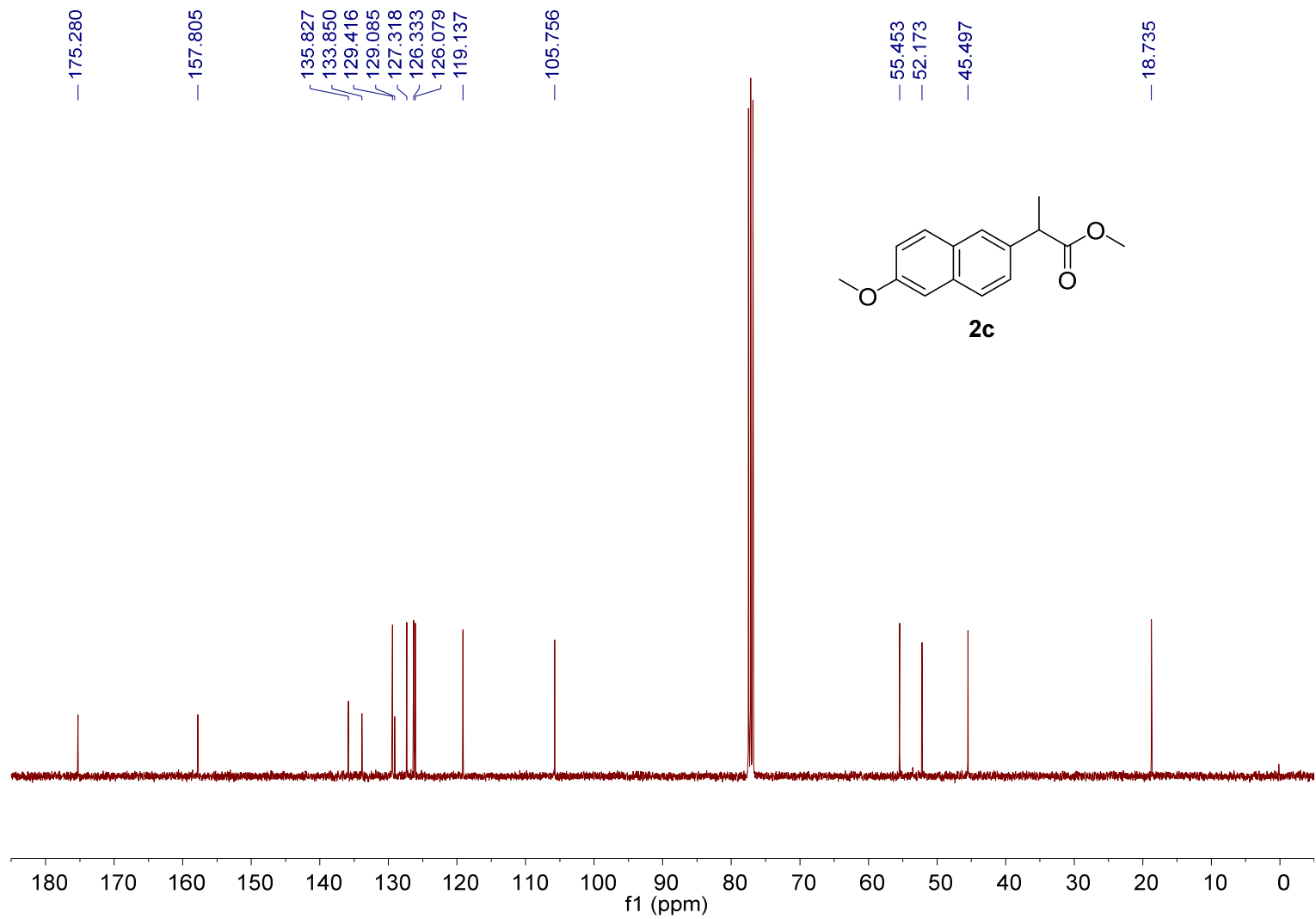


Figure S55. ¹³C NMR spectrum of **2c** (101 MHz, in CDCl₃).

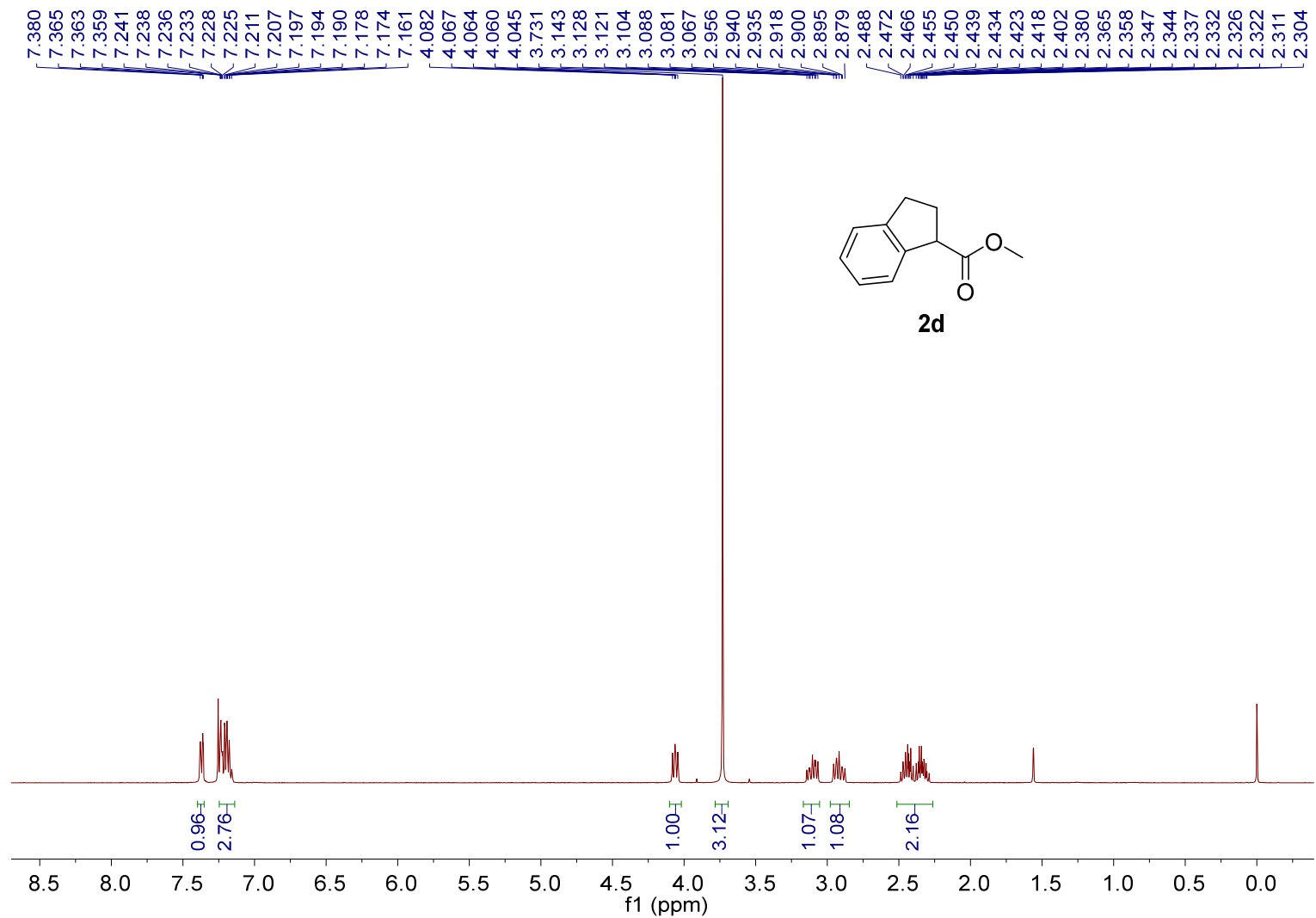


Figure S56. ¹H NMR spectrum of **2d** (400 MHz, in CDCl₃).

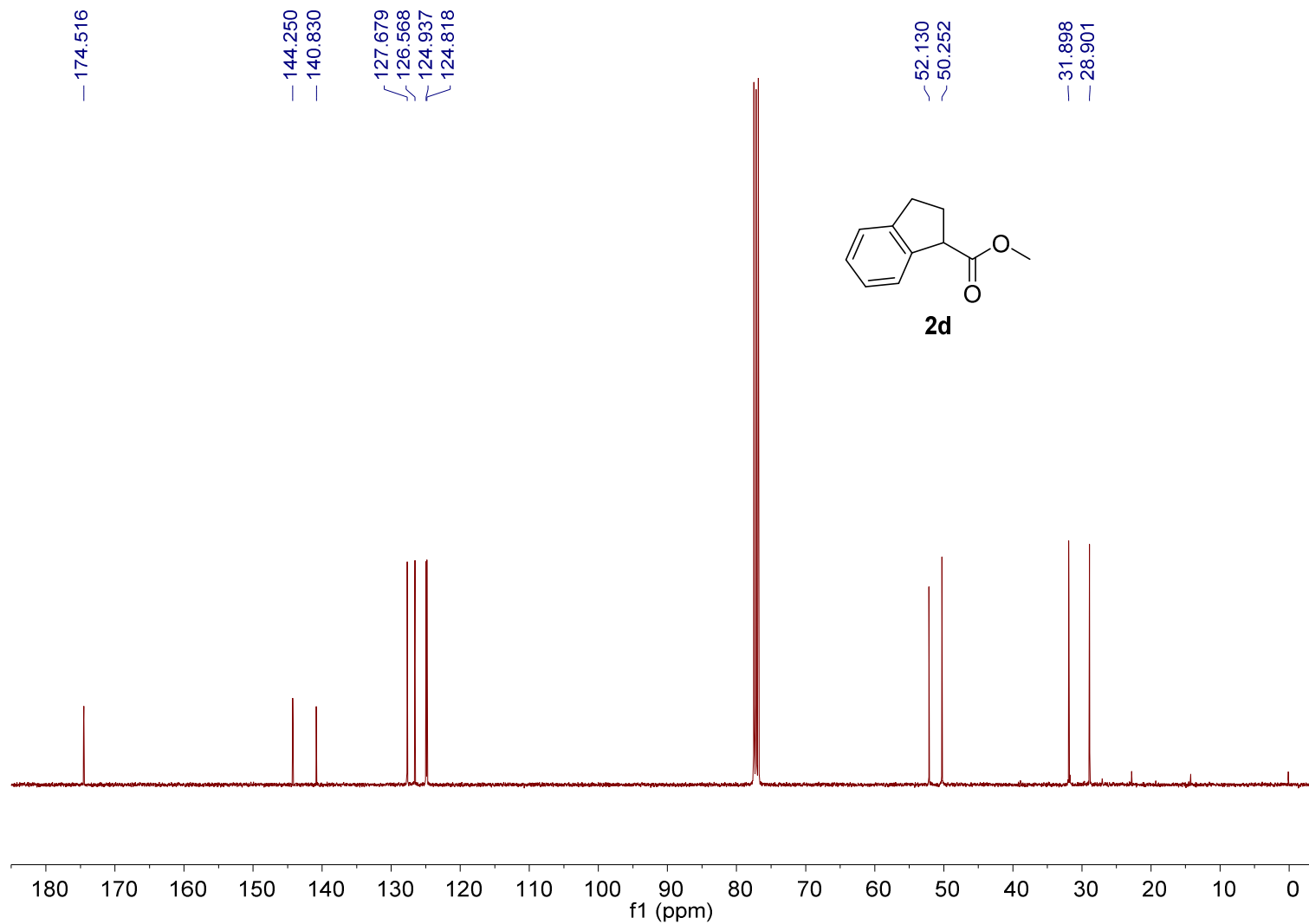


Figure S57. ^{13}C NMR spectrum of **2d** (101 MHz, in CDCl_3).

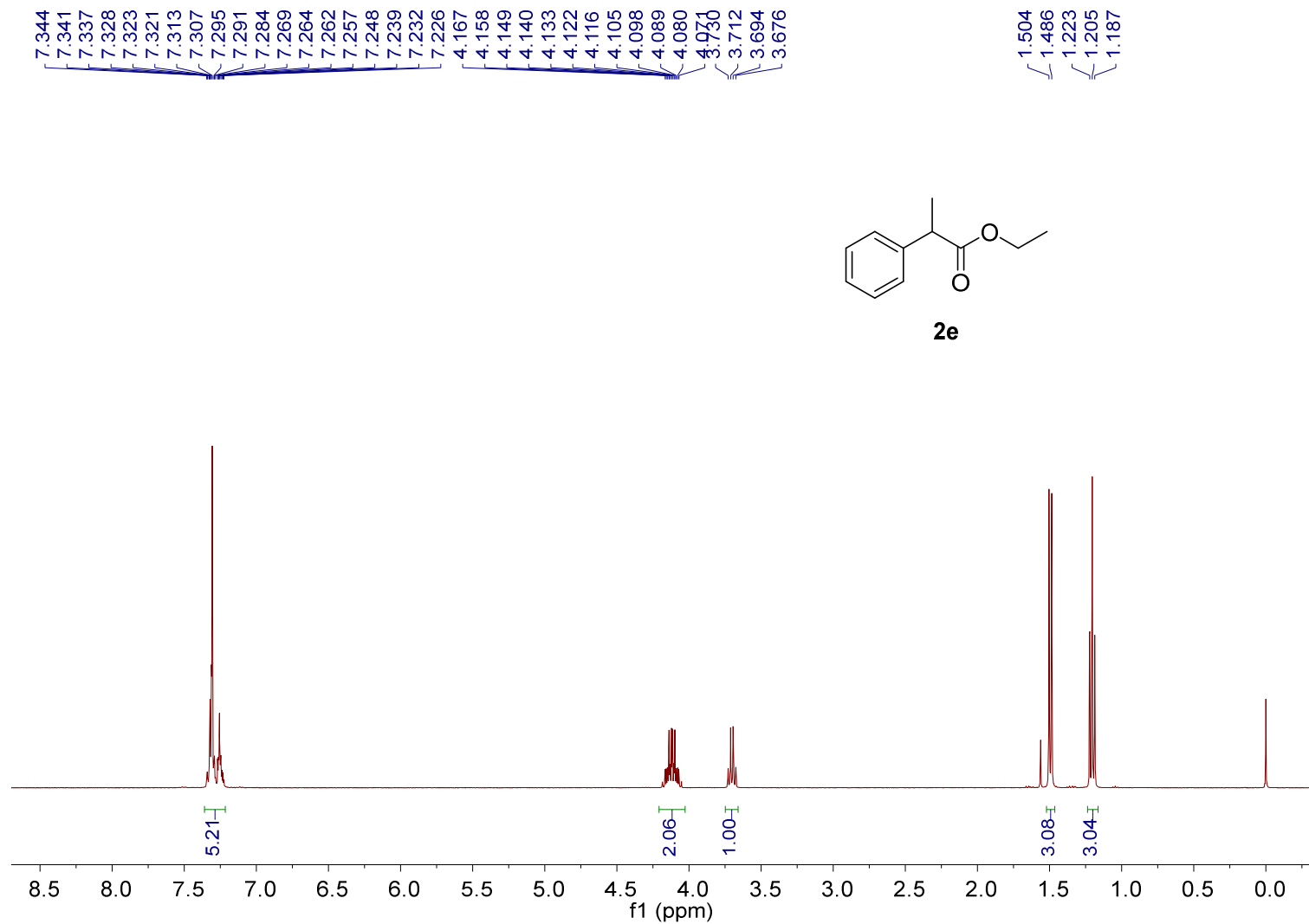


Figure S58. ¹H NMR spectrum of **2e** (400 MHz, in CDCl₃).

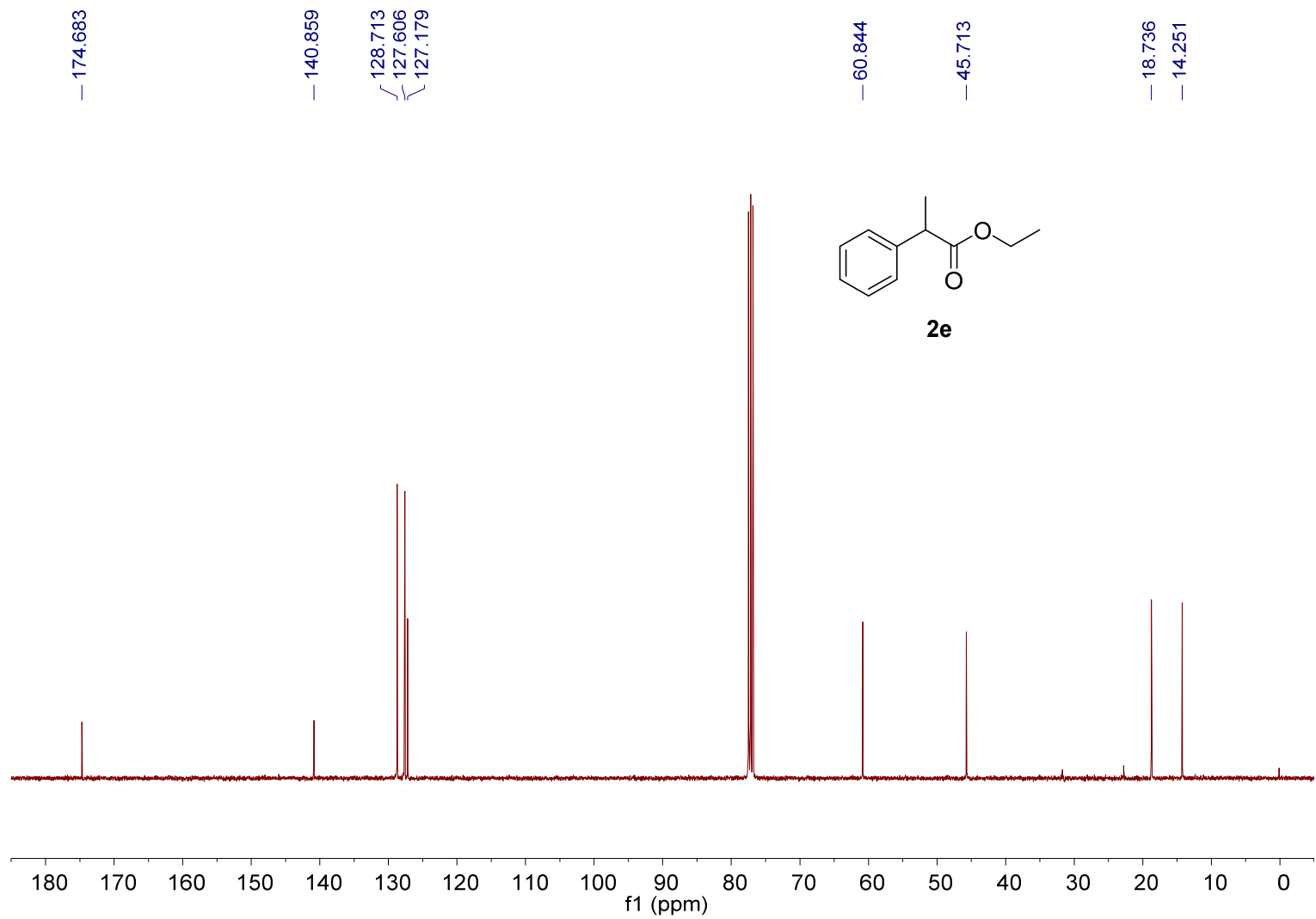


Figure S59. ¹³C NMR spectrum of **2e** (101 MHz, in CDCl₃).

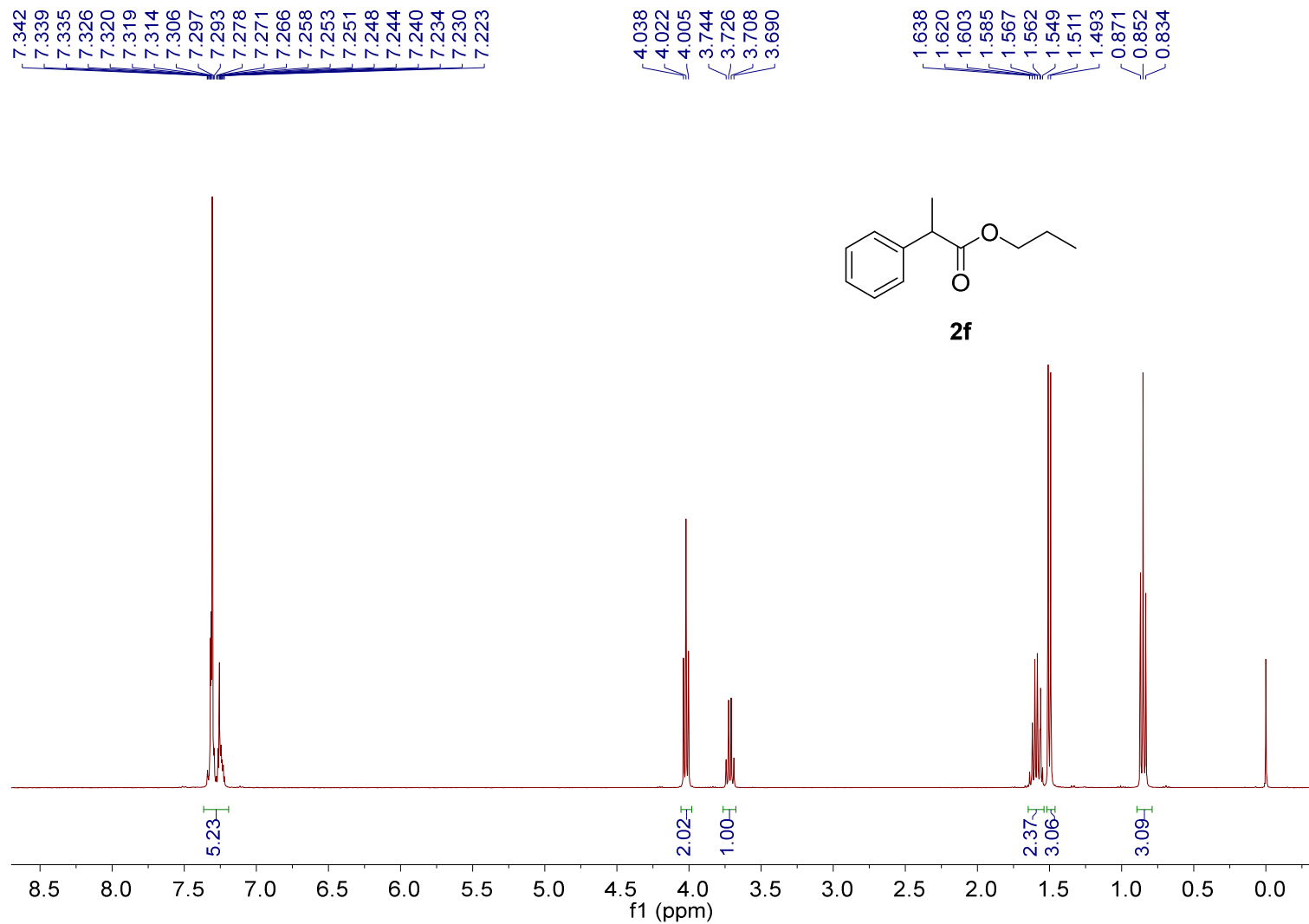


Figure S60. ¹H NMR spectrum of **2f** (400 MHz, in CDCl₃).

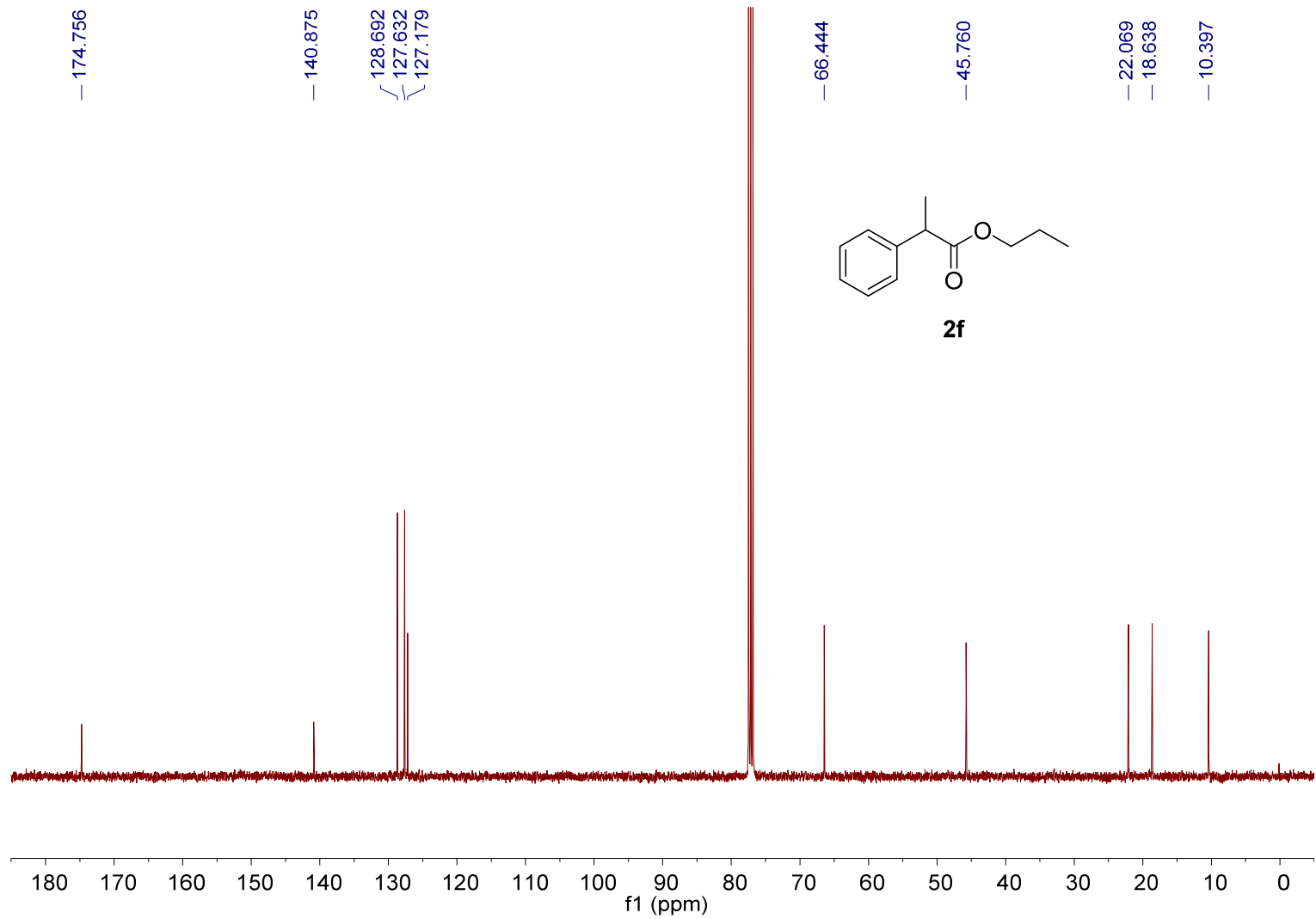


Figure S61. ¹³C NMR spectrum of **2f** (101 MHz, in CDCl₃).

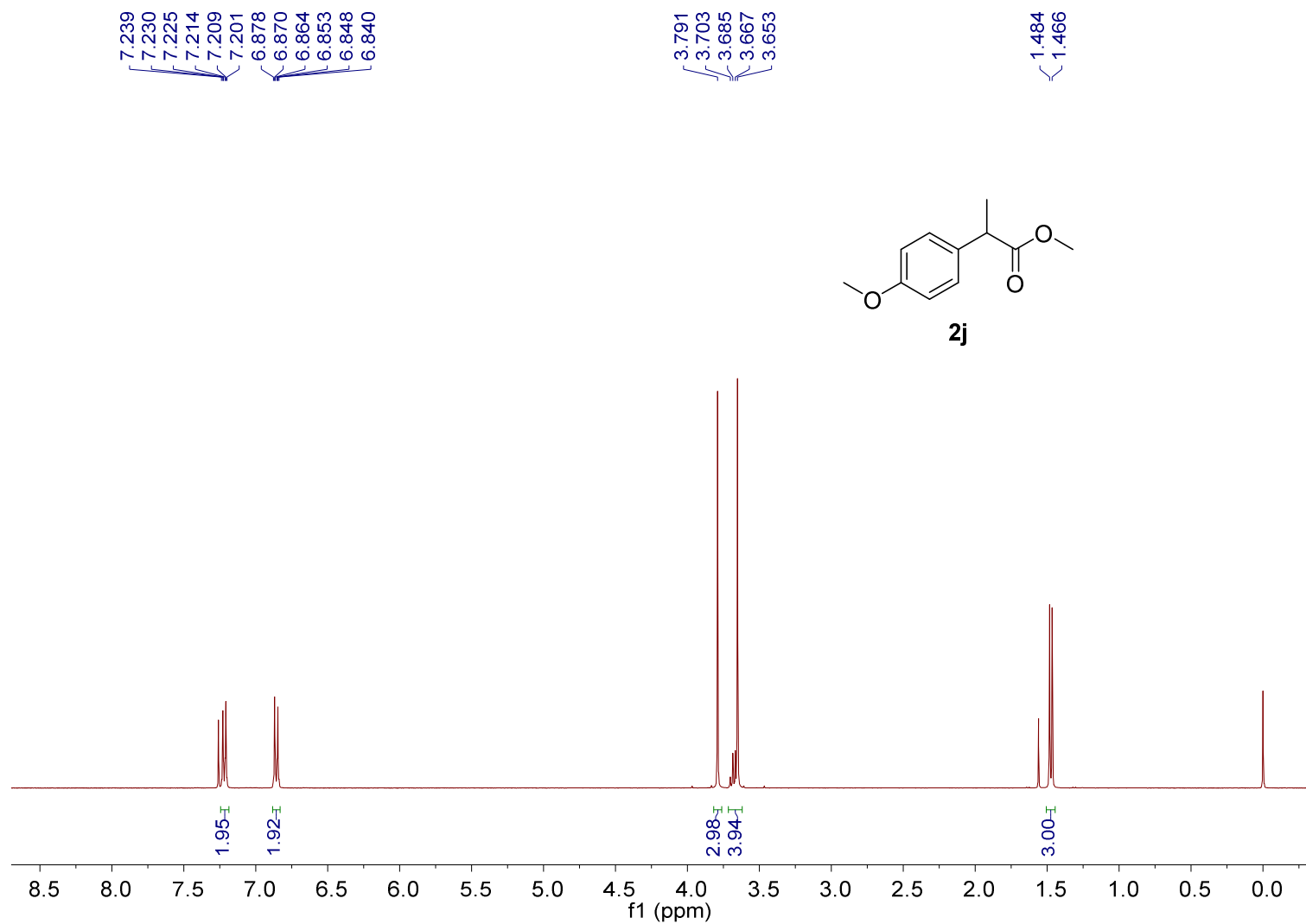


Figure S62. ¹H NMR spectrum of **2j** (400 MHz, in CDCl₃).

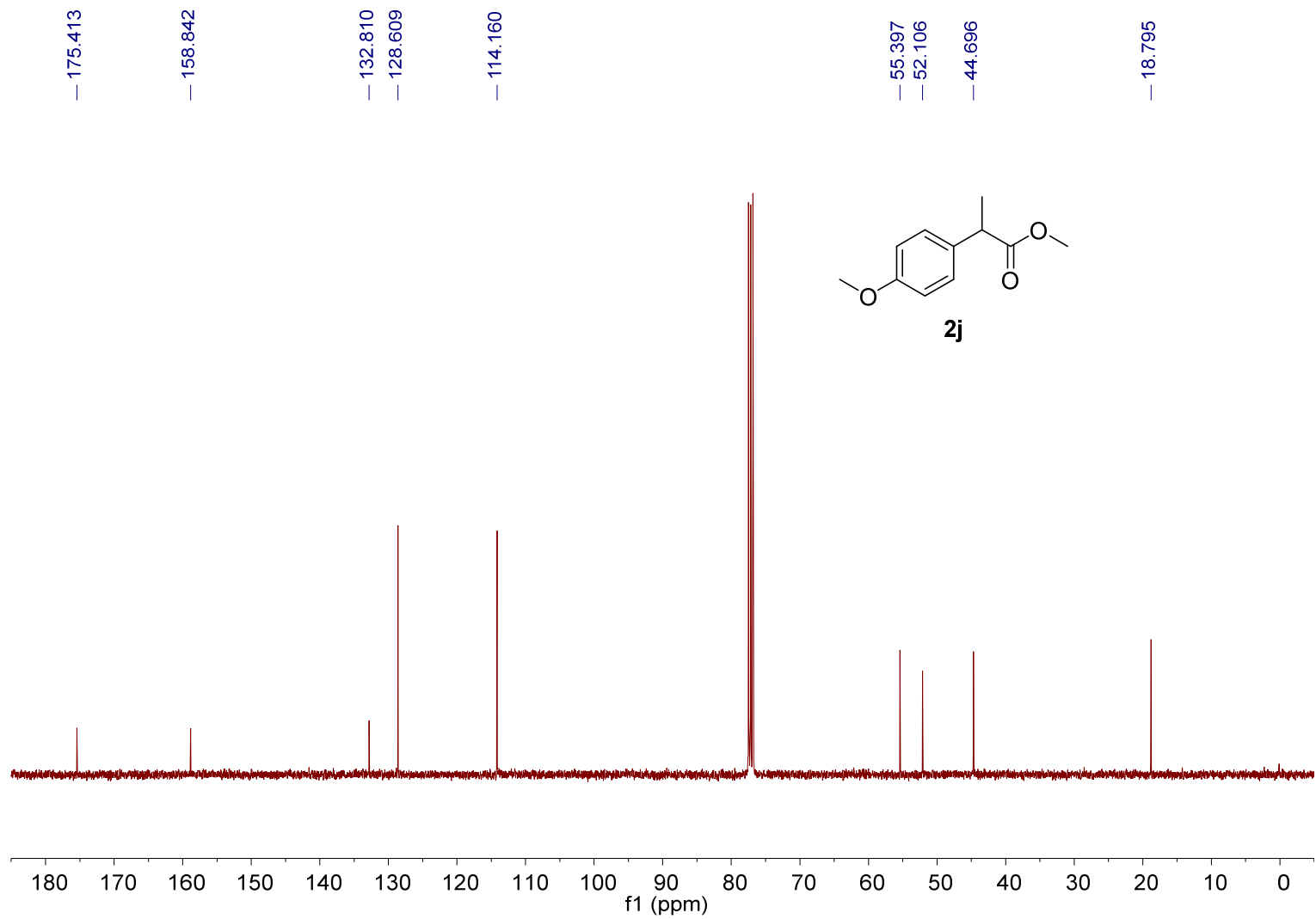


Figure S63. ¹³C NMR spectrum of **2j** (101 MHz, in CDCl₃).

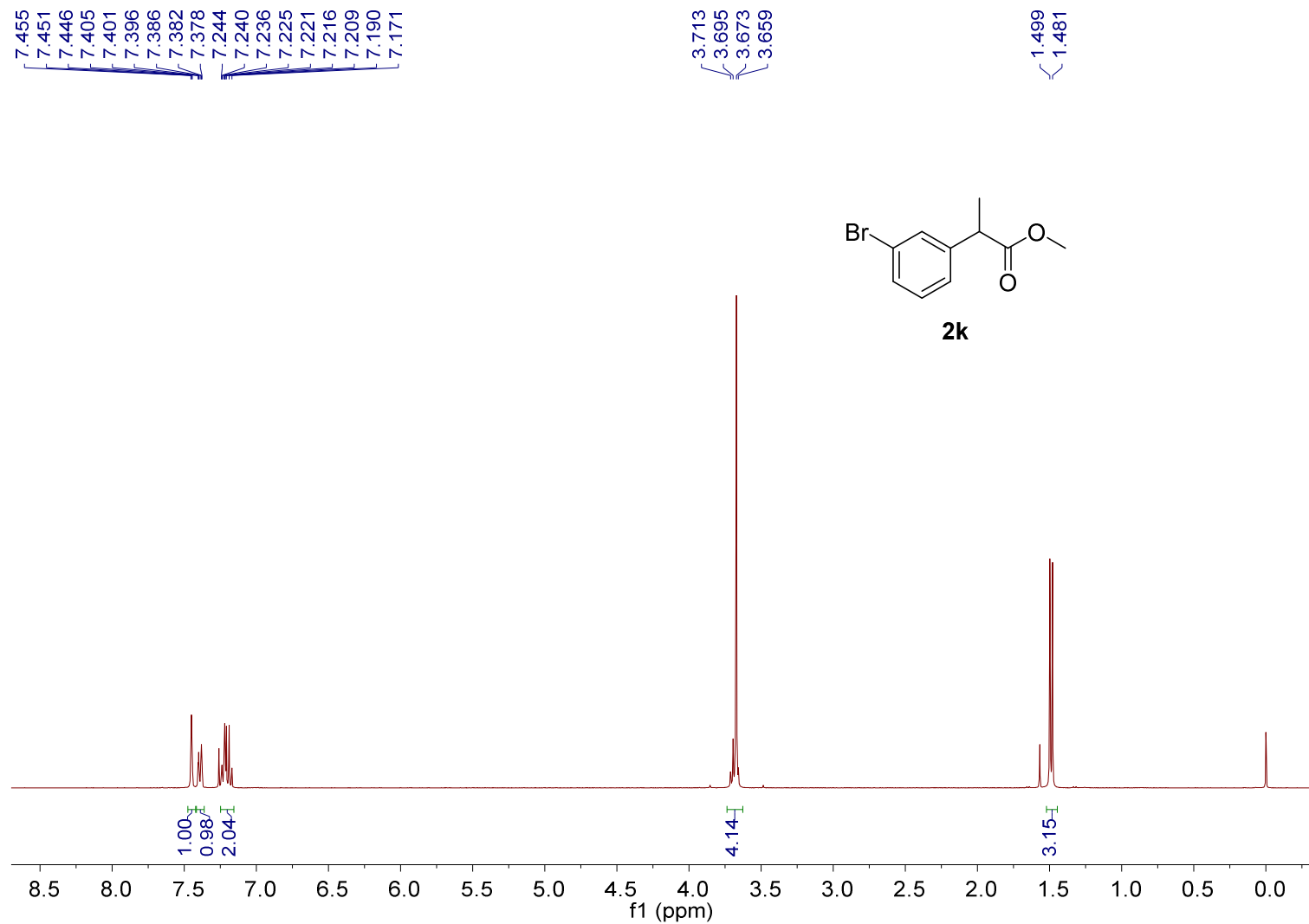


Figure S64. ^1H NMR spectrum of **2k** (400 MHz, in CDCl_3).

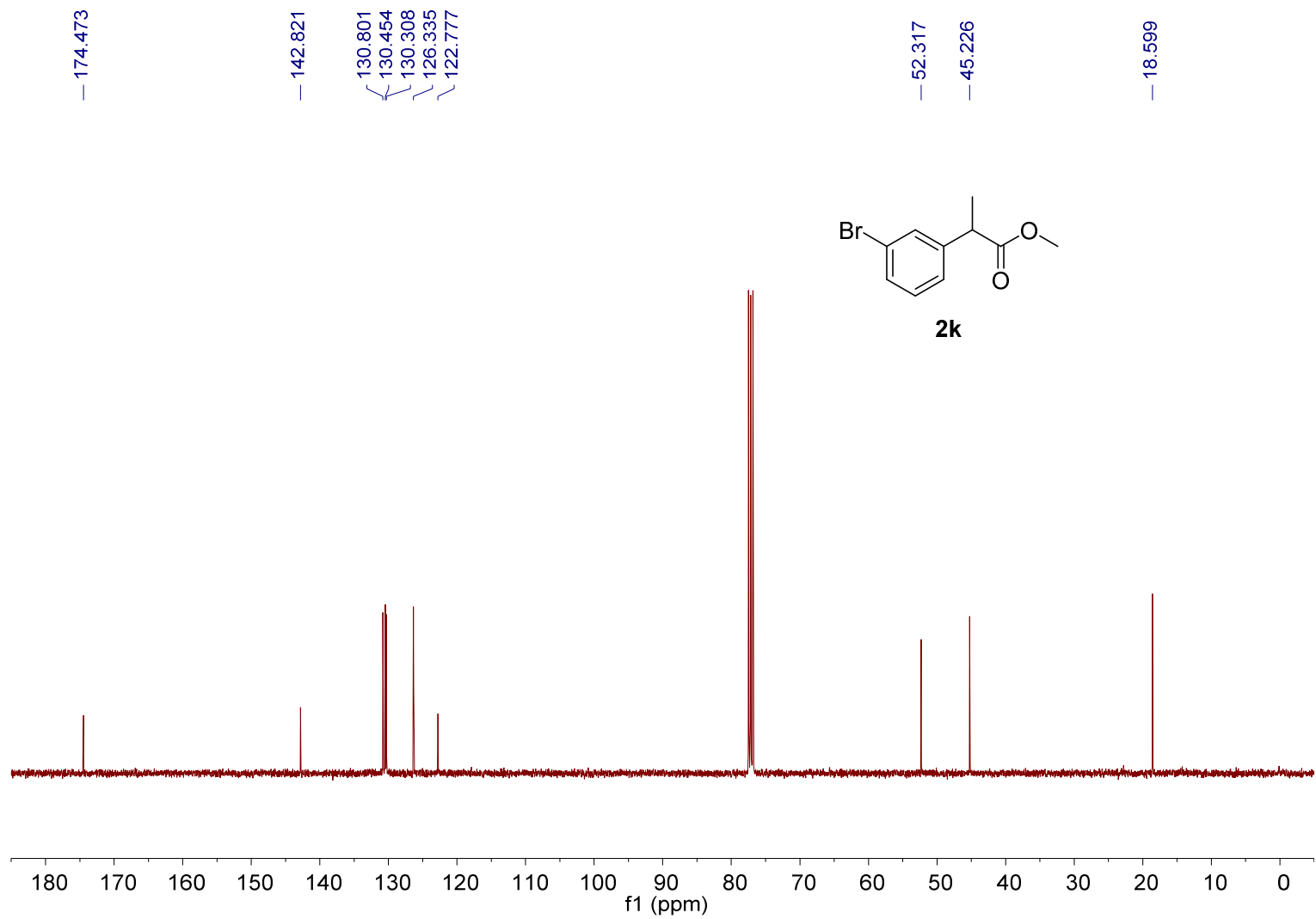


Figure S65. ^{13}C NMR spectrum of **2k** (101 MHz, in CDCl_3).

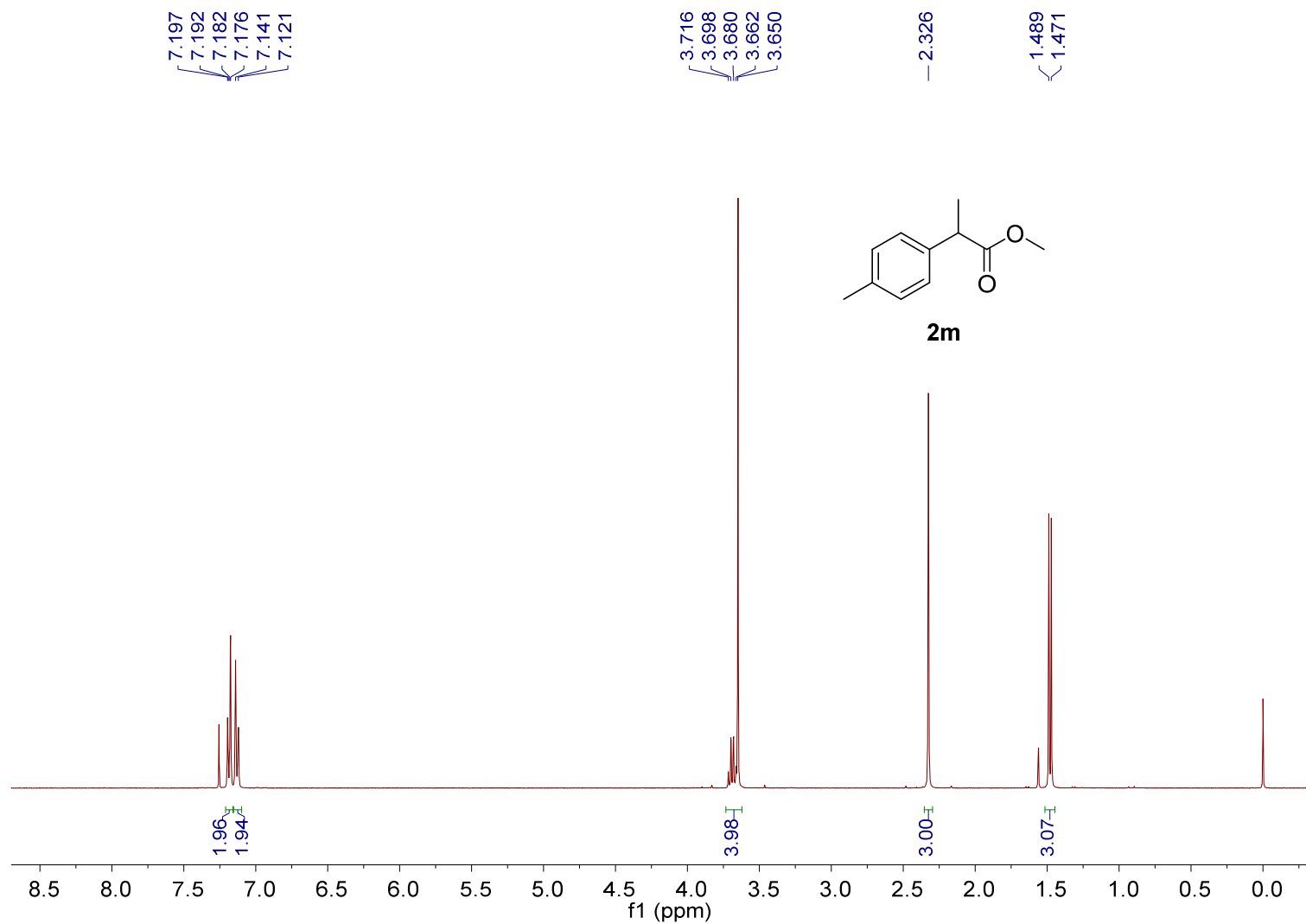


Figure S66. ^1H NMR spectrum of **2m** (400 MHz, in CDCl_3).

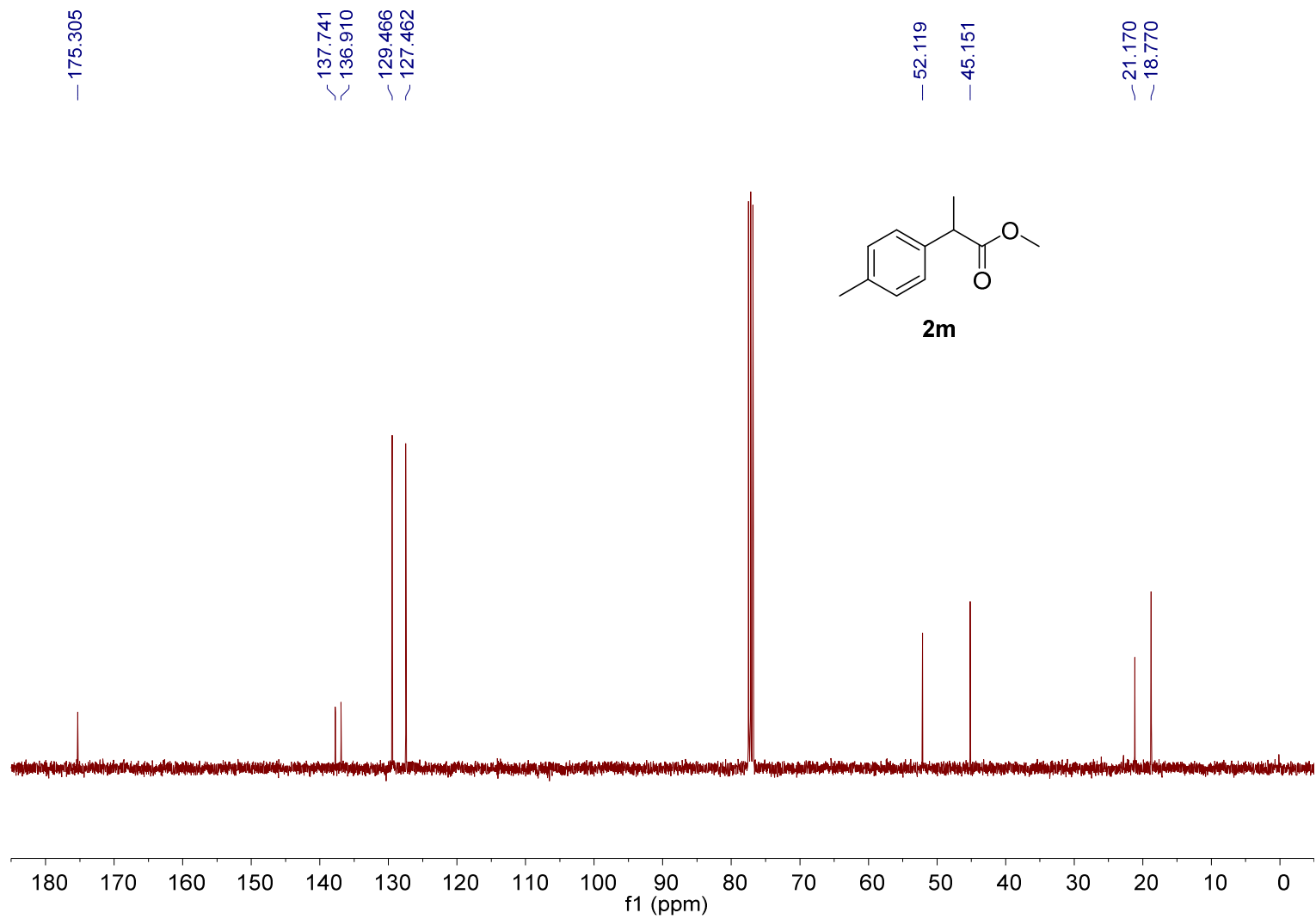


Figure S67. ^{13}C NMR spectrum of **2m** (101 MHz, in CDCl_3).

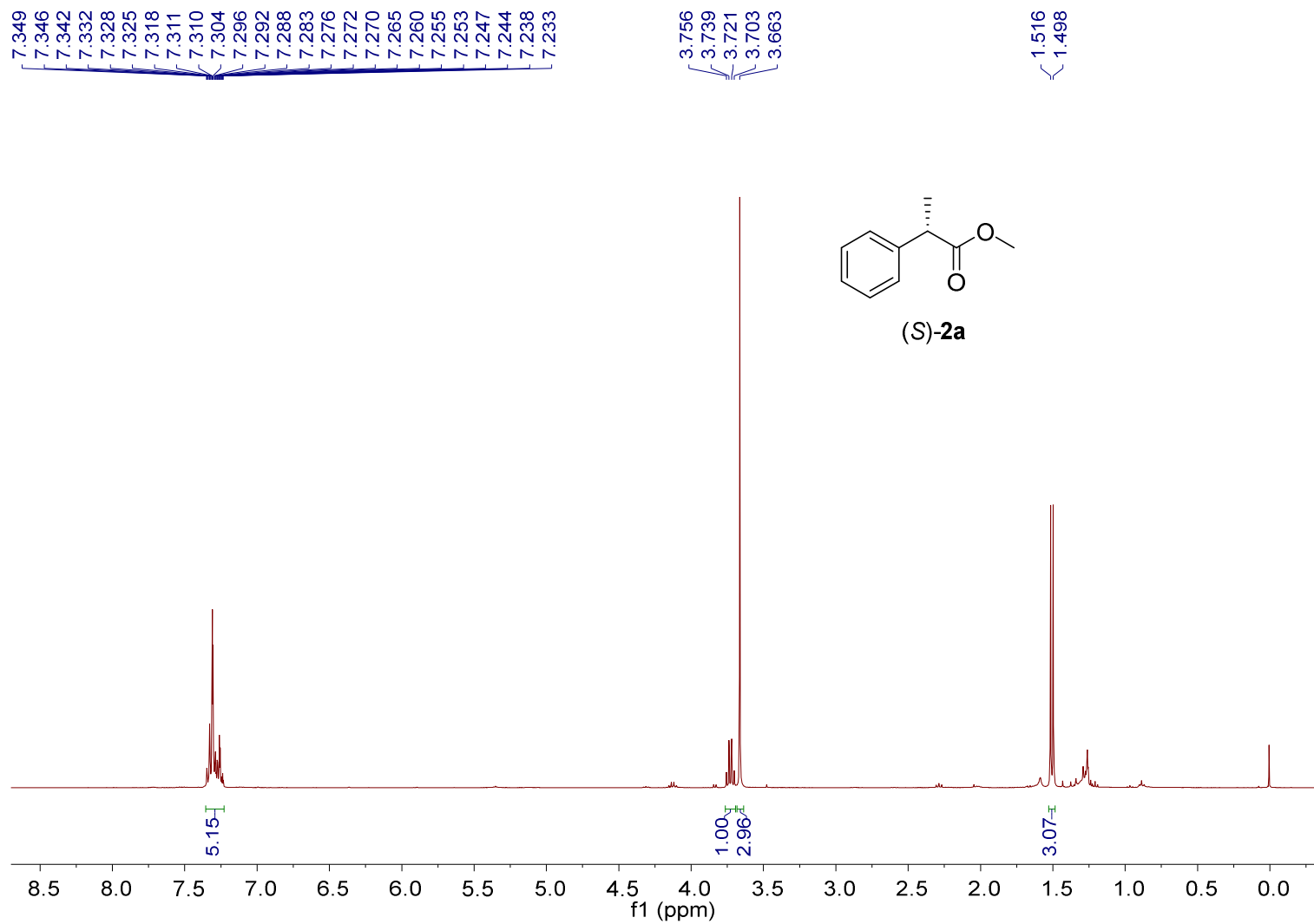


Figure S68. ^1H NMR spectrum of (S)-2a (400 MHz, in CDCl_3).

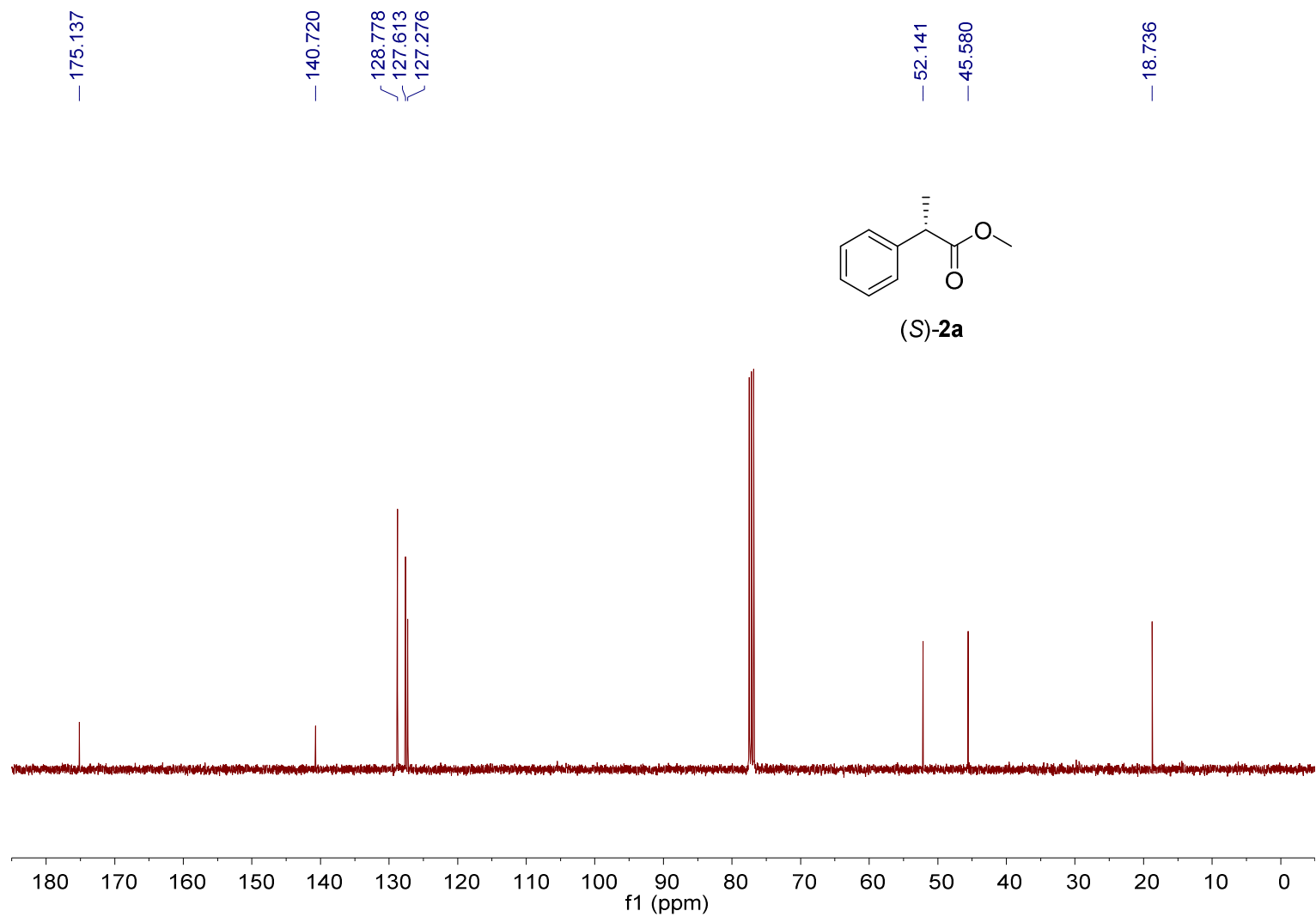


Figure S69. ^{13}C NMR spectrum of (S)-2a (101 MHz, in CDCl_3).

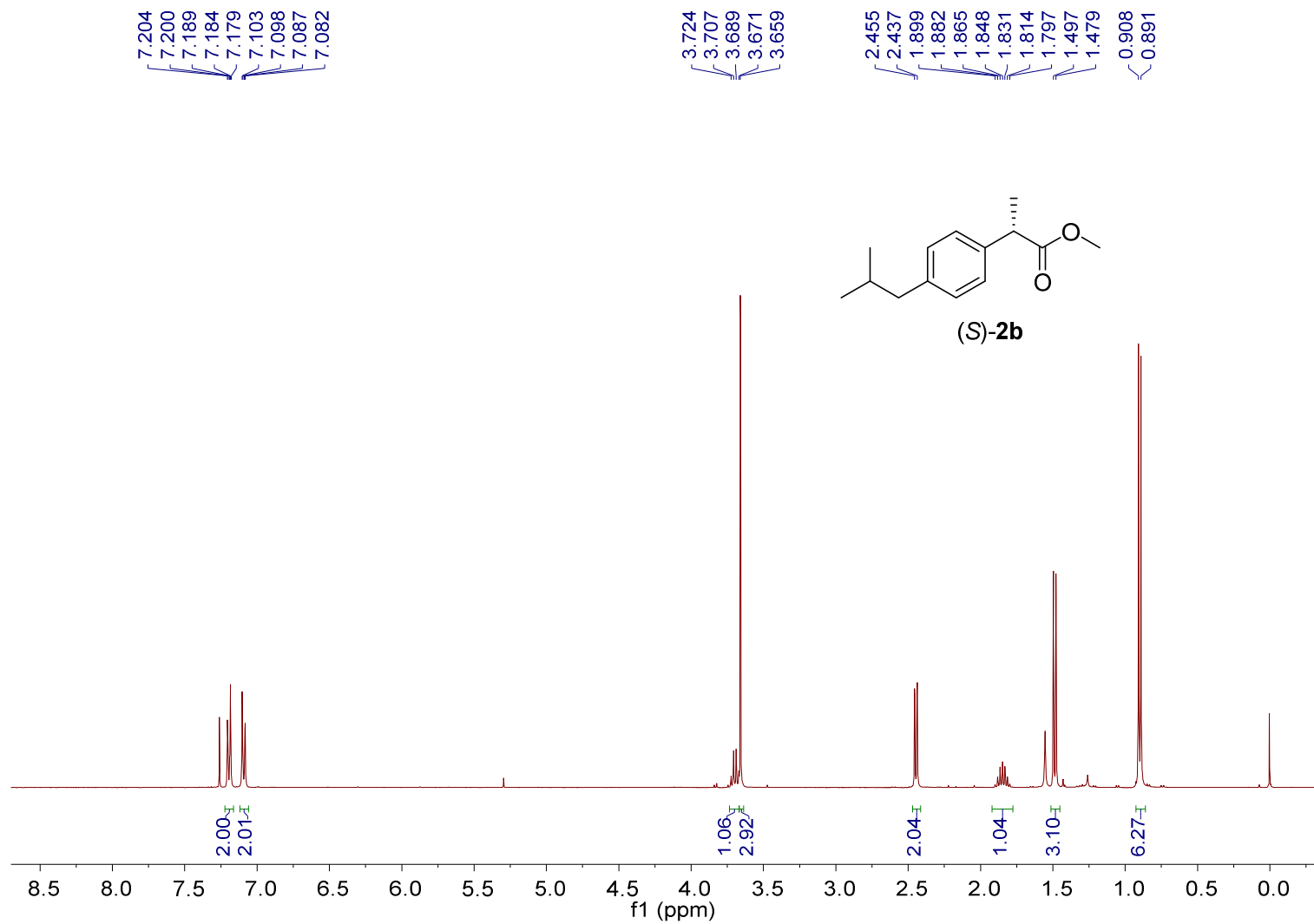


Figure S70. ^1H NMR spectrum of (*S*)-**2b** (400 MHz, in CDCl_3).

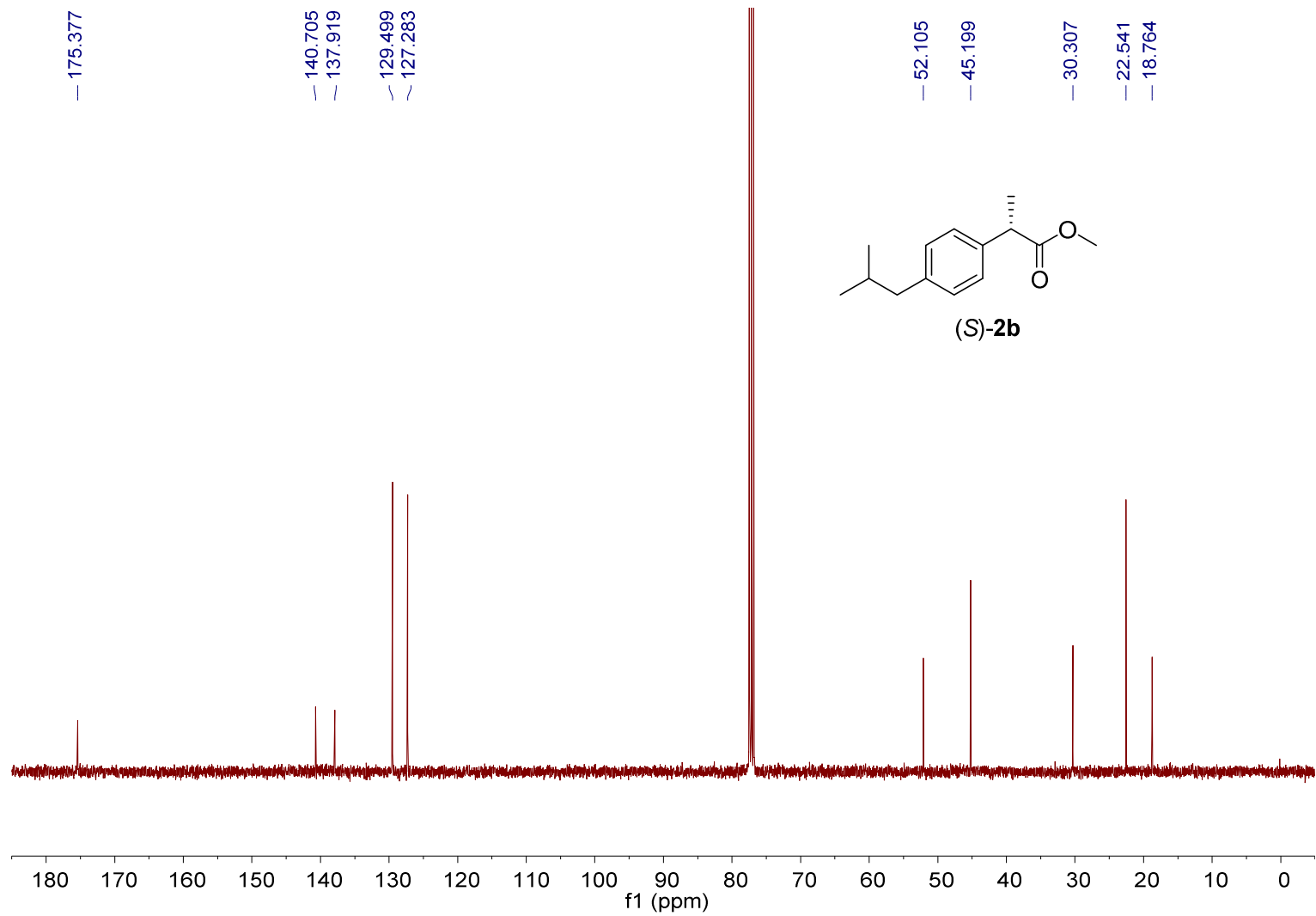


Figure S71. ^{13}C NMR spectrum of (S)-2b (101 MHz, in CDCl_3).

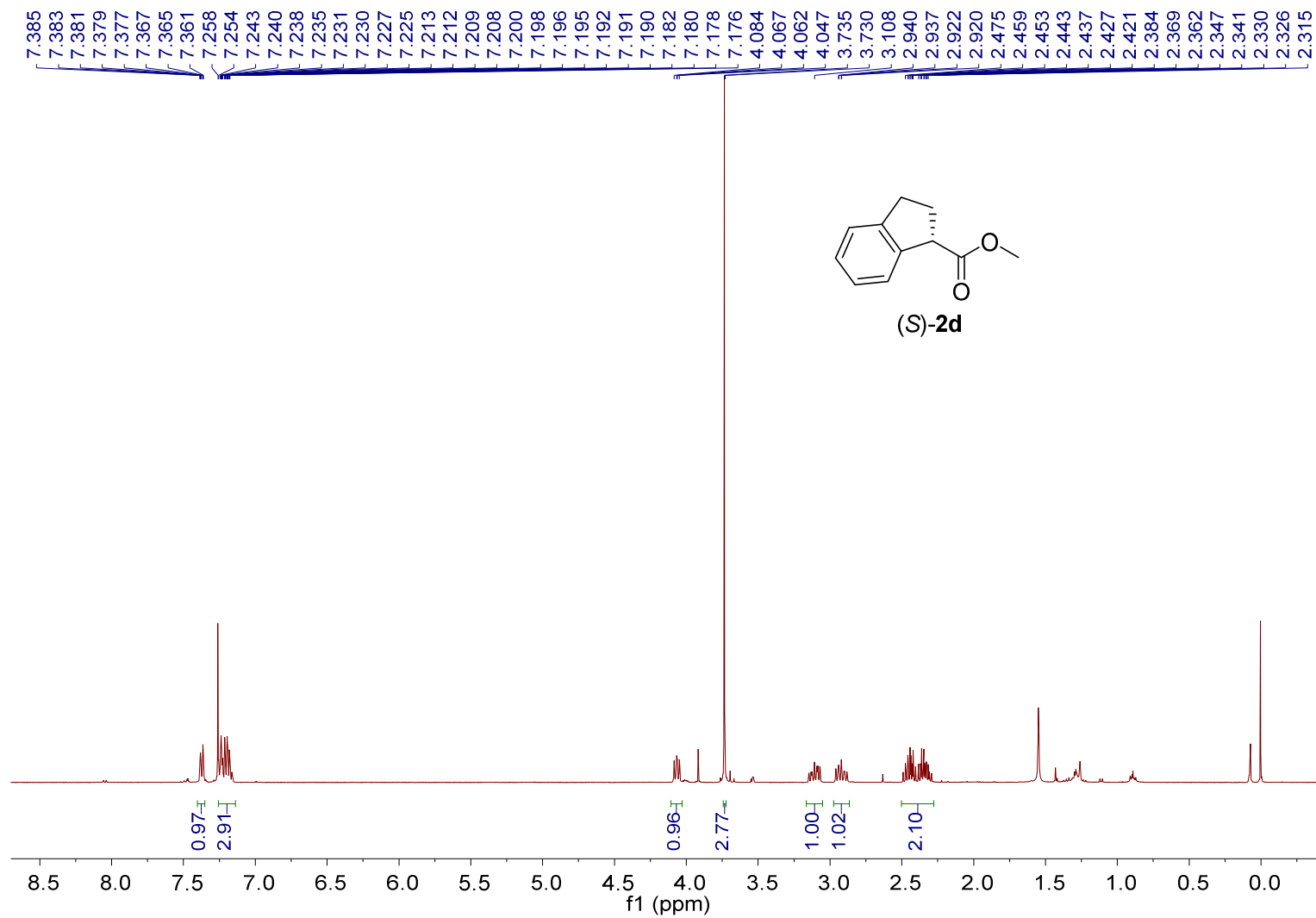


Figure S72. ¹H NMR spectrum of (S)-2d (400 MHz, in CDCl₃).

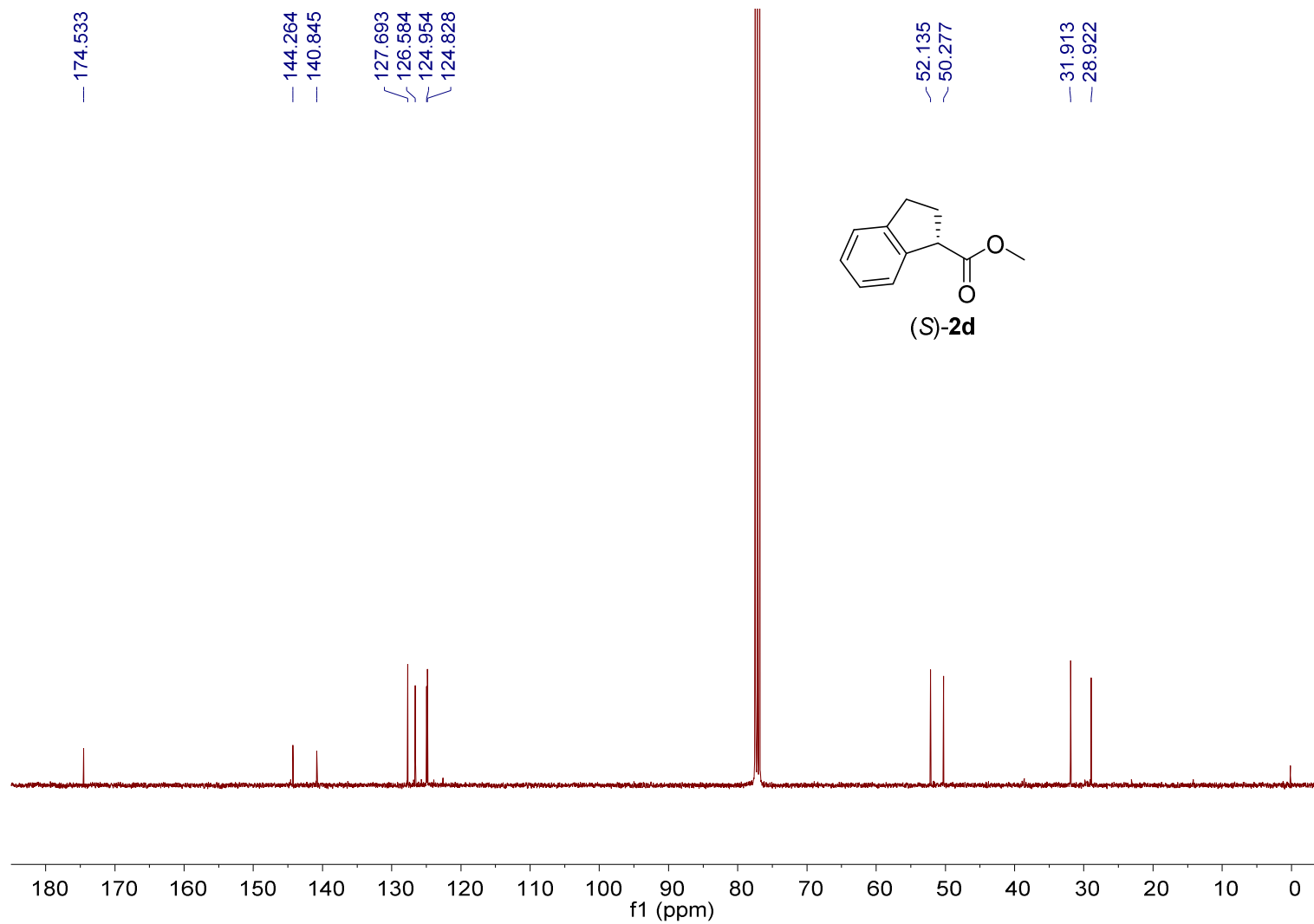


Figure S73. ^{13}C NMR spectrum of (S)-2d (101 MHz, in CDCl_3).

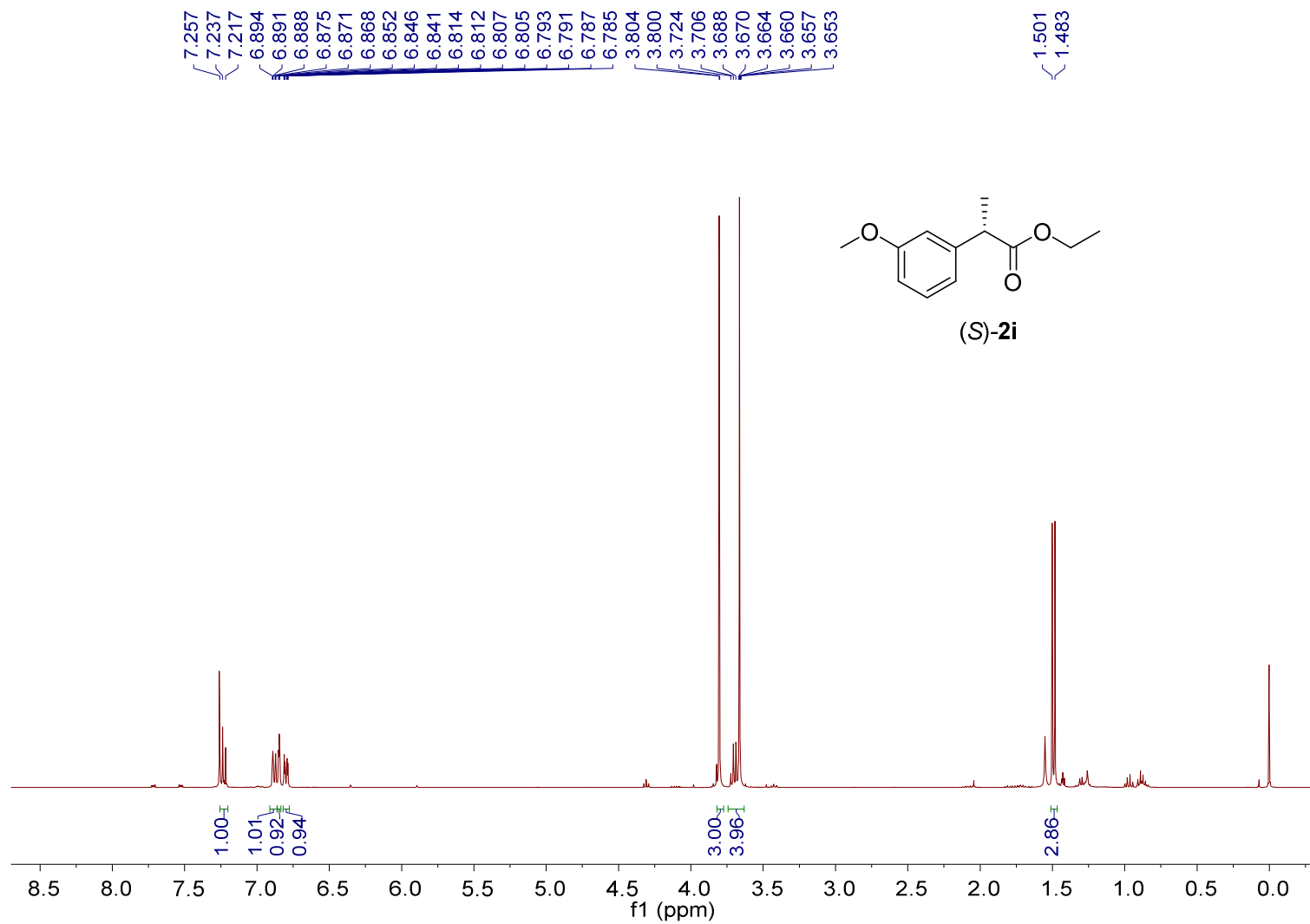


Figure S74. ¹H NMR spectrum of (S)-2i (400 MHz, in CDCl₃).

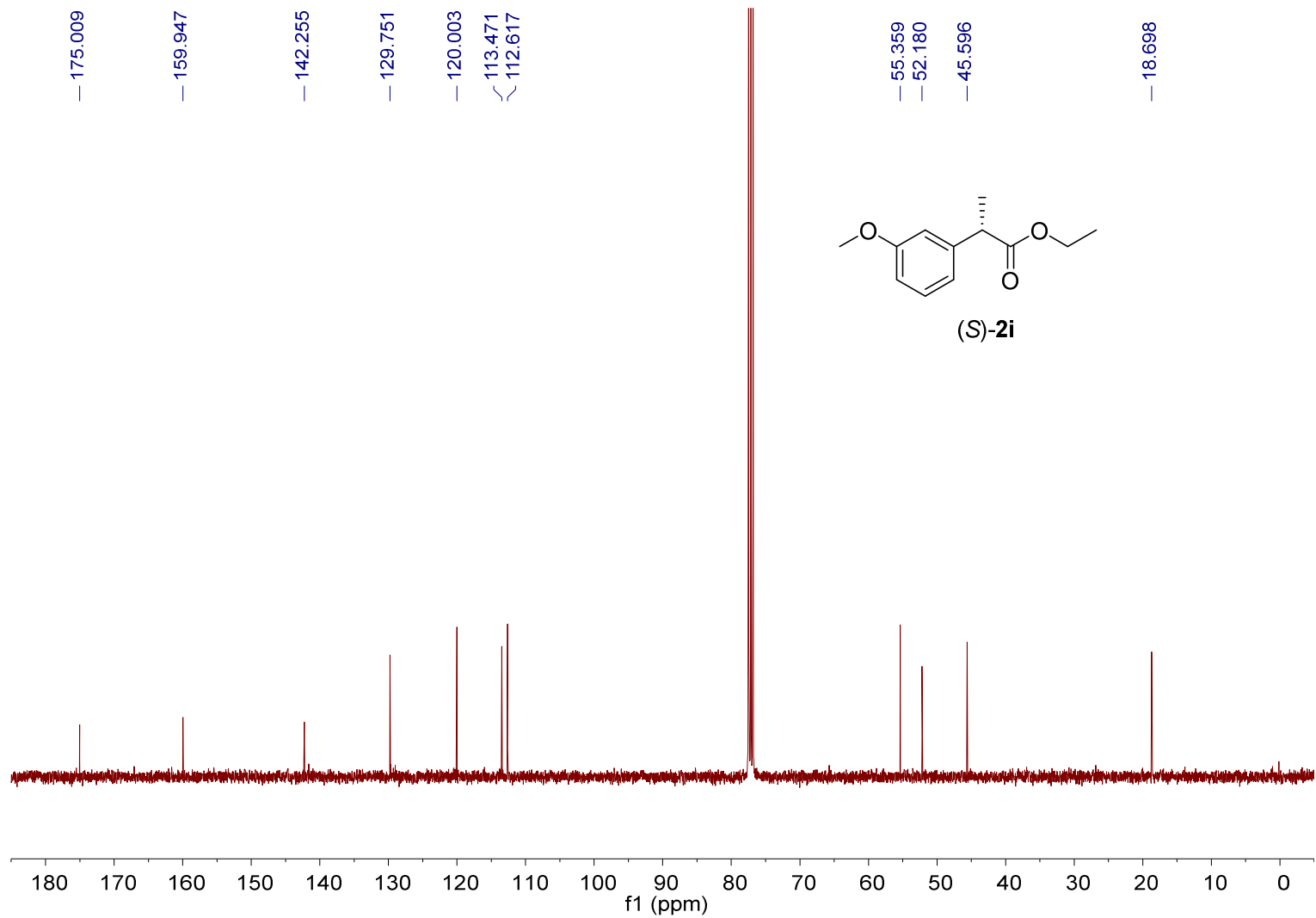


Figure S75. ¹³C NMR spectrum of (*S*)-**2i** (101 MHz, in CDCl₃).

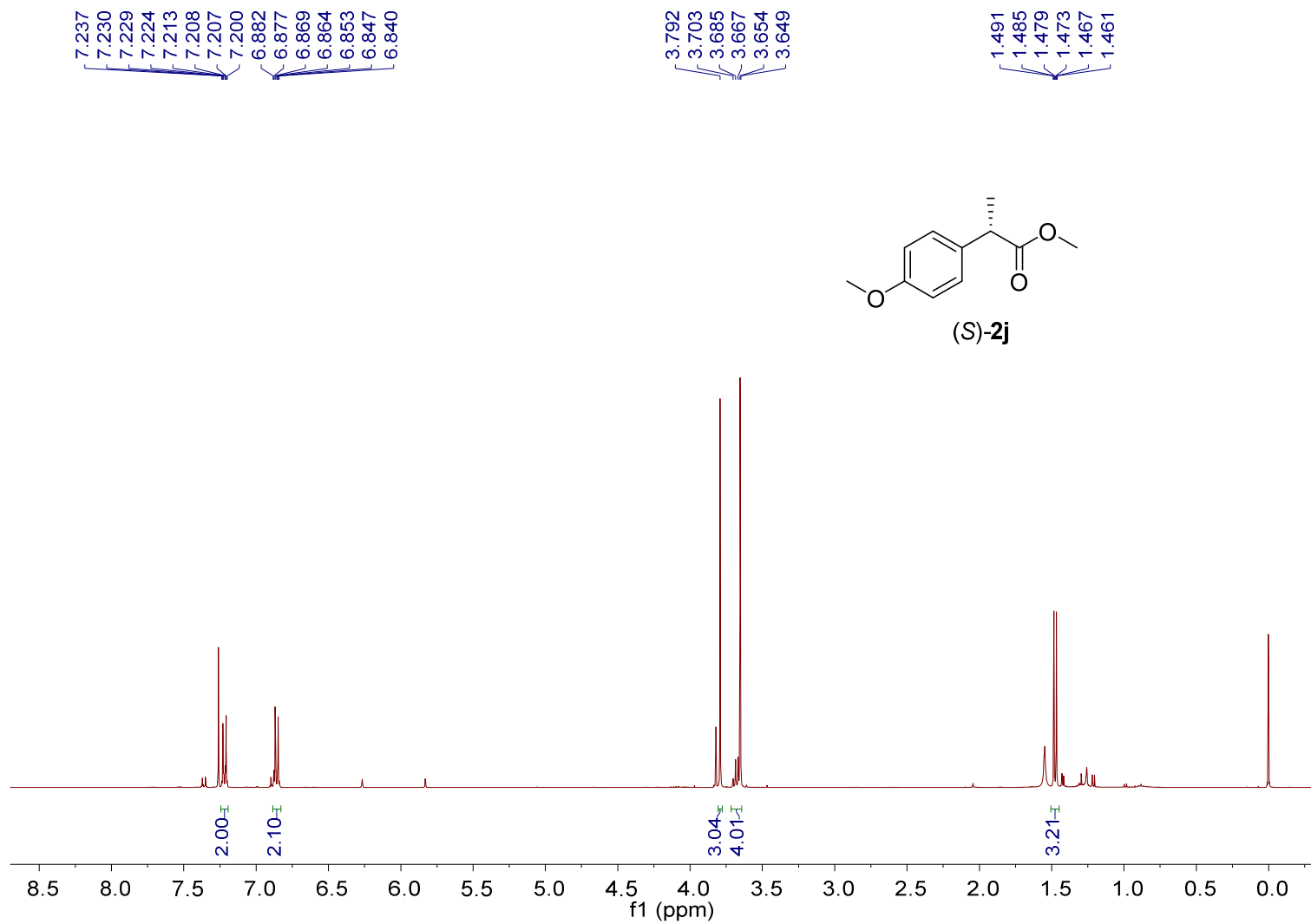


Figure S76. ^1H NMR spectrum of (S)-2j (400 MHz, in CDCl_3).

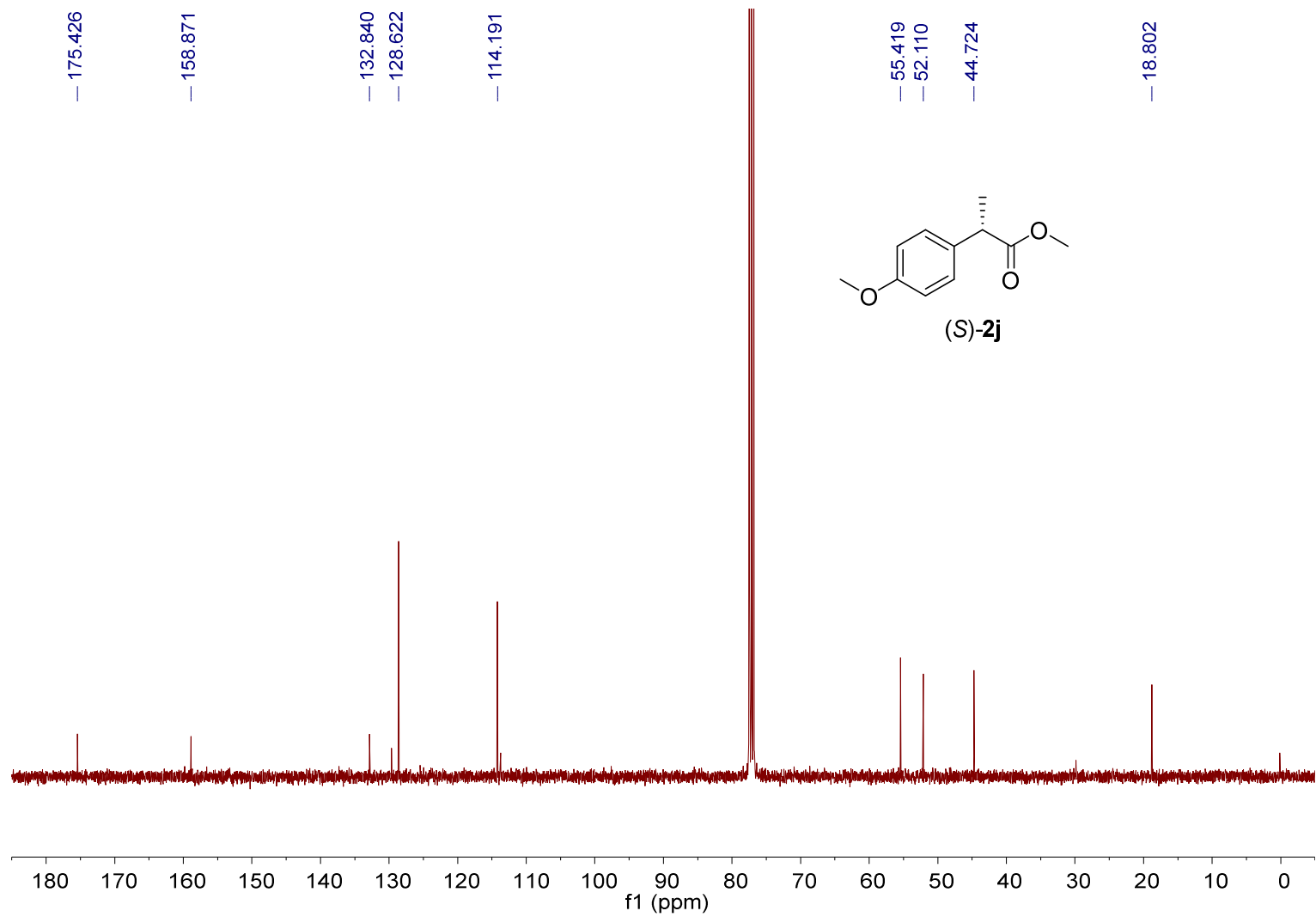


Figure S77. ^{13}C NMR spectrum of (S)-2j (101 MHz, in CDCl_3).

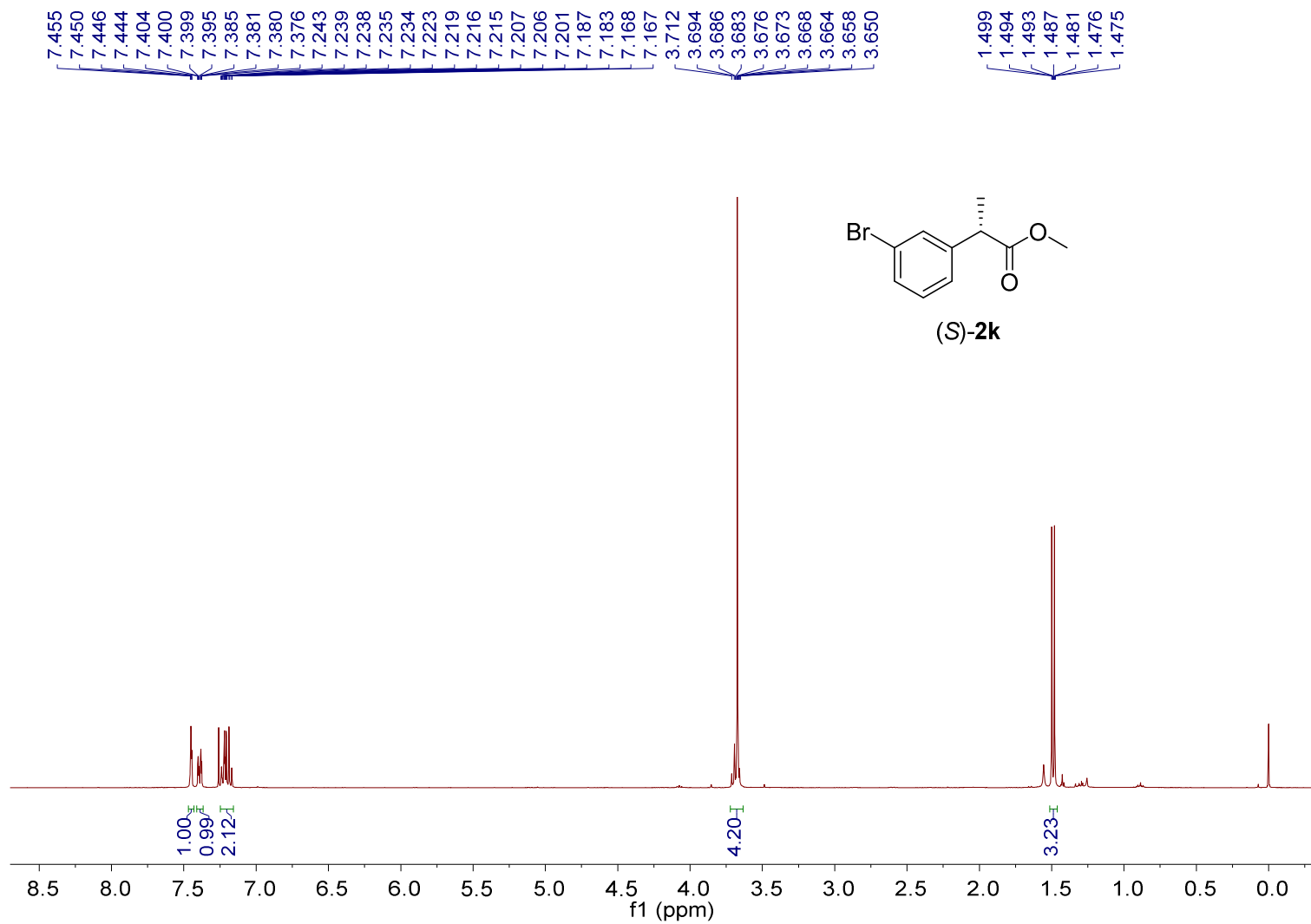


Figure S78. ^1H NMR spectrum of (*S*)-**2k** (400 MHz, in CDCl_3).

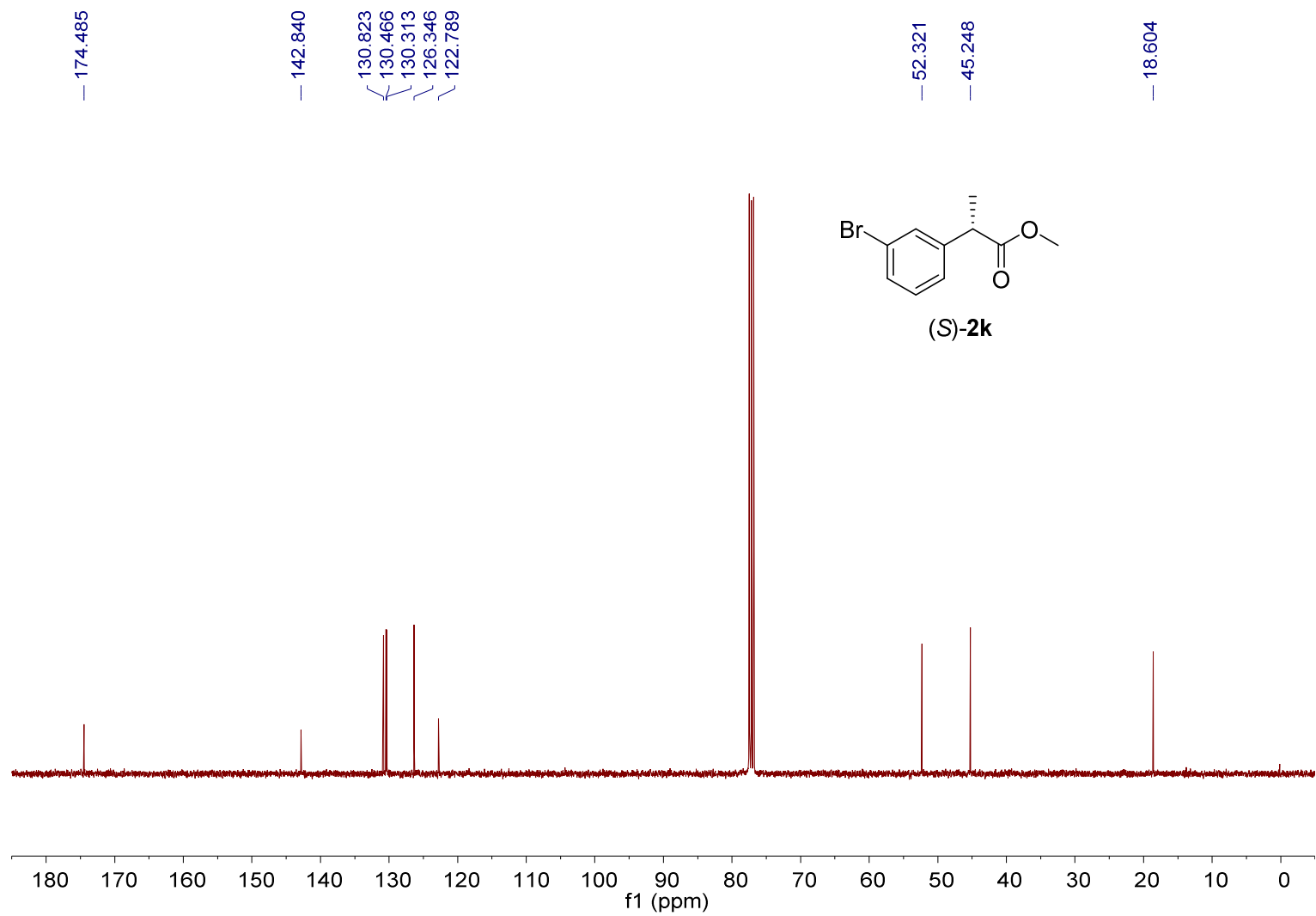


Figure S79. ^{13}C NMR spectrum of (S)-2k (101 MHz, in CDCl_3).

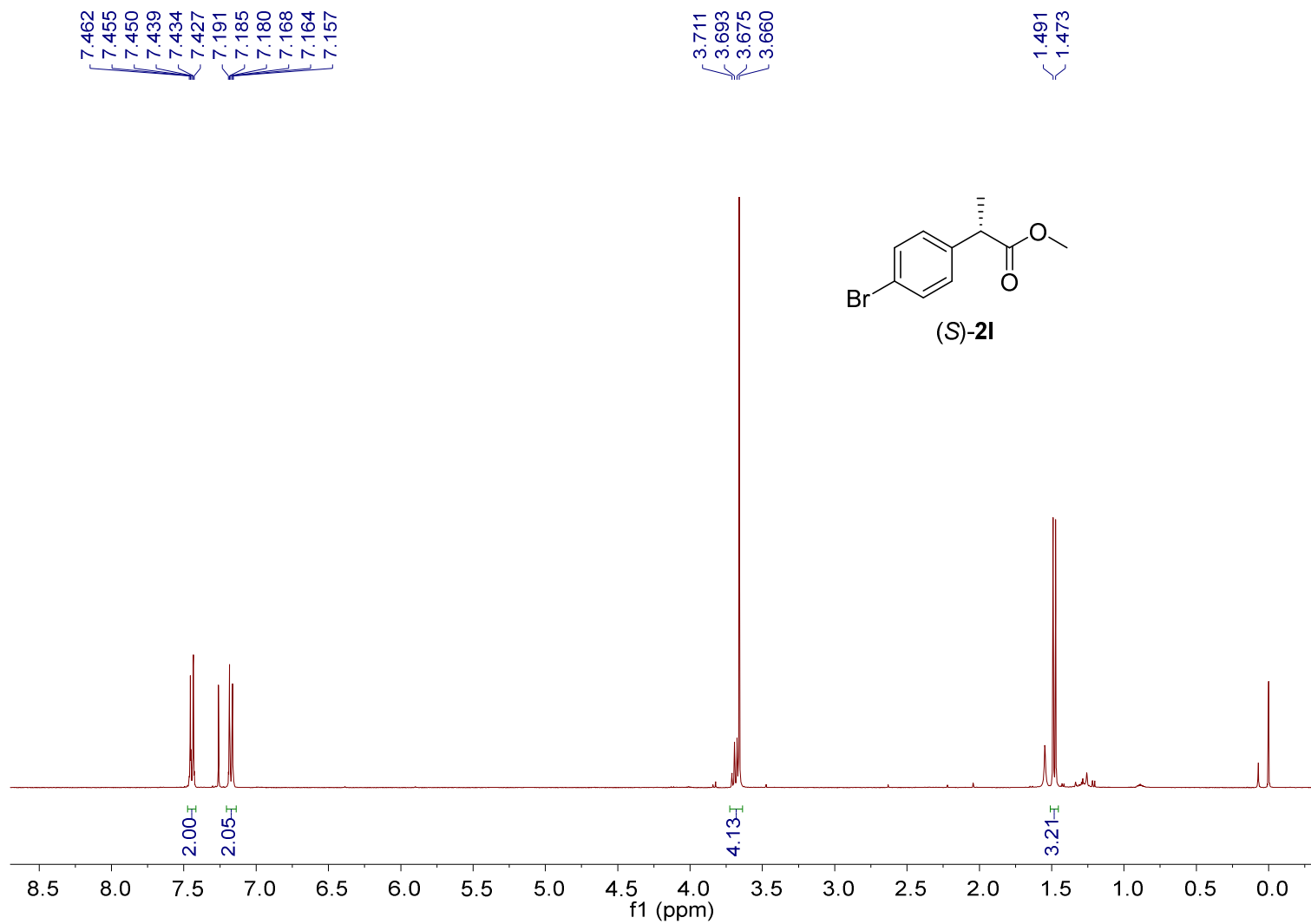


Figure S80. ^1H NMR spectrum of (S)-2I (400 MHz, in CDCl_3).

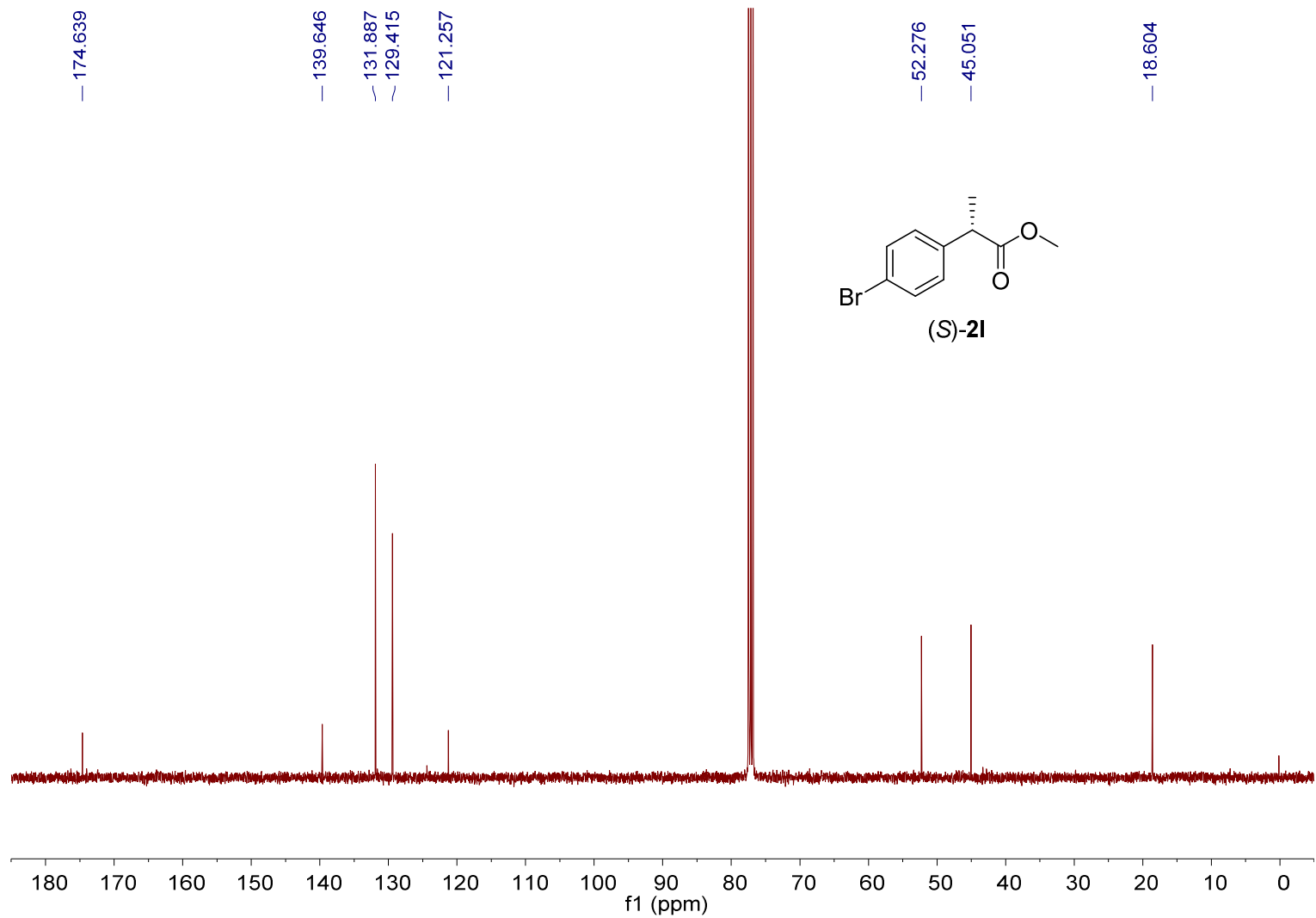


Figure S81. ^{13}C NMR spectrum of (*S*)-**2I** (101 MHz, in CDCl_3).

References

- (1) Li, Z.; Wang, Z.; Meng, G.; Lu, H.; Huang, Z.; Chen, F. Identification of an Ene Reductase from Yeast *Kluyveromyces marxianus* and Application in the Asymmetric Synthesis of (*R*)-Profen Esters. *Asian J. Org. Chem.* **2018**, *7*, 763-769.
- (2) Guo, J.; Zhang, R.; Ouyang, J.; Zhang, F.; Qin, F.; Liu, G.; Zhang, W.; Li, H.; Ji, X.; Jia, X.; Qin, B.; You, S. Stereodivergent Synthesis of Carveol and Dihydrocarveol through Ketoreductases/Eno-Reductases Catalyzed Asymmetric Reduction. *ChemCatChem* **2018**, *10*, 5496-5504.
- (3) Heckman, K. L.; Pease, L. R. Gene Splicing and Mutagenesis by PCR-Driven Overlap Extension. *Nat. Protoc.* **2007**, *2*, 924-932.
- (4) Rütthlein, E.; Classen, T.; Dobnikar, L.; Schölzel, M.; Pietruszka, J. Finding the Selectivity Switch – A Rational Approach towards Stereocomplementary Variants of the Ene Reductase YqjM. *Adv. Synth. Catal.* **2015**, *357*, 1775-1786.
- (5) Pompeu, Y. A.; Sullivan, B.; Stewart, J. D. X-ray Crystallography Reveals How Subtle Changes Control the Orientation of Substrate Binding in an Alkene Reductase. *ACS Catal.* **2013**, *3*, 2376-2390.
- (6) The PyMOL Molecular Graphics System, Version 2.0 Schrödinger, LLC. <https://www.pymol.org/>
- (7) Bowers, K. J.; Chow, D. E.; Xu, H.; Dror, R. O.; Eastwood, M. P.; Gregersen, B. A.; Klepeis, J. L.; Kolossvary, I.; Moraes, M. A.; Sacerdoti, F. D.; Salmon, J. K.; Shan, Y.; Shaw, D. E. In *Scalable Algorithms for Molecular Dynamics Simulations on Commodity Clusters*, SC '06: Proceedings of the 2006 ACM/IEEE Conference on Supercomputing, 11-17 Nov. 2006; 2006; 43-43.
- (8) Powell, I. I. I. R. W.; Buteler, M. P.; Lenka, S.; Crotti, M.; Santangelo, S.; Burg, M. J.; Bruner, S.; Brenna, E.; Roitberg, A. E.; Stewart, J. D. Investigating *Saccharomyces cerevisiae* Alkene Reductase OYE 3 by Substrate Profiling, X-Ray Crystallography and Computational Methods. *Catal. Sci. Technol.* **2018**, *8*, 5003-5016.
- (9) Waterhouse, A.; Bertoni, M.; Bienert, S.; Studer, G.; Tauriello, G.; Gumienny, R.; Heer, F. T.; de Beer, T. A P.; Rempfer, C.; Bordoli, L.; Lepore, R.; Schwede, T. SWISS-MODEL: Homology Modelling of Protein Structures and Complexes. *Nucleic Acids Res.* **2018**, *46*, W296-W303.
- (10) Kobayashi, K.; Yamamoto, Y.; Miyaura, N. Pd/Josiphos-Catalyzed Enantioselective α -Arylation of Silyl Ketene Acetals and Mechanistic Studies on Transmetalation and Enantioselection. *Organometallics* **2011**, *30*, 6323-6327.

- (11) Malmedy, F.; Wirth, T. Stereoselective Ketone Rearrangements with Hypervalent Iodine Reagents. *Chem. - Eur. J.* **2016**, *22*, 16072-16077.
- (12) Pietruszka, J.; Simon, R. C.; Kruska, F.; Braun, M. Dynamic Enzymatic Kinetic Resolution of Methyl 2,3-Dihydro-1H-indene-1-carboxylate. *Eur. J. Org. Chem.* **2009**, *2009*, 6217-6224.
- (13) Pietruszka, J.; Schölzel, M. Ene Reductase-Catalysed Synthesis of (*R*)-Profen Derivatives. *Adv. Synth. Catal.* **2012**, *354*, 751-756.
- (14) Reiß, T.; Hummel, W.; Hanlon, S. P.; Iding, H.; Gröger, H. The Organic–Synthetic Potential of Recombinant Ene Reductases: Substrate-Scope Evaluation and Process Optimization. *ChemCatChem* **2015**, *7*, 1302-1311.
- (15) Waller, J.; Toogood, H. S.; Karuppiah, V.; Rattray, N. J. W.; Mansell, D. J.; Leys, D.; Gardiner, J. M.; Fryszkowska, A.; Ahmed, S. T.; Bandichhor, R.; Reddy, G. P.; Scrutton, N. S. Structural Insights into the Ene-Reductase Synthesis of Profens. *Org. Biomol. Chem.* **2017**, *15*, 4440-4448.
- (16) Padhi, S. K.; Bougioukou, D. J.; Stewart, J. D. Site-Saturation Mutagenesis of Tryptophan 116 of *Saccharomyces pastorianus* Old Yellow Enzyme Uncovers Stereocomplementary Variants. *J. Am. Chem. Soc.* **2009**, *131*, 3271-3280.
- (17) Nett, N.; Duewel, S.; Richter, A. A.; Hoebenreich, S. Revealing Additional Stereocomplementary Pairs of Old Yellow Enzymes by Rational Transfer of Engineered Residues. *ChemBioChem* **2017**, *18*, 685-691.
- (18) Crooks, G. E.; Hon, G.; Chandonia, J.-M.; Brenner, S. E. WebLogo: A Sequence Logo Generator. *Genome Res.* **2004**, *14*, 1188-1190.
- (19) Tian, W.; Chen, C.; Lei, X.; Zhao, J.; Liang, J. CASTp 3.0: Computed Atlas of Surface Topography of Proteins. *Nucleic Acids Res.* **2018**, *46*, W363-W367.
- (20) Kayikci, M.; Venkatakrisnan, A. J.; Scott-Brown, J.; Ravarani, C. N. J.; Flock, T.; Babu, M. M. Visualization and Analysis of Non-Covalent Contacts Using the Protein Contacts Atlas. *Nat. Struct. Mol. Biol.* **2018**, *25*, 185-194.
- (21) Robert, X.; Gouet, P. Deciphering Key Features in Protein Structures with the New ENDscript Server. *Nucleic Acids Res.* **2014**, *42*, W320-W324.
- (22) Fox, K. M.; Karplus, P. A. Old Yellow Enzyme at 2 Å Resolution: Overall Structure, Ligand Binding, and Comparison with Related Flavoproteins. *Structure* **1994**, *2*, 1089-1105.

(23) Pompeu, Y. A.; Sullivan, B.; Walton, A. Z.; Stewart, J. D. Structural and Catalytic Characterization of *Pichia stipitis* OYE 2.6, a Useful Biocatalyst for Asymmetric Alkene Reductions. *Adv. Synth. Catal.* **2012**, *354*, 1949-1960.

Supplementary Information.pdf (9.96 MiB)

[view on ChemRxiv](#) • [download file](#)
